

Aus dem Institute of Pharmacology and Toxicology, Technical University of
Munich



Dissertation
zum Erwerb des Doctor of Philosophy (Ph.D.)
an der Medizinischen Fakultät der
Ludwig-Maximilians-Universität zu München

Role of miR-21 in pulmonary fibrosis

vorgelegt von:

Paula Belen Vaccarello

aus:

Cordoba, Argentina

Jahr:

2022

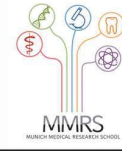
Mit Genehmigung der Medizinischen Fakultät der
Ludwig-Maximilians-Universität zu München

First evaluator (1. TAC member): Prof. Dr. Dr. Stefan Engelhardt
Second evaluator (2. TAC member): Prof. Dr. med. Christian Schulz
Third evaluator: Prof. Dr. Dr. Simone Kreth
Fourth evaluator: Prof. Dr. Andreas Schober

Dean: Prof. Dr. med. Thomas Gudermann

Date of the defense:

25.07.2022



Affidavit

Vaccarello, Paula Belen

Surname, first name

Biedersteinerstr. 29

Street

80802, Munich

Zip code, town

Germany

Country

I hereby declare, that the submitted thesis entitled

Role of miR-21 in pulmonary fibrosis

is my own work. I have only used the sources indicated and have not made unauthorised use of services of a third party. Where the work of others has been quoted or reproduced, the source is always given.

I further declare that the dissertation presented here has not been submitted in the same or similar form to any other institution for the purpose of obtaining an academic degree.

Munich, 27.07.2022

Place, date

Paula Belen Vaccarello

Signature doctoral candidate



LUDWIG-
MAXIMILIANS-
UNIVERSITÄT
MÜNCHEN

Dean's Office
Medical Faculty



Confirmation of congruency between printed and electronic version of the doctoral thesis

Vaccarello, Paula Belen

Surname, first name

Biedersteinerstr. 29

Street

80802, Munich

Zip code, town

Germany

Country

I hereby declare that the electronic version of the submitted thesis, entitled
Role of miR-21 in pulmonary fibrosis

is congruent with the printed version both in content and format.

Munich, 27.07.2022

Place, date

Paula Belen Vaccarello

Signature doctoral candidate

CONTENTS

CONTENTS	1
ABSTRACT	3
LIST OF FIGURES	5
LIST OF TABLES	6
ABBREVIATIONS	7
INTRODUCTION	8
IDIOPATHIC PULMONARY FIBROSIS	8
CELL TYPES IN THE LUNG: HOMEOSTASIS AND DISEASE	12
<i>Structural cells</i>	13
<i>Immune cells</i>	14
MICRORNAs	16
<i>MicroRNAs in lung fibrosis</i>	18
<i>MiR-21</i>	19
AIMS	22
MATERIALS AND METHODS	23
REAGENTS	23
FLOW CYTOMETRY PANELS	25
<i>Mouse</i>	25
<i>Human</i>	26
BUFFERS AND MEDIA	26
EXPERIMENTAL PROCEDURES.....	28
<i>Mice</i>	28
<i>Human samples</i>	28
<i>Bleomycin-induced pulmonary fibrosis</i>	28
<i>Lung function</i>	28
<i>Lung digestion and BAL</i>	29
<i>Single-cell suspension for flow cytometry</i>	29
<i>Magnetic separation of lung tissue CD45+/CD45- fractions</i>	30
<i>Cells staining for FACS sorting</i>	30
<i>Histology</i>	30
<i>RNA isolation</i>	31
<i>Lysis of cells for microRNA sequencing</i>	31
<i>RT-qPCR</i>	31
<i>mRNA library preparation</i>	31
<i>smallRNA library preparation</i>	31
<i>Blood monocytes isolation and differentiation to macrophages</i>	31
<i>Staining of PBMCs, monocytes and Mo-Mac for flow cytometry</i>	33
<i>Stimulation of Mo-Mac with TGF-β and antimiR-21 transfection</i>	33
<i>Cells counting</i>	33
<i>Flow cytometry analysis</i>	34
<i>PCLS preparation</i>	34
<i>PCLS fibrosis model</i>	34
<i>PCLS digestion, magnetic separation and staining for FACS</i>	34
<i>Transfection of PCLS</i>	35
<i>RNA-Seq Analysis</i>	35
RESULTS	37
CHAPTER 1: MIRNOME AND MIR-21 TARGETOME IN BLEOMYCIN-INDUCED PULMONARY FIBROSIS	37

CHAPTER 2: MIRNOME AND MIR-21 TARGETOME IN HUMAN IPF	47
CHAPTER 3: MIRNOME SIGNATURE OF MOUSE LUNG CELLS	52
CHAPTER 4: MIRNOME SIGNATURE OF HUMAN LUNG CELLS.....	56
CHAPTER 5: CHARACTERIZATION OF HUMAN BLOOD MONOCYTE-DERIVED MACROPHAGES	60
CHAPTER 6: TRANSCRIPTOME ANALYSIS OF A HUMAN <i>EX VIVO</i> MODEL OF LUNG FIBROSIS USING PCLS AND ANTIMIR-21 TREATMENT	67
DISCUSSION	77
CHAPTER 1: MIRNOME AND MIR-21 TARGETOME IN BLEOMYCIN-INDUCED PULMONARY FIBROSIS.....	77
CHAPTER 2: MIRNOME AND MIR-21 TARGETOME IN HUMAN IPF	78
CHAPTER 3: MIRNOME SIGNATURE OF MOUSE LUNG CELLS	80
CHAPTER 4: MIRNOME SIGNATURE OF HUMAN LUNG CELLS.....	82
CHAPTER 5: CHARACTERIZATION OF HUMAN BLOOD MONOCYTE-DERIVED MACROPHAGES	83
CHAPTER 6: TRANSCRIPTOME ANALYSIS OF A HUMAN <i>EX VIVO</i> MODEL OF LUNG FIBROSIS USING PCLS AND ANTIMIR-21 TREATMENT	86
CONCLUSION AND FUTURE PERSPECTIVES.....	89
REFERENCES.....	91
ACKNOWLEDGMENTS.....	102

ABSTRACT

Idiopathic pulmonary fibrosis (IPF) is a chronic and irreversible lung disease with a low median survival of only 3-5 years after diagnosis. The absence of a cure is due, in part, to the incomplete understanding of the underlying molecular mechanisms. Emerging evidence points towards an important participation of microRNAs (miRs), small non-coding RNAs that regulate gene expression in a variety of biological processes.

This work aims to 1) gain a better understanding of the roles of miRs in lung homeostasis and in pulmonary fibrosis, with a special focus on the most abundant upregulated miR, miR-21, and 2) to assess the efficacy of anti-miR-21 treatment against lung fibrosis in a relevant human model.

To tackle the first objective, microRNA sequencing (miRNA-Seq) was carried out on lungs from bleomycin-exposed mice and IPF patients, confirming the deregulation of previously reported miRs and discovering new ones, and finding that miR-21 was the upregulated miR with the highest expression. Furthermore, the enrichment of miRs in the CD45⁺/⁻ murine cell fractions of fibrotic lungs was determined and it was found that miR-21 was enriched in the immune cell fraction. These findings together with the widely accepted notion that macrophages play a decisive role in the development of fibrosis led to the investigation of the miR-21 targetome in murine macrophages. Strong repression of miR-21 targets was observed in a population of fibrosis-associated macrophages and putative cellular and molecular pathways where these deregulated targets might be involved were defined.

Likewise, the miR-21 targetome was analyzed in IPF and it was observed that miR-21 target repression was stronger in scarred IPF tissue compared to non-scarred IPF or healthy tissue and BALF. Potential pathways associated with the downregulated miR-21 targets were similar to those found in bleomycin-induced pulmonary fibrosis in mice.

Next, the miRnome profile of individual lung cell types in mouse and human were determined by microRNA-Seq. A miRnome signature profile distinguishes each cell type from the other and a small number of miRs represents the majority of total miR reads in a given cell population. This provides additional clues in the investigation of the mechanisms of action of miRs. Both in human and mice, miR-21 was expressed at highest levels in macrophages, giving further evidence of a putative key role of macrophage-derived miR-21 in lung biology.

Finally, analysis of the transcriptome in a human lung fibrosis model using precision-cut lung slices (PCLS) revealed important similarities with IPF. Notably, inhibition of miR-21 reduced fibrosis-associated gene expression, potentially by suppressing inflammation. These findings support the efforts of devising a therapy against lung fibrosis by targeting miR-21.

LIST OF FIGURES

FIGURE 1	YEARLY INCIDENCE OF IDIOPATHIC PULMONARY FIBROSIS ACCORDING TO DIFFERENT STUDIES.....	8
FIGURE 2	HISTOLOGY OF USUAL INTERSTITIAL PNEUMONIA BY HEMATOXYLIN-EOSIN STAINING.	9
FIGURE 3	SURVIVAL CURVE OF IPF PATIENTS TREATED OR NOT TREATED WITH ANTIFIBROTIC DRUGS.....	10
FIGURE 4	CURRENT MODEL FOR THE CELLULAR AND MOLECULAR MECHANISMS DRIVING LUNG FIBROSIS.....	11
FIGURE 5	STRUCTURE AND CELLS OF THE HUMAN LUNG.	13
FIGURE 6	BIOGENESIS OF MICRORNAs.	17
FIGURE 7	SURVIVAL, FIBROSIS AND LUNG FUNCTION CHANGES UPON BLEOMYCIN-INDUCED PULMONARY FIBROSIS.	38
FIGURE 8	IMMUNE CELL CHANGES UPON BLEOMYCIN-INDUCED LUNG FIBROSIS.....	40
FIGURE 9	MIRNOME CHANGES IN BLEOMYCIN-INDUCED LUNG FIBROSIS.	42
FIGURE 10	ENRICHMENT OF MIRNAs IN THE CD45+ AND CD45- FRACTIONS IN THE LUNGS OF BLEOMYCIN-EXPOSED MICE. .	44
FIGURE 11	ANALYSIS OF THE MIR-21 TARGETOME IN MURINE MACROPHAGE SUBPOPULATIONS.	46
FIGURE 12	MIRNOME OF HUMAN LUNGS FROM DONORS AND PATIENTS WITH IPF.	49
FIGURE 13	ANALYSIS OF THE MIR-21 TARGETOME IN LUNG TISSUE AND BALF FROM IPF PATIENTS AND HEALTHY CONTROLS.	52
FIGURE 14	SORTING OF MOUSE LUNG CELLS.	53
FIGURE 15	MIRNOME OF SORTED MOUSE LUNG CELLS AT BASAL STATE.	55
FIGURE 16	SORTING OF HUMAN LUNG CELLS FOR MICRORNA SEQUENCING.	57
FIGURE 17	MIRNOME OF HUMAN SORTED LUNG CELLS.	59
FIGURE 18	DIFFERENTIATION OF HUMAN BLOOD MONOCYTES TO MACROPHAGES.....	61
FIGURE 19	INFLUENCE OF CELL CULTURE SURFACE IN MACROPHAGE DIFFERENTIATION.	63
FIGURE 20	CHARACTERIZATION OF GM- AND M-MAC.....	65
FIGURE 21	MIR-21 LEVELS IN GM- AND M-MAC UPON TGF- B TREATMENT.	66
FIGURE 22	TRANSCRIPTOMIC ANALYSIS OF A HUMAN <i>EX VIVO</i> FIBROSIS MODEL USING PCLS.	69
FIGURE 23	COMPARISON OF HUMAN <i>EX VIVO</i> PCLS FIBROSIS MODEL TO IPF.	71
FIGURE 24	MIR-21 INHIBITION REDUCES THE FIBROTIC PHENOTYPE OF FC-PCLS.	74
FIGURE 25	COMPARISON OF TRANSCRIPTOME CHANGES BETWEEN IPF AND FC-PCLS TREATED WITH A-21.	75

LIST OF TABLES

TABLE 1 EXPERIMENTALLY VALIDATED MIR-21 TARGETS. 20
TABLE 2. REAGENTS USED. 25

ABBREVIATIONS

AEC	alveolar epithelial cell
AM	alveolar macrophage
BAL	bronchoalveolar lavage
BALF	bronchoalveolar lavage fluid
CC	control cocktail
CC-PCLS	precision-cut lung slices treated with control cocktail
DEG	differentially expressed genes
ECM	extracellular matrix
EMT	epithelial-to-mesenchymal transition
EnC	endothelial cell
EpC	epithelial cell
FACS	fluorescence-activated cell sorting
Fb	fibroblast
FC	fibrosis cocktail
FC-PCLS	precision-cut lung slices treated with fibrosis cocktail
GM-CSF	granulocyte macrophage colony stimulating factor
GM-Mac	monocyte-derived macrophages in the presence of GM-CSF
ILD	interstitial lung disease
iPSC	induced pluripotent stem cells
IM	interstitial macrophage
IPF	idiopathic pulmonary fibrosis
IPFn	IPF normal tissue
IPFs	IPF scarred tissue
M-CSF	macrophage colony stimulating factor
M-Mac	monocyte-derived macrophages in the presence of M-CSF
Mac	macrophages
MACS	magnetic-activated cell sorting
MFI	median fluorescence intensity
microRNA-Seq	microRNA sequencing
miR	microRNA
miRNA	microRNA
Mo-Mac	monocyte-derived macrophages
ON	overnight
PBMC	peripheral blood mononuclear cell
PCLS	precision-cut lung slices
RNA-Seq	RNA sequencing
RT	room temperature
UIP	usual interstitial pneumonia

INTRODUCTION

Idiopathic pulmonary fibrosis

Idiopathic pulmonary fibrosis (IPF) is a chronic, progressive and irreversible interstitial lung disease of unknown etiology that affects approximately 3 million people per year worldwide [1], especially middle-aged to elder people (**Figure 1**), most commonly men. Even though a rare disease, with an estimated yearly incidence of 2.8–9.3 per 100.000 in North America and Europe [2], it is one of the two most common forms of interstitial lung diseases (ILD) [3].

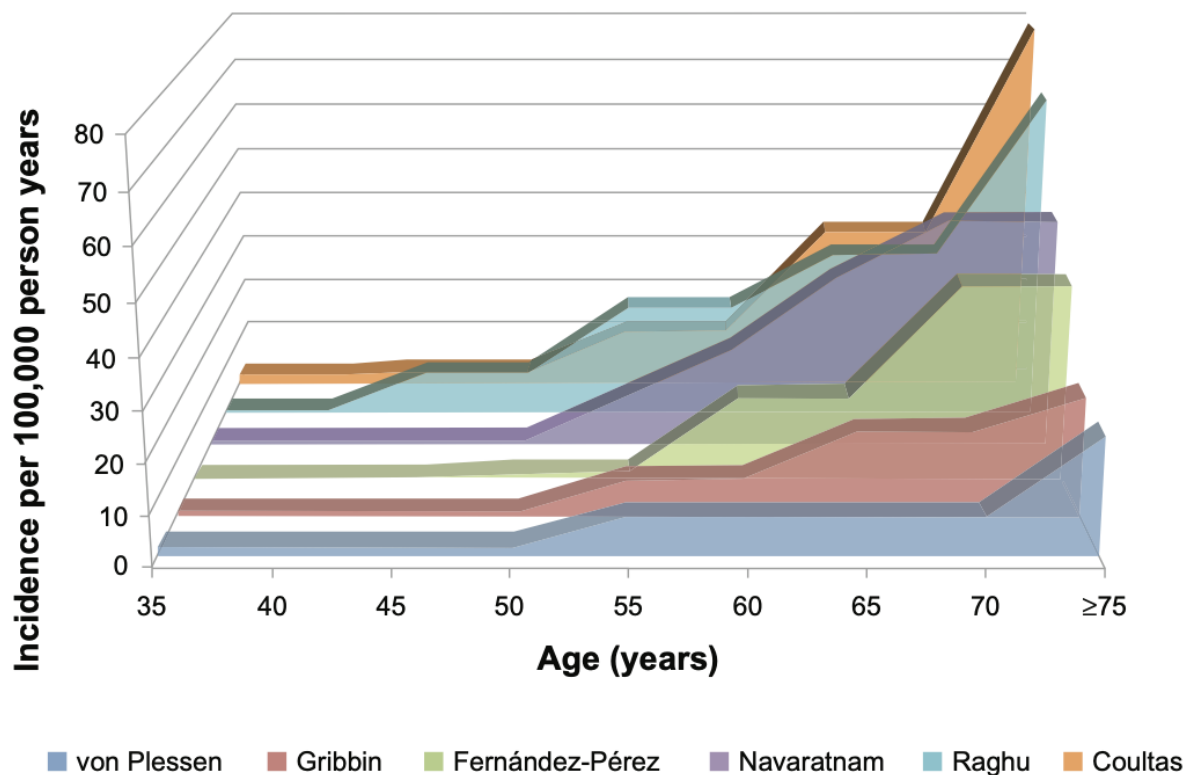


Figure 1 Yearly incidence of idiopathic pulmonary fibrosis according to different studies.

The incidence of idiopathic pulmonary fibrosis increases with age. Figure adapted from [4].

ILDs are a group of heterogeneous lung diseases characterized by inflammation and fibrosis, in varying degrees, that include idiopathic pulmonary fibrosis, sarcoidosis, hypersensitivity

pneumonia and systemic sclerosis ILD, among others. Common symptoms include difficulty to breathe, coughing, tiredness and loss of weight [5].

In IPF, the cause of disease is, by definition, unknown. Therefore, the diagnosis starts by excluding other ILDs, together with measurements of the pulmonary function, chest X-rays, CT scans, bronchoalveolar lavage (BAL) and lung biopsies [6].

The main pathological feature of IPF at the histological level is the presence of usual interstitial pneumonia (UIP), which includes honeycombing and fibroblastic foci (**Figure 2**). UIP is characterized by a patchy structure with areas of dense fibrosis alternating with normal areas. Honeycombing refers to cyst-like enlarged airspaces with thickened walls surrounded by fibrosis, and sometimes filled with mucus and inflammatory cells. Fibroblastic foci are areas of the lung densely populated by fibroblasts and myofibroblasts which are proliferating and secreting large amounts of extracellular matrix (ECM) proteins. The scarring of the tissue due to excessive deposition of ECM causes lung stiffness, the destruction of lung structure and an impairment of air exchange in the alveoli, resulting in shortness of breath, weakness and an overall low quality of life [7].

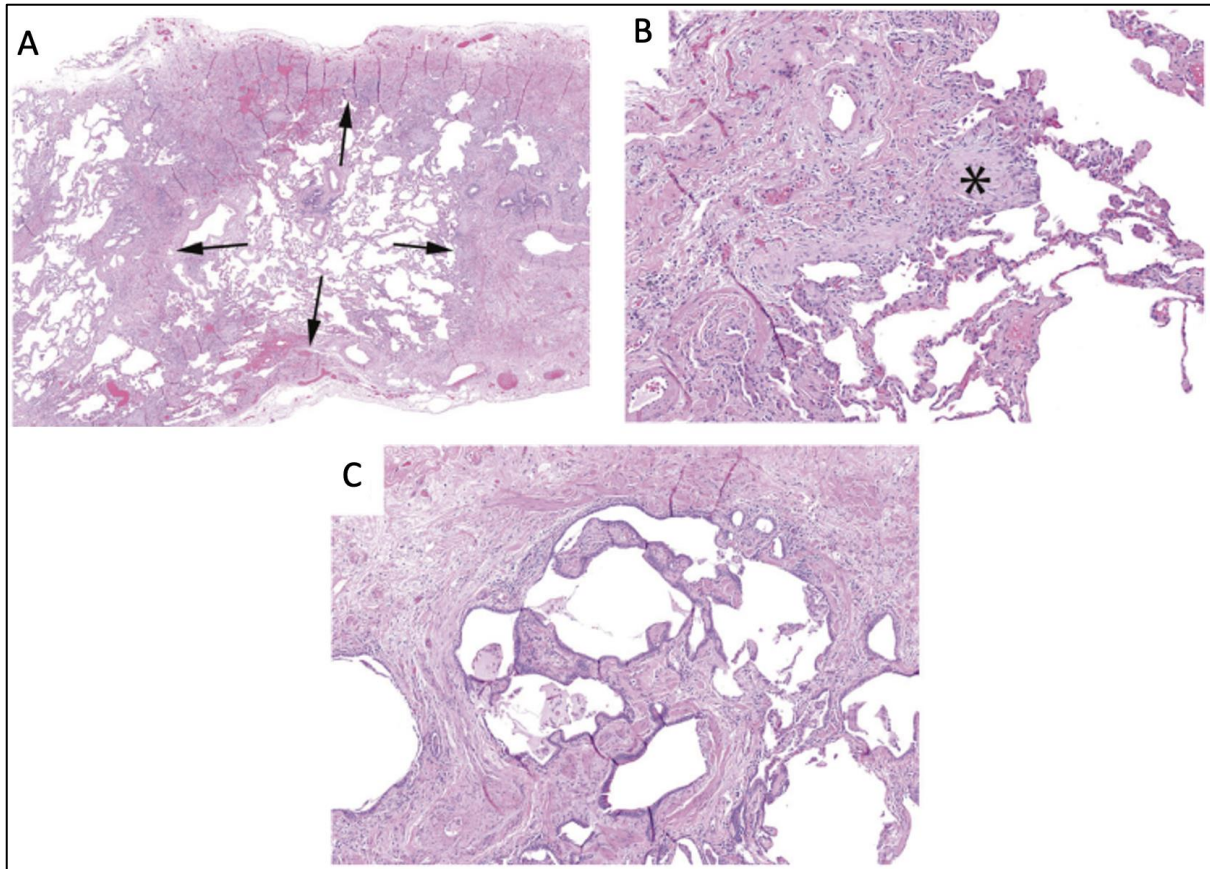


Figure 2 Histology of usual interstitial pneumonia by hematoxylin-eosin staining.

A. Abrupt alternation of fibrotic (arrows) and normal (areas in the center and left) lung. **B.** A fibroblastic focus (*), i.e., an area characterized by accumulation of myofibroblasts immersed in extracellular matrix. **C.** Area with honeycombing, i.e., enlarged airspaces in the shape of cysts, lined by bronchial epithelium, often filled with mucus and surrounded by scars. Figure from [8].

IPF is an aggressive and gradually progressing disease; patients who are diagnosed with IPF have a median survival afterwards of only 3-5 years [9]. Treatment options are scarce, two drugs have been approved by the FDA and the European Medicines, Nintedanib and Pirfenidone, which slow the progression of the disease to some extent but provide no cure (**Figure 3**). In many cases, the last hope is lung transplantation [9].

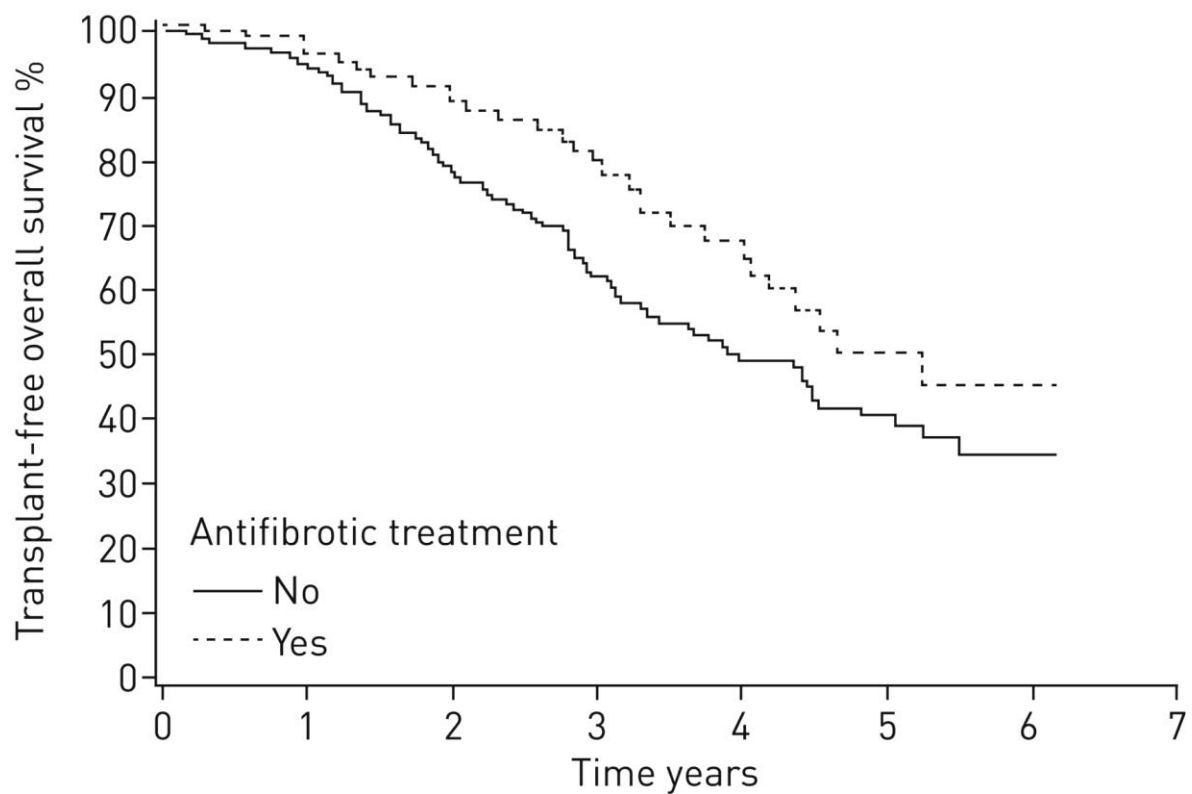


Figure 3 Survival curve of IPF patients treated or not treated with antifibrotic drugs.

Treatment with Nintedanib or Pirfenidone slows the progression of IPF, but does not stop it. Figure from [10].

Even though the etiology is unknown, IPF has been associated mainly to lifestyle and environmental factors such as smoking, air pollution, asbestos or silica exposure, bacterial and viral infections, radio and chemotherapy, but also genetic factors.

At the molecular level, the current hypothesis is that these insults produce repetitive alveolar microinjuries which induce epithelial cells to secrete inflammatory mediators that in turn recruit and activate immune cells, leading to a signaling cascade that promotes wound healing, where fibroblasts are activated to proliferate and secrete extracellular matrix components (ECM) and epithelial cells undergo a process called epithelial-to-mesenchymal transition (EMT), i.e., they lose epithelial cells characteristics and acquire a mesenchymal cell phenotype that enables them to also secrete ECM (**Figure 4**). This process is necessary to repair wounds and, in normal conditions, the scar that was formed would be replaced by regenerated epithelium and endothelium. Lung fibrosis occurs when this process is aberrantly activated and instead of progressing to a resolution phase, fibrosis continues and the lung is left permanently scarred [11].

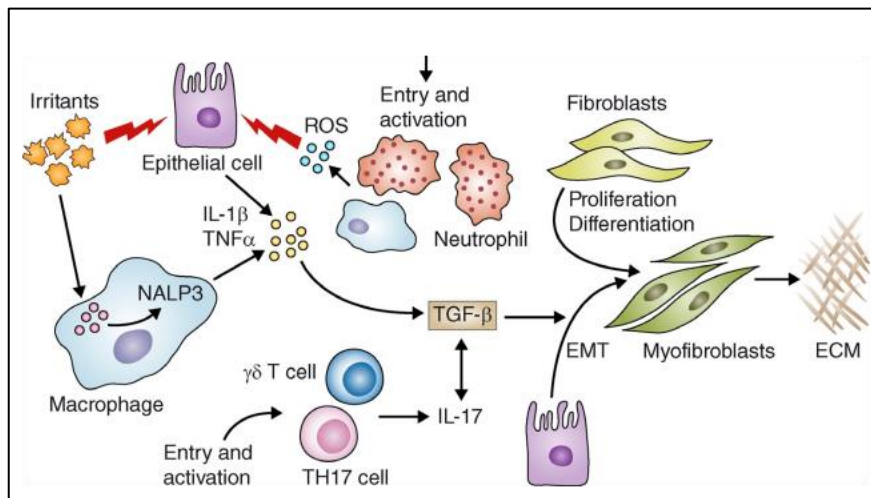


Figure 4 Current model for the cellular and molecular mechanisms driving lung fibrosis.

Repetitive alveolar microinjuries derived from exposure to certain pollutants, drugs or pathogens initiate proinflammatory and profibrotic pathways in structural and immune cells both in a paracrine and autocrine manner, leading in the end to fibroblasts proliferation and transdifferentiation into myofibroblasts that secrete high amounts of ECM, scarring the lung tissue and obstructing gas exchange in the alveoli. Figure from [11]

Several *in vivo* rodent models of pulmonary fibrosis exist, including exposure to bleomycin, radiation, asbestos and silica, as well as genetic deletions or mutations. While none of them reproduces exactly the pathogenesis of IPF, they give a good approximation to understand the molecular and cellular mechanisms of disease and potential drugs. Of these, the most commonly used is bleomycin-induced pulmonary fibrosis.

Bleomycin is an anti-cancer drug which produces DNA damage in cells. Its use as a fibrosing agent derives from the clinical observation that, in patients undergoing cancer therapy, it led to lung fibrosis. It is believed that this results from the fact that the lungs, unlike other organs, are deficient in the enzyme required for its metabolism [12].

Bleomycin is administered to mice via (oro)intratracheal liquid or aerosolized instillation. The first days after bleomycin administration are characterized by a state of inflammation and recruitment of inflammatory cells. After 7-14 days, high collagen deposition, presence of fibroblastic foci and upregulation of fibrosis signaling molecules and ECM components are observed, similar to IPF. The major differences of this model in comparison to human IPF are that it is rapidly established, it is not progressive and resolves over time, usually after 28 days [13], [14].

Cell types in the lung: homeostasis and disease

The lungs are the main components of our respiratory system whose main function is gas exchange. The airways have a tree-like structure, where the trachea would be the trunk that progressively branches into the bronchi, bronchioles and alveolar ducts, terminating in the alveoli, where gas exchange occurs (**Figure 5**).

At the cellular level, the lung tissue is composed of various cell types, namely epithelial cells, endothelial cells, fibroblasts and immune cells.

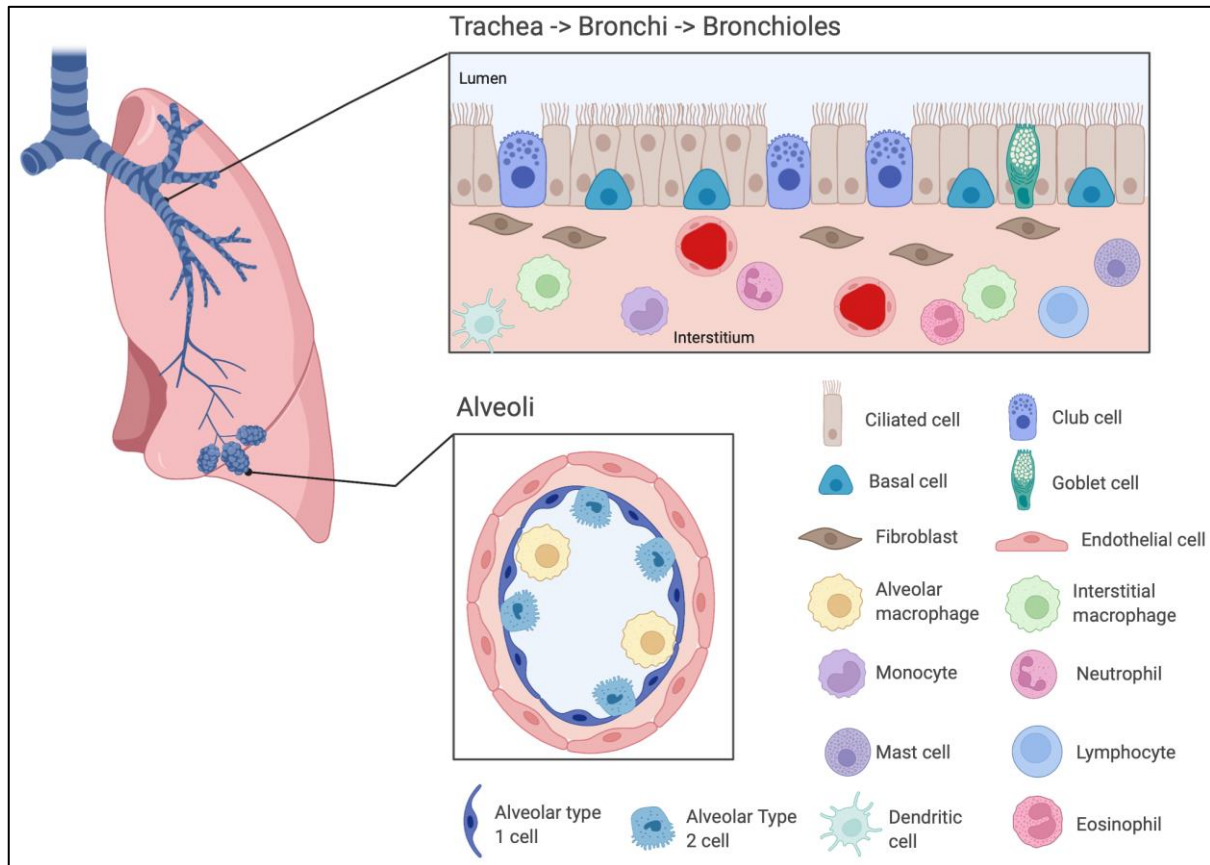


Figure 5 Structure and cells of the human lung.

Structure of the lung airways, starting in the trachea, branching to the bronchi, bronchioles and ending in the alveoli. Close-ups: Lungs are composed of several types of structural and immune cells. Created with BioRender.com.

Structural cells

Epithelial cells are present from the trachea down to the alveoli, though in varying abundance. In the upper airways, the epithelium is composed mainly by ciliated, goblet and basal cells, in the bronchioles there are mainly ciliated, club and basal cells and the alveoli are composed of alveolar type 1 (AT1) and 2 (AT2) cells. Goblet and ciliated cells take care of mucociliary clearance, protecting the body from harmful substances and pathogens by secreting mucus and transporting the trapped particles up to the trachea, respectively. Basal cells are progenitors of ciliated and secretory cells. Club cells are also secretory and provide the lining fluid of the epithelium in the distal airways, which includes antimicrobial peptides; as basal cells, they are progenitors for ciliated and secretory cells. AT1 cells are the cells in charge of gas exchange and AT2 produce surfactants and give rise to AT1 cells.

In lung fibrosis, alveolar epithelial cells (AECs) undergo apoptosis and the loss of these cells is not replenished by reepithelization, exposing the basement membrane to damage. The decline in AECs is accompanied by higher proportions of airway epithelial cells.

Furthermore, AECs from IPF patients have been shown to display genomic instability, mitochondrial dysfunction, express several chemokines and growth factors that promote activation of fibroblasts and to undergo a transdifferentiation process, EMT, where they lose epithelial cell characteristics and acquire a fibroblast-like phenotype [15], [16].

Fibroblasts are mesenchymal cells located in the interstitial space or immediately below the epithelium and constitute the main providers of ECM, which serves as a scaffold to maintain lung structure. In homeostatic conditions, fibroblasts are in a quiescent state and tightly regulate the production and turnover of ECM. However, upon injury, they differentiate to activated myofibroblasts, which produce large amounts of matrix proteins, have increased migration and contractile properties, become more resistant to apoptosis and secrete signals to recruit inflammatory cells to the site of injury [17], [18].

Endothelial cells are in direct contact with the blood and therefore permit the transport of oxygen from the air in the alveoli into the blood and carbon dioxide from the blood to the air[19]. Upon injury, they are involved in blood clotting to seal wounds, and the vascular permeability increases, allowing for entry of inflammatory cells and coagulation and fibrosis-associated proteins. Moreover, dysregulated angiogenesis is observed in IPF lung tissue, being decreased in fibroblastic foci and increased in areas of milder fibrosis [20].

Immune cells

Even though epithelial cells have an important role in host defense by providing a physical barrier, mucociliary clearance and the secretion of antimicrobial peptides, in this work, immune cells will refer to those cells of hematopoietic origin.

In the lungs we can find all kinds of myeloid and lymphoid cells, namely, macrophages (further divided into interstitial and alveolar macrophages), monocytes, B cells, T cells, natural killer cells (NK), dendritic cells (DCs), mast cells, neutrophils and eosinophils.

Alveolar macrophages (AM), as their name indicates, reside in the alveolar space, while **interstitial macrophages** (IM) reside in the interstitium, they are smaller and more heterogenous in shape. Alveolar macrophages are the first cells to come into contact with inhaled particles and pathogens. In this interaction they determine whether the substance or

microorganism is harmless or harmful and elicits an appropriate response. They are also in charge of clearing apoptotic cells, debris and surfactant by phagocytosis. In humans, little is known about the functional differences between both macrophage subtypes under homeostatic conditions, but interstitial macrophages also perform classic macrophage functions such as immune regulation and phagocytosis, and seem to have higher antigen-presentation properties than AM [21].

Macrophages are by far the most studied immune cells in IPF, where they have a highly complex role, as they can exert both pro- and anti-fibrotic effects depending on the stage of fibrosis, macrophage subtype and origin, and the specific milieu surrounding them.

Macrophage-derived cytokines, chemokines and growth factors such as TGF-beta, PDGF and IL-1beta promote fibroblast proliferation and ECM production. On the other hand, macrophages also produce matrix metalloproteinases (MMPs) that degrade ECM, and they phagocytose dying cells which would otherwise continue secreting inflammatory signals[11], [22].

In this context, **monocytes** have a prominent role. Under homeostatic conditions, they contribute to immune defense by phagocytosis, antigen presentation, exerting cytotoxicity and giving rise to macrophages and dendritic cells. Upon lung injury, they are recruited to the site of injury where they differentiate into macrophages. Several mouse studies have shown that monocyte-derived macrophages but not tissue-resident macrophages are the main drivers of fibrosis [23]–[26].

Neutrophils protect the host by killing bacteria through phagocytosis, degranulation and the formation of neutrophil extracellular traps. They are not abundant in the lung under homeostatic conditions, but their numbers are increased in the BALF of IPF patients, together with one of their classic proteins, neutrophil elastase, which seems to activate TGF-beta signaling and myofibroblast differentiation [27].

It is believed that the majority of tissue-resident **T cells** in the lung consists of memory T cells that derive from lymphoid organs and persist in the lung after a respiratory infection, protecting it from future exposure to those pathogens. In fibrosis, the most studied T cells are T helper cells 1 and 2 (Th1 and Th2); Th2 cells can activate fibroblasts and macrophages via IL-4 and IL-13, while Th1 cells secrete cytokines with anti-fibrotic properties [28], [29].

Other immune cells in the lung have been studied mainly in association with other pulmonary diseases, such as allergy and asthma, respiratory infections and cancer.

Mast cells mainly exert their inflammatory function by degranulation, secreting, among others, histamine, prostaglandin D₂ and tryptase. They are well known in asthma because they get activated when allergen-bound IgE binds to the mast cells' high affinity IgE receptor[30].

Eosinophils are similar to mast cells in that they are granulated tissue-resident cells, but they originate from a different precursor. Likewise, they are mainly involved in allergic reactions, but in a later phase; they are recruited to the airways by activated mast cells-secreted cytokines and the release of their cytotoxic granules leads to airway damage and inflammation [31].

Dendritic cells are professional antigen-presenting cells and represent the link between innate and adaptive immunity. DCs sample their environment and, when activated by pathogens, pollutants or signals from damaged lung cells, they migrate to the lymph nodes and initiate the adaptive immune response by interacting with T cells [32].

B cells are present in the lung as circulating B cells, but also as resident B cells, namely, plasma cells that secrete immunoglobulins, and memory B cells that arise after respiratory infections. B cells contribute to allergic inflammation by secreting IgE but are also involved in other lung diseases, such as COPD and lung cancer[33], [34].

MicroRNAs

MicroRNAs (miRs) are a type of endogenous non-coding RNAs of only ~22 nucleotides in length that regulate diverse biological processes in cells such as differentiation, apoptosis and metabolism. The way microRNAs exercise this regulation is by binding to mRNAs that share a complimentary sequence, usually in the 3'-untranslated region (UTR), and inducing transcript degradation or translational repression, depending on the degree of complementarity; when high, it leads to mRNA degradation and when low, repression of translation, the former being the predominant mechanism in mammals [35]. Given their short nature, a single microRNA can have hundreds of target mRNAs and, at the same time, a single mRNA can have complimentary sequences to several microRNAs.

In the genome, microRNAs can be located between genes (intergenic), within introns (intronic) or clustered with other miRs (polycistronic). They are first transcribed in the nucleus as a longer primary transcript (pri-miRNA) with a stem-loop, which is cleaved by the

endonuclease Drosha, giving rise to a shorter precursor miR (pre-microRNA). The pre-miR is then transported from the nucleus to the cytoplasm, where it is further cleaved by the nuclease Dicer into a mature duplex. One of the strands from the miRNA:miRNA duplex is degraded, while the other is loaded into the miRNA-induced silencing complex (miRISC) that guides it to the target mRNA[36], [37] (**Figure 6**).

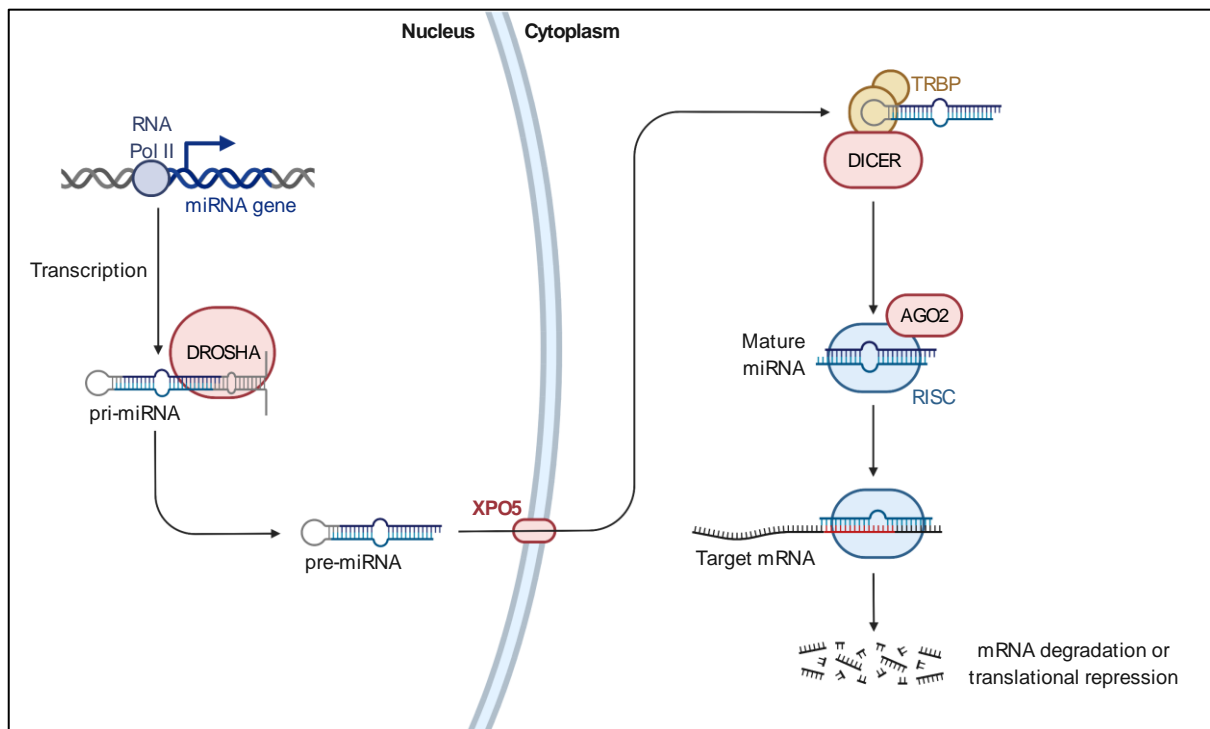


Figure 6 Biogenesis of microRNAs.

In the nucleus, miRNAs are first transcribed as a long pri-miRNA, which is cleaved by the enzyme Drosha into a pre-miRNA that is subsequently transported into the cytoplasm assisted by Exportin5. In the cytoplasm, the pre-miRNA is further cleaved by the enzyme Dicer, forming a miRNA duplex. One of the strands in this duplex is degraded and the other loaded into the AGO2-RISC complex that guides the miRNA to its target mRNA by sequence complementarity. The binding of the miR to its target induces transcript degradation or translational repression. Adapted from “microRNA in Cancer”, by BioRender.com (2022). Retrieved from <https://app.biorender.com/biorender-templates>.

Apart from microRNAs involvement in physiological processes, their dysregulation has been linked to several disorders and diseases, including fibrosis, cancer and atherosclerosis, making them valuable as biomarkers or therapeutic targets, both based on inhibition with

antisense oligonucleotides (antimiRs) or increasing their levels with miR mimics. Some of these antimiRs or miR mimics have been tested in clinical trials[38], [39].

For an antimiR to be effective in silencing a target microRNA *in vivo*, it should exhibit good pharmacokinetic characteristics, bind to its target with high affinity and resist nuclease cleavage. To achieve this, the antisense oligonucleotides are chemically modified, e.g., with a bicyclic locked nucleic acid modification (LNA), which enhances stability and affinity, or phosphorothioate linkages in replacement of phosphodiester ones, which improves stability and pharmacokinetics, among others [38].

MicroRNAs in lung fibrosis

MicroRNAs dysregulation has been extensively studied in the pathogenesis of lung fibrosis, both in human IPF as well as in animal models. *Pandit et al 2010* [40] performed miR array of normal and IPF lung tissues and found over 15 downregulated miRs and over 40 upregulated miRs, including the downregulation of let-7d and members of the miR-30 family, and the upregulation of miR-31, miR-376a. They further confirmed the downregulation of let-7d by *in situ* hybridization and found that its inhibition in different epithelial cell lines induces EMT and that it promotes fibrosis *in vivo*. *Lacedonia et al 2021* [41] also found let-7d to be downregulated in the serum exosomes of IPF patients and *Yu et al 2019* [42] showed that restoring let-7d expression with mimics attenuated EMT in cultured epithelial cells by reducing the expression of the let-7d target HMGA2.

Confirming the findings of *Pandit et al 2010* [40], *Mao et al 2014* [43] and *Zhang et al 2017* [44] later also observed the downregulation of miR-30a in the lungs of bleomycin-exposed rats and in the plasma of IPF patients, respectively. Furthermore, treatment of mice exposed to bleomycin-induced pulmonary fibrosis with miR-30a mimics significantly decreased the severity of fibrosis [44].

Another well-studied miRNA is miR-21. *Liu et al 2010* [45] showed that miR-21 is upregulated in the lungs of IPF patients and bleomycin-induced pulmonary fibrosis in mice, *Yamada et al 2013* [46] found that miR-21 is upregulated in epithelial, endothelial and mesenchymal lung cells from mice with bleomycin-induced pulmonary fibrosis and in AT2 cells from IPF patients and *Dirol et al 2022* [47] recently observed elevated levels of miR-21 in the plasma of IPF patients. Furthermore, miR-21 inhibition reduces the progression of bleomycin-induced lung fibrosis [45], reverses TGF- β -induced EMT in cultured mouse epithelial cells [46] and TGF- β -induced human fibroblasts activation [45], [48].

In another miRNA array, *Milosevic et al 2012* [49] identified 94 differentially expressed microRNAs between IPF and normal lungs, including the upregulation of miR-154, which was also increased in isolated human lung fibroblasts from IPF lungs. They also found that miR-154 induces fibroblasts proliferation and migration and the activation of the WNT/ β catenin pathway, all processes activated in IPF [11].

Like these examples, several other miRNAs have been implicated in idiopathic pulmonary fibrosis and animal models [50]–[53].

MiR-21

MiR-21 is a 22 nucleotides-long microRNA located on chromosome 17 in the intronic region of the TMEM49 gene and it possesses its own promoter. It has been classified as an oncogenic miRNA (“oncomiR”) because it is upregulated in many forms of cancer, including lung, breast, ovarian, colorectal, gastric, esophageal, oral, prostate and glioma [54]–[58].

Nevertheless, one could as well call it a “fibromiR” or “inflamiR” given that it is also upregulated in fibrosis of several tissues and inflammatory diseases, such as lung, renal, liver and cardiac fibrosis, asthma, atherosclerosis and osteoarthritis, among others [37], [50], [59]–[63].

The clinical relevance of inhibiting miR-21 as therapeutic strategy is highlighted by the fact that it has reached clinical trials. RG-012, a miR-21 inhibitor, completed phase I clinical trials in the treatment of Alport syndrome, a kidney disease [64].

Mechanistically, several miR-21 targets have been experimentally validated and associated with important signaling pathways and biological processes. **Table 1** gives a summary of some of those validated targets.

miR-21 target	Signaling pathway / Biological process	Species/model	Disease	Methods	References
SMAD7	TGF- β 1 pathway	Human Fb cell line, mouse	Pulmonary fibrosis	Luciferase assay, WB	[65], [66]
PDCD4	TGF- β 1 pathway, invasion, proliferation, PDCD4-c-Jun-AP-1 pathway	Human Fb cell line, human esophageal squamous cell carcinoma cell line, esophageal squamous cell carcinoma tumors, colorectal tumors, blood Mo-Mac	Ovarian, cervical, colon and esophageal cancer, LPS-induced inflammation	WB, Luciferase assay, RT-qPCR	[48], [67]–[69]
PTEN	PI-3K pathway, apoptosis, proliferation, PTEN-AKT-phosphorylation-dependent-pathway, migration, efferocytosis, NF- κ B pathway	Cholangio-carcinoma and hepatocellular carcinoma cell lines, mouse heart tissue, primary mouse cardiac Fb, hepatocellular cancer tumors, blood Mo-Mac	Cholangio-carcinoma, myocardial ischemia-reperfusion, hepato-cellular carcinoma, LPS-induced inflammation	WB, RT-qPCR, Luciferase assay, microarray, IF	[69]–[72]
SPRY1	ERK-MAPK pathway, apoptosis	Rat and mouse primary cardiac Fb, mouse Fb cell line, mouse and human heart tissue	Heart failure	RT-qPCR, ISH, WB, Luciferase assay	[73]
SPRY2	ERK-MAPK pathway, invasion, migration, proliferation, apoptosis	Human and rat liver tissue, rat primary HSCs, HEK cells, breast tissue, human breast cancer cell lines	Liver cirrhosis, breast cancer	RT-qPCR, Luciferase assay, WB	[74], [75]
HNF4a	EMT	Human and rat liver tissue, rat primary HSCs, HEK-293 cell line	Liver cirrhosis	RT-qPCR, Luciferase assay, WB	[74]
BMPR2	Proliferation, apoptosis	HEK-293 cell line, mouse lung tissue, human pulmonary arterial SMCs	Chronic hypoxia	RT-qPCR, Luciferase assay, WB, ISH, NB	[76], [77]

Table 1 Experimentally validated miR-21 targets.

EMT: epithelial-to-mesenchymal transition, Fb: fibroblast, Mo-Mac: monocyte-derived macrophages, HSCs: hepatic stellate cells, SMCs: smooth muscle cells, RT-qPCR: reverse

transcription quantitative polymerase chain reaction, WB: Western blot, IF: immunofluorescence, ISH: in situ hybridization, NB: Northern blot.

Apart from regulating the expression of target mRNAs, miR-21 itself is also subject to regulation at the transcriptional and post-transcriptional level. Some transcription factors such as NFI, C/EBP α and Gfi1 bind to the promoter region of miR-21 and suppress its transcription. Zhou *et al* 2018 [78] showed that TGF- β 1 induces miR-21 expression through Smad proteins and this enhancement seems to be primarily mediated by a post-transcriptional mechanism where Smad3 assists Drosha in the processing of the already transcribed pri-miR-21[79].

AIMS

- 1) To gain a better understanding of the roles of miRNAs in the healthy and fibrotic lung, with a special focus on miR-21, the most abundant upregulated miR in IPF.
- 2) To assess the therapeutic potential of miR-21 inhibition against lung fibrosis in a relevant human model.

MATERIALS AND METHODS

Reagents

Reagent	Company	Catalogue N°
1-Oleoyl Lysophosphatidic Acid (sodium salt)	Biomol	Cay62215-1
Albumin Fraction V	Carl Roth	8076.4
Albumin Fraction V, biotin-free	Carl Roth	0163.4
Ammonium chloride (NH ₄ Cl)	Carl Roth	P726.1
Amphotericin B	Gibco	15290018
AMPure XP	Beckman Coulter	A63881
Animal-Free Recombinant Human TGF-β1 (CHO derived)	Peprotech	AF-100-21C
ArC™ Amine Reactive Compensation Bead Kit	Invitrogen	A10628
Atipamezol (Revertor® 5 mg/ml)	cp pharma	799-588
Automatic Setup Beads Kit	SONY biotechnology	LE-B3001
Bleomycin sulfate from Streptomyces verticillus	Sigma Aldrich	B8416-15UN
Burprenophrine (Buprenovet® Multidose 0.3 mg/ml)	Bayer	2541
Calcium chloride dihydrate (CaCl ₂)	Sigma-Aldrich	C3881
CD45 MicroBeads	Miltenyi	130-052-301
CD45 MicroBeads, human	Miltenyi	130-045-801
Chloroform	Roth	3313.1
Collagenase Type 2	Worthington	LS004176
Collagenase Type 4	Worthington	LS004188
D-(+)-Trehalose dihydrate	Sigma	T0167
Diazepam		
Dimethylsulfoxide (DMSO)	Roth	4720.4
Direct Red 80	Sigma Aldrich	365548-5g
Dispase	Corning Life Sciences	734-1312
Dispase® II (neutral protease, grade II)	Roche	4942078001
DMEM	Gibco	41966-029
DMEM/F-12 (1:1)	Thermo Fisher	11330-032
DNase I	Roche	11284932001
DPBS	LifeTechnologies	14190-169
Elastase	Worthington	LS002292
Ethanol 99,8%	Carl Roth	9065.4
Ethylendiaminetetraacetic acid (EDTA)	Sigma-Aldrich	03690
Fast Green FCF	Sigma Aldrich	F7252
FcR Blocking Reagent, human	Miltenyi	130-059-901
Fentanyl hameln 50 microgram/ml	hameln	ZI 15923002
Fetal bovine serum (FBS)	Sigma	F7524
Ficoll-Paque™ PLUS Media	Thermo Fisher Scientific	11768538
Flumazenil	hikma	PZN 01326057

Reagent	Company	Catalogue N°
FluoroFix Buffer	BioLegend	BLD-422101
Glycogen, RNA Grade	LifeTechnologies	R0551
HBSS	LifeTechnologies	14175129
Heparin		
hsa-miR-21-5p miRCURY LNA miRNA PCR Assay	Qiagen	339306 GeneGlobe ID: YP00204230
Insulin-Transferrin-Selenium-Ethanolamine (ITS -X)	Life Technologies	51.500.056
Isoflurane CP®	cp pharma	798-932
Isopropanol	Roth	6752.4
Lipofectamine RNAiMAX Transfection Reagent	Life Technologies	13778-075
LNA-antimiR-21 5'-TCAGTCTGATAAGCT-3'	Exiqon	199900
LNA-antimiR-scr 5'-ACGTCTATACGCCCA -3'	Exiqon	199900
Medetomidine (Dorbene vet® 1 mg/ml)	Zoetis	796-435
Metamizol (Novalgin® Tropfen 500 mg/ml)	SANOFI	797-976
Midazolam (Dormicum® 5 mg/ml)	Roche	799-237
miRCURY LNA RT Kit	Qiagen	339340
miRCURY LNA SYBR Green PCR Kit	Qiagen	339346
Mouse BD Fc Block™	BD Biosciences	553142
Naloxon	PUREN	PZN 11356645
NEBNext Cell Lysis Buffer	New England Laboratories	E5530S
NEBNext® Multiplex Oligos for Illumina®	New England Laboratories	E6440S
NEBNext® Single Cell/Low Input RNA Library Prep Kit for Illumina®	New England Laboratories	E6420L
NEBNext® Small RNA Library Prep Set for Illumina	New England Laboratories	E7330L
Nuclease-free H2O	Invitrogen	10977-049
Opti-MEM medium	Thermo Fisher Scientific	31985062
Pan Monocyte Isolation Kit	Miltenyi	130-096-537
Pen/Strep	LifeTechnologies	15070063
Platelet Derived Growth Factor-AB, human recombinant (rHuPDGF-AB)	Biomol	94949.10
Recombinant Human GM-CSF	Peptotech	300-03
Recombinant Human M-CSF	Peptotech	300-25
RNase Inhibitor, Human Placenta	New England Laboratories	M0307L
RPMI 1640	Gibco	21875-034
SNORD44(hsa) miRCURY LNA miRNA PCR Assay	Qiagen	339306 GeneGlobe ID: YP00203902
SNORD68 miRCURY LNA miRNA PCR Assay	Qiagen	339306 GeneGlobe ID: YP00203911

Reagent	Company	Catalogue N°
Tris-HCl	Carl Roth	9090.2
TRIzol™ Reagent	Thermo Fisher Scientific	15596026
TrueQuant SmallRNA Seq Kit	GenXPro	16047
Trypan blue stain 0.4%	Invitrogen	T10282
Tumor Necrosis Factor alpha, human recombinant (rHuTNF-a)	Biomol	50435.10
Tween® 20 for molecular biology	Hartenstein	CT21
UltraComp eBeads™ Plus Compensation Beads	Invitrogen	01-3333-42

Table 2. Reagents used.

Flow cytometry panels

Mouse

Macrophages

Antibody	Clone	Fluorophore	Dilution	Company	Cat. N
CD45	30-F11	FITC	1:100	BioLegend	103108
CD11b	M1/70	PE	1:160	BioLegend	101208
CD24	M1/69	PE/Dazzle 594	1:80	BioLegend	101838
SiglecF	1RNM44N	PerCP-eFluor-710	1:100	Invitrogen	46-1702-82
F4/80	BM8	PECy7	1:100	Invitrogen	25-4801-82

Neutrophils, B cells and T cells

Antibody	Clone	Fluorophore	Dilution	Company	Cat. N
CD45	30-F11	FITC	1:100	BioLegend	103108
CD11b	M1/70	PE	1:160	BioLegend	101208
Ly6G	1A8	PE/Dazzle 594	1:80	BioLegend	127648
CD19	1D3	PECy5	1:80	Invitrogen	15-0193-82
CD3	17A2	PECy7	1:100	BioLegend	100220

CD45- fraction

Antibody	Clone	Fluorophore	Dilution	Company	Cat. N
CD45	30-F11	FITC	1:100	BioLegend	103108
CD105	MJ7/18	PE	1:100	eBioscience	12-1051-82
EpCAM	G8.8	PE/Dazzle 594	1:100	BioLegend	118236
CD140a	APA5	PECy7	1:100	eBioscience	25-1401-82

Human

PBMCs, blood monocytes and Mo-Mac

Antibody/dye	Clone	Fluorophore	Dilution	Company	Cat. N
Zombie violet			1:1000	BioLegend	423114
CD206	15-2	FITC	1:25	BioLegend	321104
CD169	7-239	PE	1:25	BioLegend	346004
CD45	HI30	PerCP	1:25	BioLegend	304026
CD14	63D3	Brilliant Violet 711	1:25	BioLegend	367140
CD68	Y1/82A	PECy7	1:25	BioLegend	333816

PCLS CD45+ fraction

Antibody/dye	Clone	Fluorophore	Dilution	Company	Cat. N
Zombie Violet			1:1000	BioLegend	423114
CD45	HI30	FITC	1:20	proteintech	FITC-65109
CD206	15-2	PECy5	1:20	Sony Biotechnology	2205540

PCLS CD45- fraction

Antibody/dye	Clone	Fluorophore	Dilution	Company	Cat. N
Zombie Violet			1:1000	BioLegend	423114
CD45	HI30	FITC	1:20	proteintech	FITC-65109
CD144	BV9	PE/Dazzle™ 594	1:20	BioLegend	348520
CD90	5E10	PECy5	1:20	Sony Biotechnology	2240560
EpCAM	9C4	Brilliant Violet 711	1:20	Sony Biotechnology	2221200
CD31	WM59	PECy7	1:20	Sony Biotechnology	2115590

Buffers and media

FACS buffer

- EDTA 2 mM
 - BSA 0.5 % w/V
- in DPBS

Permeabilizing FACS buffer

- Tween 20 0.5% V/V
 - BSA 0.5 % w/V
 - EDTA 2 mM
- in DPBS

Macrophage medium

- Heat-inactivated FBS 10 % V/V
- Penicillin/Streptomycin 1% V/V
in RPMI

M-CSF medium

M-CSF 50 ng/mL in Macrophage medium

GM-CSF medium

GM-CSF 20 ng/mL in Macrophage medium

Cryopreservation medium

- Heat-inactivated FBS 10 % V/V
- DMSO 10 % V/V
in RPMI

PCLS medium

- Penicillin/Streptomycin 1% V/V
- ITS-X 1X
- Amphotericin B 0.25 ug/mL
In DMEM/F-12

Fibrosis cocktail (FC)

- TGF- β 5 ng/mL
- TNF- α 10 ng/mL
- PDGF-AB 10 ng/mL
- LPA 5 μ M
In PCLS medium

Control cocktail (CC)

- Trehalose 0.25 mg/mL
- BSA 20 μ g/mL
In PCLS medium

Experimental procedures

Mice

8-12 weeks old C57BL/6N mice from in-house breeding were used. All procedures were approved by the Government of Upper Bavaria (ROB-55.2-2532.Vet_02-19-82).

Human samples

Lung tissue samples from healthy subjects and IPF patients used for microRNA-Seq were kindly provided by Dr. Claudia Staab-Weijnitz, Comprehensive Pneumology Center, Helmholtz Center Munich.

Lung tissue from patients undergoing lung cancer resection used for PCLS preparation were obtained from the Klinikum Rechts der Isar hospital under the approval of the Ethics Committee from the Technical University of Munich (59/21 S).

Bleomycin-induced pulmonary fibrosis

Mice were anesthetized with MMF (0.5 mg/kg Medetomidine, 5 mg/kg Midazolam, 0.05 mg/kg Fentanyl and 200 mg/kg Metamizol) and 2 U/kg weight of bleomycin solution in DPBS were instilled intratracheally using a microsyringe (Penn-Century). For the control group, 50 μ L of DPBS were used. After the instillation, anesthesia was antagonized by subcutaneous injection of 2.5 mg/kg Atipamezol, 0.5 mg/kg Flumazenil and 0.4 mg/kg Naloxon. Afterwards, mice were kept in O₂-enriched (30% V/V) cages for 7 days.

Buprenorphine 0.05 mg/kg and Diazepam 1.5 mg/kg were administered as analgesics every 6-8 h in case of need.

Lung function

Mice were injected intraperitoneally with 200 μ L heparin in 0.9 % w/V NaCl and anesthetized with MMF. Lung function measurements were made using the flexiVent system (SCIREQ, Montreal, Canada) and analyzed with the flexiWare 8.1 software. Mice were mechanically ventilated at a rate of 150 breaths/min and a tidal volume of 15 mL/kg. Inspiratory capacity (IC) was obtained from the Deep Inflation perturbation; airway resistance (Rn), tissue damping (G) and tissue elastance (H) values were obtained after the Prime-8 perturbation. A pressure-volume curve was constructed with the PVi-P perturbation and the value of quasi-static compliance (Cst) was obtained. Data were analyzed using

Student's unpaired t-tests and outliers were identified with the ROUT method (Q=1%), There were single outliers in the values for Cst, G and H.

Lung digestion and BAL

Mice were injected intraperitoneally with 100 μ L heparin to prevent blood coagulation and then killed with isoflurane. For the bronchoalveolar lavage, the mouse trachea was exposed and a small incision was made to cannulate the trachea with a blunt 20G needle, which was kept in place with suture and forceps. Using a 1 mL syringe, 1 mL of ice-cold 2 mM EDTA in DPBS was instilled into the lungs via the needle. After a few seconds, the solution was aspirated and the recovered lavage fluid was collected in a 15 mL tube on ice. The lavage procedure was repeated for a total of 7 instillations. After the lavage, the thoracic cavity was exposed and the lungs were perfused with DPBS through the right ventricle using a 20G needle until the DPBS came out clear. The lungs were removed, placed on a small beaker with 3 mL mouse digestion buffer (1 mg/mL Collagenase Type II, 0.3 mg/mL DNase I, 50 U/mL Dispase, 0.3 mM CaCl₂ in DMEM) and cut into small pieces with scissors. The digestion mixture was transferred to a 5 mL tube and the lung was digested for 30 min in an incubator at 37°C with rocking.

Single-cell suspension for flow cytometry

Mouse BALF cells

The BALF was centrifuged and erythrocyte lysis was performed by resuspending the cells in 300 μ L lysis buffer (139.5 mM NH₄Cl, 0.01 M Tris-HCl) and incubating for 2-3 min at RT. Lysis was stopped by adding 1 mL DPBS, and cells were centrifuged. To prevent unspecific antibody binding, cells were resuspended in Fc Block 1:50 and incubated at 4°C for 10 min. Cells were filtered through a 40 μ m filter and the filter was washed with 1 mL DPBS. All centrifugation steps were done at 4°C, 400 g for 7 min.

Mouse lung cells

The enzymatic digestion was stopped with the addition of 500 μ L FBS. The digestion mix was mixed up and down with a 1 mL syringe at least 20 times to finish the disaggregation of the tissue. The cell suspension was filtered through a 100 μ m filter to a 15 mL tube and the filter was washed with 4 mL DPBS. Cells were centrifuged and erythrocyte lysis was performed by resuspending the cells in 1 mL erythrocyte lysis buffer (139.5 mM NH₄Cl, 0.01 M Tris-HCl) and incubating for 2-10 min at RT. Erythrocyte lysis was stopped by adding 4

mL DPBS. Cells were centrifuged, resuspended in 3 mL DPBS, filtered through a 40 μ m filter to a new 15 mL tube and the filter was washed with 2 mL DPBS. Cells were centrifuged and unspecific antibody binding was prevented by resuspending the cells in 1 mL Fc block 1:50 and incubating for 10 min at 4 °C. All centrifugation steps were done at 4°C, 400 g for 7 min.

Magnetic separation of lung tissue CD45+/CD45- fractions

Cells were centrifuged, resuspended in 90 μ L MACS buffer + 10 μ L of CD45 microbeads. They were then incubated for 15 min at 4 °C and washed by adding 1-2 mL MACS buffer. Cells were centrifuged and resuspended in MACS buffer (10E8 cells/500 μ L). Magnetic separation was performed using the autoMACS separator with the program *possel*. All centrifugation steps were done at 4°C, 400 g for 7 min.

Cells staining for FACS sorting

Cells were resuspended in Zombie dye 1:1000 in DPBS (1-10E6 cells/100 μ L) and incubated at RT for 15 min. Cells were washed with 2 mL FACS buffer and centrifuged, followed by resuspension in the antibody mix solution (1E6 cells/100 μ L) and incubation at 4 °C for 30 min, protected from light. After the antibody staining, cells were centrifuged, washed twice with 1 mL DPBS and resuspended in FACS buffer. Before sorting the cells, 15 mL tubes were coated with FBS by filling the tube with FBS and incubating for 30 min at 4 °C. Cells were analyzed and sorted with either SONY SH800 or BD-Aria Fusion. Cells were sorted in 15 mL FBS-coated tubes with 3-4 mL FBS as bed volume. After sorting, cells were centrifuged, resuspended in 700 μ L TRIzol and stored at -80 °C until RNA isolation. All centrifugation steps were done at 4°C, 400 g for 7 min.

Histology

Mice were injected intraperitoneally with 100 μ L heparin to prevent blood coagulation and then killed with isoflurane. The thoracic cavity was exposed and the lungs were perfused with DPBS through the right ventricle using a 20G needle until the liquid came out clear. The lungs were removed, placed in a 15 mL tube containing 10 mL of 4% V/V PFA and incubated ON at RT with rocking. Afterwards, lungs were paraffin-embedded, sectioned and stained with the Sirius Red & Fast Green Staining (0.01% w/V Sirius Red, 0.1% Fast Green).

RNA isolation

RNA isolation was performed using TRIzol following the manufacturer's protocol with the exception that the isopropanol precipitation was done ON instead of for 10 min for higher yield. RNA concentration and quality were measured with the 4200 TapeStation System (Agilent).

Lysis of cells for microRNA sequencing

Cells were centrifuged and the pellet resuspended in 5 μ L containing 1X NEBNext Cell Lysis Buffer and 2000 U/mL RNase inhibitor.

RT-qPCR

Reverse transcription was done using the miRCURY LNA RT Kit and qPCR with the miRCURY LNA SYBR Green PCR Kit following the manufacturer's protocols on a StepOnePlus or a QuantStudio5 Real-Time PCR Systems (Applied Biosystems). SNORD44 and SNORD68 were used as endogenous controls for human and mouse, respectively.

mRNA library preparation

mRNA libraries were prepared either from cell lysates or isolated RNA with NEBNext® Single Cell/Low Input RNA Library Prep Kit for Illumina® following the manufacturer's protocol. Indexing of samples was made using the primers from the NEBNext® Multiplex Oligos for Illumina kit, following the manufacturer's protocol.

smallRNA library preparation

smallRNA libraries were prepared either from cell lysates or isolated RNA using the NEBNext® Small RNA Library Prep Set for Illumina® or the TrueQuant SmallRNA Seq Kit following the manufacturer's protocol.

Blood monocytes isolation and differentiation to macrophages

Isolation of PBMCs from blood

Blood was diluted 1:2 with $\text{Ca}^{2+}/\text{Mg}^{2+}$ -free DPBS and mixed by inverting several times. Ficoll-Paque media was layered onto the blood in a sterile 50 mL tube in a ratio 4:3 diluted blood:Ficoll. Centrifugation was performed at 400 g for 30 min at 18 °C in a swing-out rotor centrifuge with the brake off. The upper layer containing plasma and platelets was drawn off,

leaving the mononuclear cell layer undisturbed at the interface. The mononuclear cells layer was promptly transferred to a 50 mL tube. Cells were washed by adding at least 3 volumes of DPBS and pipetting up and down. Cells were centrifuged at 500 g for 10 min at 18 °C, the supernatant was discarded and the washing with DPBS was repeated. For the following steps, the centrifuge was cooled down to 4 °C and the break was turned on.

Purification of monocytes from PBMCs

Cells were resuspended in 10 mL FACS buffer prepared with biotin-free BSA, filtered through a 30 µm filter and the filter was washed with biotin-free FACS buffer. 2E5 cells were separated for flow cytometry analysis. The rest of the cells were centrifuged at 300 g at 4 °C for 10 min and resuspended in biotin-free FACS buffer (1E7 cells/ 30 µL FACS buffer).

‘Fully automated cell labeling and separation using the Pan Monocyte Isolation Kit and the autoMACS® Pro Separator in *Deplete* program’ was performed following the manufacturer’s protocol. From the negative fraction containing the monocytes, 2E5 cells were separated for flow cytometry analysis, 1E5 cells were separated for RNA isolation and the rest of the cells were cryopreserved.

Cryopreservation of monocytes

Cells were centrifuged at 300 g at 4 °C for 10 min, resuspended in freshly-prepared cryopreservation medium (3-5.10⁶ cells/mL cryopreservation medium) and transferred to a 1.8 mL cryovial. The cryovial was placed in a frosty box at -80 °C for 24 h and then transferred to a regular box.

Differentiation of monocytes to macrophages

Cryopreserved monocytes were thawed by briefly incubating the vials in a water bath at 37°C. The vial was promptly removed from the water bath before complete thawing and wiped with ethanol 80 % V/V. The cells were transferred from the vial to a tube containing warm macrophage medium and the vials were flushed with warm macrophage medium to ensure complete transfer of cells. Cells were centrifuged at 300 g at 4 °C for 10 min, resuspended in M- or GM-CSF medium, plated into the tissue culture plates and incubated under cell culture conditions for 6 days, after which the monocytes differentiated into macrophages. Cells were regularly tested for mycoplasma contamination and the results were always negative. Monocytes and macrophages morphology were assessed by light microscopy with the Evos FL Auto 2.

Harvesting macrophages

Cells were washed twice with ice-cold DPBS, Accutase (1.3 mL for 6-well plates) was added and the cells were returned to the cell culture incubator for 20-30 min until cells detached. Plates were gently agitated and cells were flushed with medium to finish detaching cells.

Staining of PBMCs, monocytes and Mo-Mac for flow cytometry

Cells were centrifuged, resuspended in Zombie dye 1:1000 in DPBS (1-10E6 cells / 40 μ L) and incubated at RT for 10 min, protected from light. Unspecific antibody binding was prevented by adding 10 μ L FcR blocking reagent every 1E7 cells, followed by incubation for 10 min at 4 °C. 50 μ L of the cell surface antibody cocktail was added and cells were incubated for 20 min at 4 °C. Cells were washed by adding 1 mL FACS buffer and centrifuging. Then, they were fixed by resuspension in 500 μ L FluoroFix Buffer and incubated ON at 4 °C. Cells were centrifuged and permeabilized by resuspension in 100 μ L Tween 20 0.5 %V/V and incubation at RT for 15 min. Cells were washed by adding 1 mL permeabilizing FACS buffer and centrifugation. Cells were resuspended in 96 μ L permeabilizing FACS buffer and 4 μ L of CD68, and incubated at RT for 20 min, followed by filtration through a 40 μ M filter and washing of the filter with permeabilizing FACS buffer. Cells were centrifuged, washed with permeabilizing FACS buffer and resuspended in permeabilizing FACS buffer for flow cytometry analysis. All centrifugation steps were done at 300 g at 4 °C for 10 min.

Stimulation of Mo-Mac with TGF- β and antimiR-21 transfection

Monocytes isolated from three different donors were seeded in a 48-well plate at a density of 1.2E5 monocytes/well and differentiated to macrophages as described above. On day 6, macrophages were treated with 0, 5, 20 or 50 ng/mL TGF- β for 48 h. On day 8, macrophages were transfected with 50 nM antimiR-21/scr using the Lipofectamine RNAiMAX protocol. 48 h later, cells were lysed directly in the plates with 300 μ L TRIzol, transferred to 1.5 mL tubes, 100 μ L more of TRIzol were added and the lysate was stored at -80 °C until RNA isolation.

Cells counting

10 μ L of cells were mixed with 10 μ L of Trypan Blue and automatic cell counting was done using an Invitrogen Countess Automated Cell Counter (Thermo Fisher).

Flow cytometry analysis

Single-color compensations were done using UltraComp eBeads™ Plus Compensation Beads for the antibodies, and ArC™ Amine Reactive Compensation Bead Kit for the Zombie Violet dye. Flow cytometry analysis and sorting was done using the cell sorter SONY SH800 or BD-Aria Fusion. Flow cytometry data was analyzed with the software FlowJo 10.8.1.

PCLS preparation

In the surgery room, immediately after the lung piece was available, lung pieces were cleaned in cold PCLS medium to remove clotted blood and subsequently inflated with a syringe through visible bronchioles with warm low-melting point agarose (3 % w/V in PCLS medium). The lung blocks were transported to the laboratory in cold PCLS medium to the laboratory and placed on ice to allow the agarose to solidify. The lung block was then cut into smaller pieces with a scalpel and sliced into 400 µm thick slices with the Leica Vibratome VT1200 under sterile conditions. 10 mm punches were made with a puncher and kept in cell culture. PCLS viability was regularly assessed with the MTT assay. For this, culture medium was removed and replaced with 500 µL of 0.48 mg/mL MTT in PCLS medium and incubated under culture conditions for 30 min-1 h until the formation of blue color.

PCLS fibrosis model

PCLS were cultured in 24-well tissue culture plates in 1 mL PCLS medium at 37 °C in 5% CO₂. For the fibrosis model, PCLS were treated with the fibrosis cocktail (FC) or control cocktail (CC) on days 0 and 2.

PCLS digestion, magnetic separation and staining for FACS

PCLS were washed with DPBS and weighted. 4 mL of human digestion buffer (Collagenase Type IV 575 U/mL, DNase I 0.3 mg/mL, Dispase II 2 U/mL, Elastase 1.5 U/mL, CaCl₂ 5 mM in HBSS) were added every 1 g of PCLS, and PCLS were cut into smaller pieces with a scalpel. PCLS were incubated in the digestion solution at 37 °C for 1 h with rocking, pipetting up and down every 20 min. The cell suspension was filtered through a 100 µm filter and the filter was washed with Stop Digestion Buffer (EDTA 50 mM, FBS 10 % V/V in DPBS). Cells were centrifuged and erythrocyte lysis was performed by resuspending the cells in 1 mL Red Blood Lysis Buffer and incubating for 5-10 min at RT. The lysis was stopped by adding 10 mL of DPBS, cells were filtered through 40 µm, the filter was washed with DPBS

and cells were centrifuged. Cells were resuspended in 40 μ L FACS buffer+10 μ L of FcR Blocking Reagent and they were incubated for 10 min at 4 °C. 30 μ L of FACS buffer+10 μ L of CD45 microbeads were added, and cells were incubated for 15 min at 4 °C. Then, cells were washed by addition of 1 mL FACS buffer and centrifugation. Next, they were resuspended in 500 μ L FACS buffer and magnetic separation was performed using the autoMACS separator in *possel* mode. Cells were washed by addition of 1 mL DPBS and centrifugation, after which they were resuspended in 50 μ L Zombie Violet dye 1:1000 in DPBS and incubated for 10 min at RT, protected from light. 50 μ L of antibody cocktail were added, followed by incubation for 30 min at 4 °C. Cells were washed twice with 1 mL FACS buffer and resuspended in FACS buffer for cell sorting using the SONY SH800. All centrifugation steps were done at 300 g at 4 °C for 10 min.

Transfection of PCLS

15 μ L 1X Metafectene® SI+ Buffer were mixed with 0.8 μ L of Metafectene® SI+ Transfection Reagent and 30 pmol of antimiR-21/antimiR-scr, and incubated at RT for 15 min. Afterwards, this lipoplex was added to the PCLS cultured in 500 μ L of PCLS medium, and PCLS were incubated at 37°C/5% CO₂ for 48 h.

RNA-Seq Analysis

Transcriptome

Sequencing was performed on an Illumina NextSeq 2000, generating 2x110 bp reads with an average of 41 million reads per sample. Adaptor trimming was performed with Flexbar 3.5.0. Within the Galaxy platform (www.usegalaxy.eu), quality trimming was done using fastp 0.20.1, quality was checked using FastQC 0.73, reads were aligned with RNA STAR 2.7.8a using the built-in human reference genome hg38 and the gene annotation GRCh38.p13, and genes were quantified with StringTie 2.1.7.

Public RNA-Seq datasets were downloaded from the Gene Expression Omnibus (GEO) database with accession numbers GSE99621, GSE134692, GSE79544, GSE122960, GSE94135, GSE94699.

miRnome

Sequencing was performed on either an Illumina NextSeq or MiSeq, generating 50-75 bp single-end reads. Within the Galaxy platform, adaptor and quality trimming were done using Cutadapt 3.4 in the case of the libraries prepared with the GenXPro kit, and with Trim

Galore! 0.4.3.1 in the case of the libraries prepared with the NEB kit. GenXPro libraries were subjected in addition to UMIs trimming using fastp 0.20.1. Quality of the reads was checked using FastQC 0.73. Reads were mapped with MiRDeep2 Mapper using the built-in reference genome hg38 canonical for human samples or mm10 for mouse samples, and quantified with MiRDeep2 Quantifier using the hairpin and mature sequences from miRbase version 22.1.

miRnome and transcriptome

Downstream analysis was performed using R software. Differential expression analysis was performed using the DESeq2 package 1.32.0 and plots were generated using ggplot2 3.3.5, ggrepel 0.9.1 and pheatmap 1.0.12.

For the analysis of CC- vs FC-treated-PCLS, RUVg was performed with the RUVSeq package 1.26.0 to minimize the effect of inter-patient differences.

Gene ontology analysis for the PCLS transcriptome was performed using Enrichr (<https://maayanlab.cloud/Enrichr/>) and plots were generated in R software with the package GOplot 1.0.2 and enrichplot 1.12.3. Gene set enrichment analysis was performed using the R packages clusterProfiler 4.0.5, AnnotationDbi 1.54.1, org.Hs.eg.db 3.13.0 and DOSE 3.18.3. Gene ontology analysis for the public RNA-Seq datasets from mouse and human was performed with the R packages clusterProfiler 4.0.5, AnnotationDbi 1.54.1, org.Hs.eg.db 3.13.0 and org.Mm.eg.db 3.13.0.

MiR-21 predicted targets were obtained from TargetScan 8.0.

RESULTS

Chapter 1: miRnome and miR-21 targetome in bleomycin-induced pulmonary fibrosis

Extensive evidence has demonstrated microRNA dysregulation in pulmonary fibrosis; nevertheless, studies till date have mostly made use of targeted techniques such as RT-qPCR and microarrays. Since the aim of this work was to study the whole miRnome changes in pulmonary fibrosis in an unbiased way, here microRNA sequencing was applied for the first time in lung cells from a mouse model of bleomycin-induced lung fibrosis.

In order to establish this model, 2 U/kg body weight bleomycin (or PBS as control) were administered to mice as an aerosol with the use of a microsyringe. 1 week later the lung function was assessed with the use of the flexiVent system, the BALF was collected for FACS analysis, and the lungs were removed for histology staining, microRNA sequencing and FACS analysis (**Figure 7 A**).

At this early stage of the disease, survival was minimally decreased in the bleomycin group (from a 100% to 92%) (**Figure 7 B**) and there was no change in fibrosis at the histological level when assessed by Sirius Red & Fast Green staining (**Figure 7 C**). However, changes in lung function were already observed (**Figure 7 D**). Tissue damping, which is related to the tissue resistance and the resistance to air flow in the peripheral airways, was significantly increased. In addition, a downward shift of the pressure-volume curve was observed as well as a decrease in the maximum volume at the highest pressure, indicating decreased elastic properties of the respiratory system.

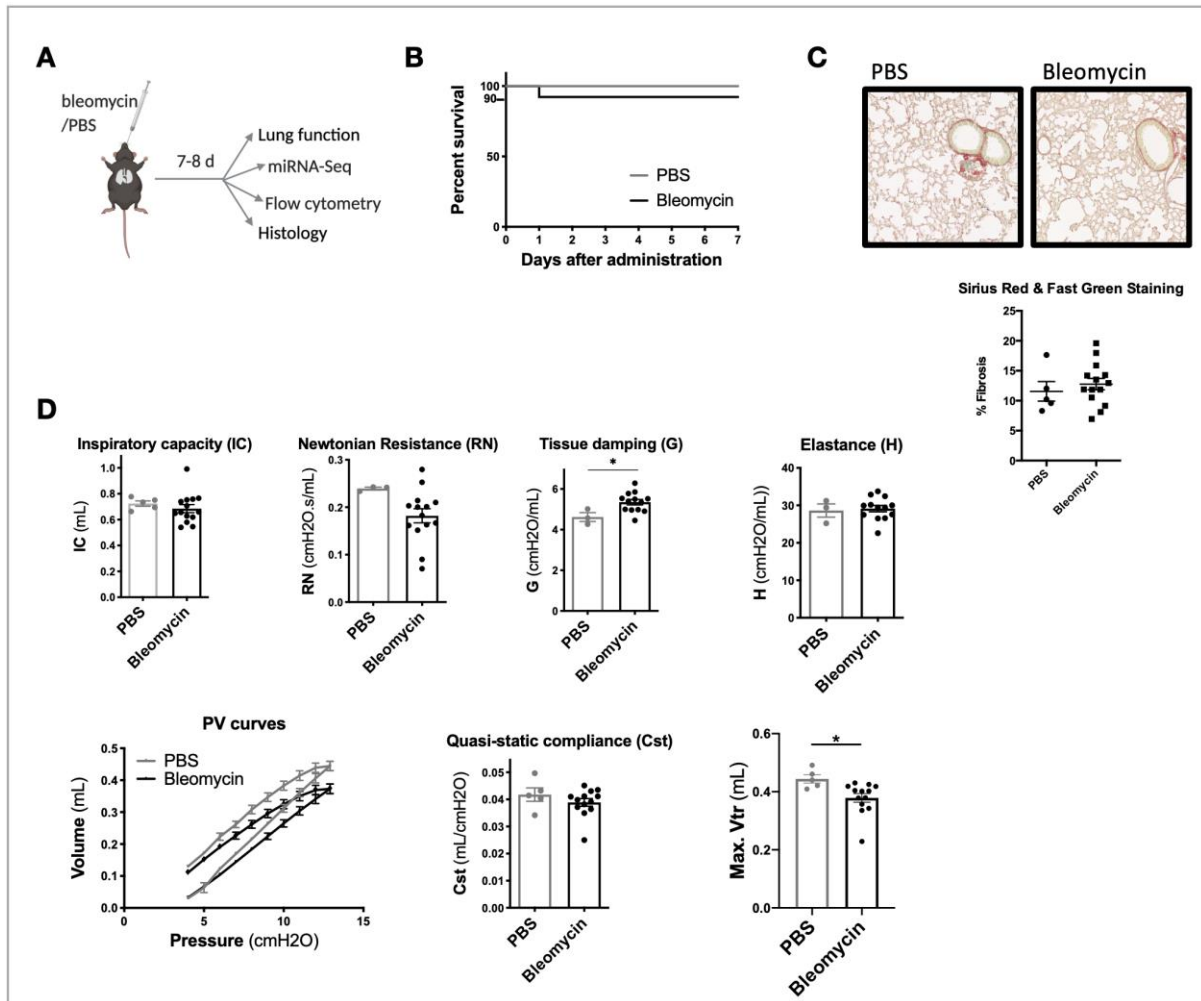


Figure 7 Survival, fibrosis and lung function changes upon bleomycin-induced pulmonary fibrosis.

A. Experiment outline: bleomycin or PBS was administered to mice using a microsyringe and mice were sacrificed a week later. **B.** Survival curve from PBS-treated (n=5) and bleomycin-treated (n=26) mice. **C.** Sirius Red & Fast Green staining of representative lung sections and quantification of fibrosis in PBS-treated (n=5) and bleomycin-treated (n=14) mice. **D.** Lung function parameters assessed with the flexiVent system. IC (PBS n=5, Bleomycin n=14), RN (PBS n=3, Bleomycin n=14), G and H (PBS n=3, Bleomycin n=12), Cst and PV-curve (PBS n=5, Bleomycin n=13). Data are individual values and mean \pm SEM and the data were analyzed using Student's unpaired t-tests. *p<0.05. IC: inspiratory capacity, RN: Newtonian resistance, G: tissue damping, H: elastance, Cst: quasi-static compliance, PV: pressure-volume.

In the first week after bleomycin administration, the model is characterized by inflammatory infiltrates. Therefore, the composition of macrophages and eosinophils in the BALF and the CD45+ fraction of the lung tissue were analyzed after enzymatic digestion and magnetic separation with CD45 beads (**Figure 8**). In the BALF it was observed that, under basal and PBS conditions, the CD45+ cells were exclusively (95.9±1.3%) SiglecF^{hi} CD11b^{lo} resident alveolar macrophages, whereas in bleomycin conditions this population was reduced to 29.1±5.7%; a population of SiglecF^{lo} CD11b^{hi} recruited macrophages accounted for 17.7±2.1% and eosinophils 7.7±1.5%, in accordance with previous studies reporting the infiltration of monocyte-derived macrophages to the lungs upon lung injury. Similarly, in the lung tissue the percentage of SiglecF^{hi} CD11b^{lo} macrophages decreased (4.2 ±0.9 to 0.9 ± 0.2), while the percentage of SiglecF^{lo} CD11b^{hi} macrophages increased (8.4 ± 1.1 to 13.3±0.9); the percentage of eosinophils remained statistically unchanged (4.9±1.3 to 7.0±0.9).

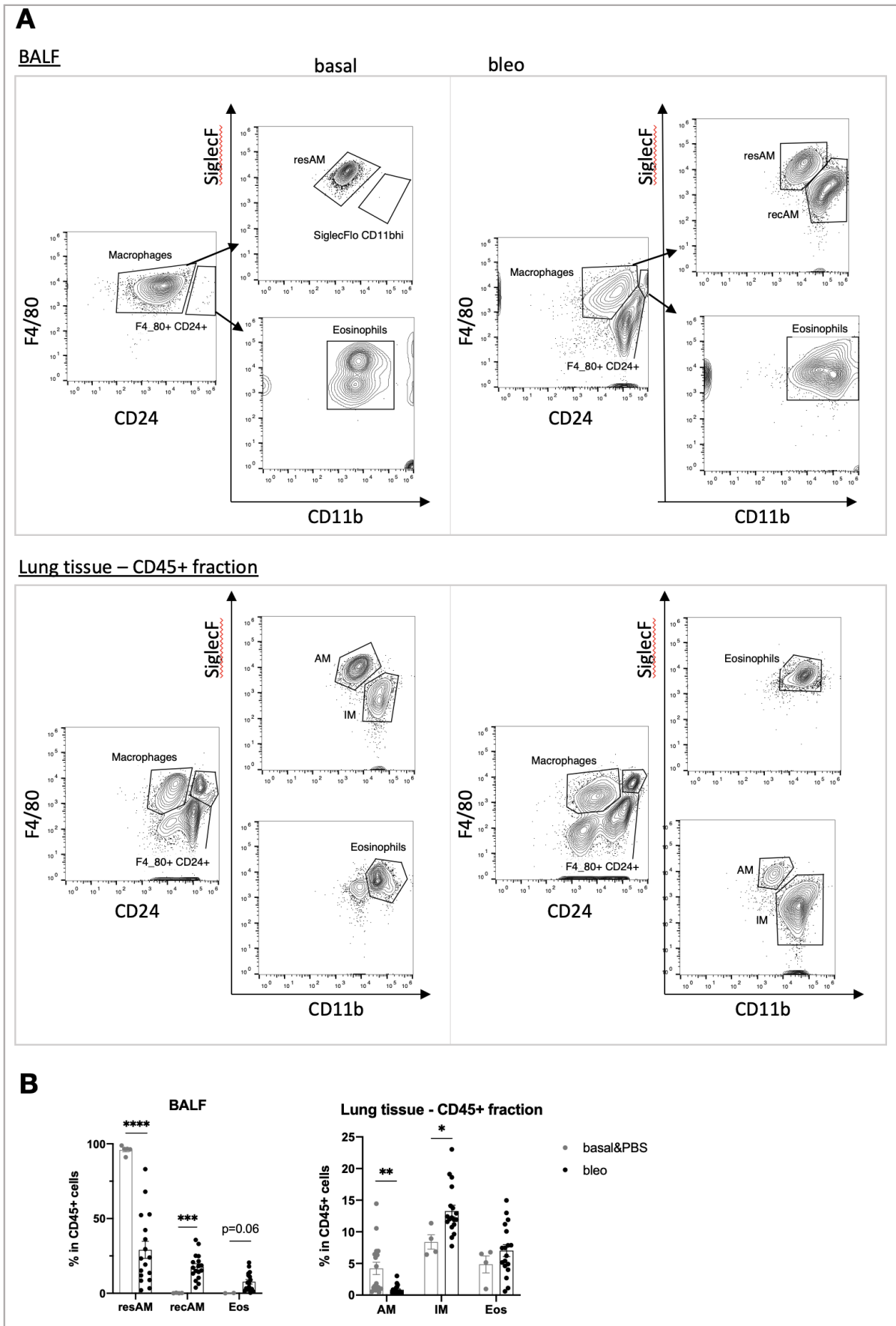


Figure 8 Immune cell changes upon bleomycin-induced lung fibrosis.

A. Flow cytometry analysis of macrophages and eosinophils in BALF cells and CD45+ lung tissue cells under basal conditions and bleomycin-induced lung fibrosis (bleo). **B.** Quantification of cells composition within the BALF and CD45+ lung tissue cells, both in the basal/PBS group and the bleomycin group. resAM (Basal&PBS n=5, bleo n=17), recAM (Basal&PBS n=4, bleo n=17), BALF Eos (Basal&PBS n=3, bleo n=17), AM (Basal&PBS n=17, bleo n=18), IM and tissue Eos (Basal&PBS n=4, bleo n=18). Data are individual values and mean \pm SEM, and were analyzed using Student's unpaired t-tests; *p<0.05, **p<0.01, ***p<0.001, ****p<0.0001. BALF: bronchoalveolar lavage fluid, resAM: resident alveolar macrophages, recAM: recruited alveolar macrophages, AM: alveolar macrophages, IM: interstitial macrophages, Eos: eosinophils, bleo: bleomycin.

In order to study the whole miRnome changes upon pulmonary fibrosis, microRNA sequencing was performed on cells isolated from lung tissue from mice under basal conditions and from mice exposed to bleomycin (**Figure 9 A**). After filtering out miRs with low expression (mean expression ≤ 10), 96 differentially expressed microRNAs (p-adj <0.05, $|\log_2FC| \geq 1$) were found, from which 49 were upregulated and 47 downregulated (**Figure 9 B**).

Among the upregulated microRNAs, miR-21a-5p was the highest expressed miR. In terms of abundance, from representing 4% of total miR reads and being the top 5 abundant miR in the basal lung, its expression increased to 14% in bleomycin-treated lungs and represented the top 2 abundant miR (**Figure 9 C and D**).

Interestingly, out of more than 300 detected microRNAs, only 3 of them contribute to more than 50% of total reads in both healthy and fibrosis lungs.

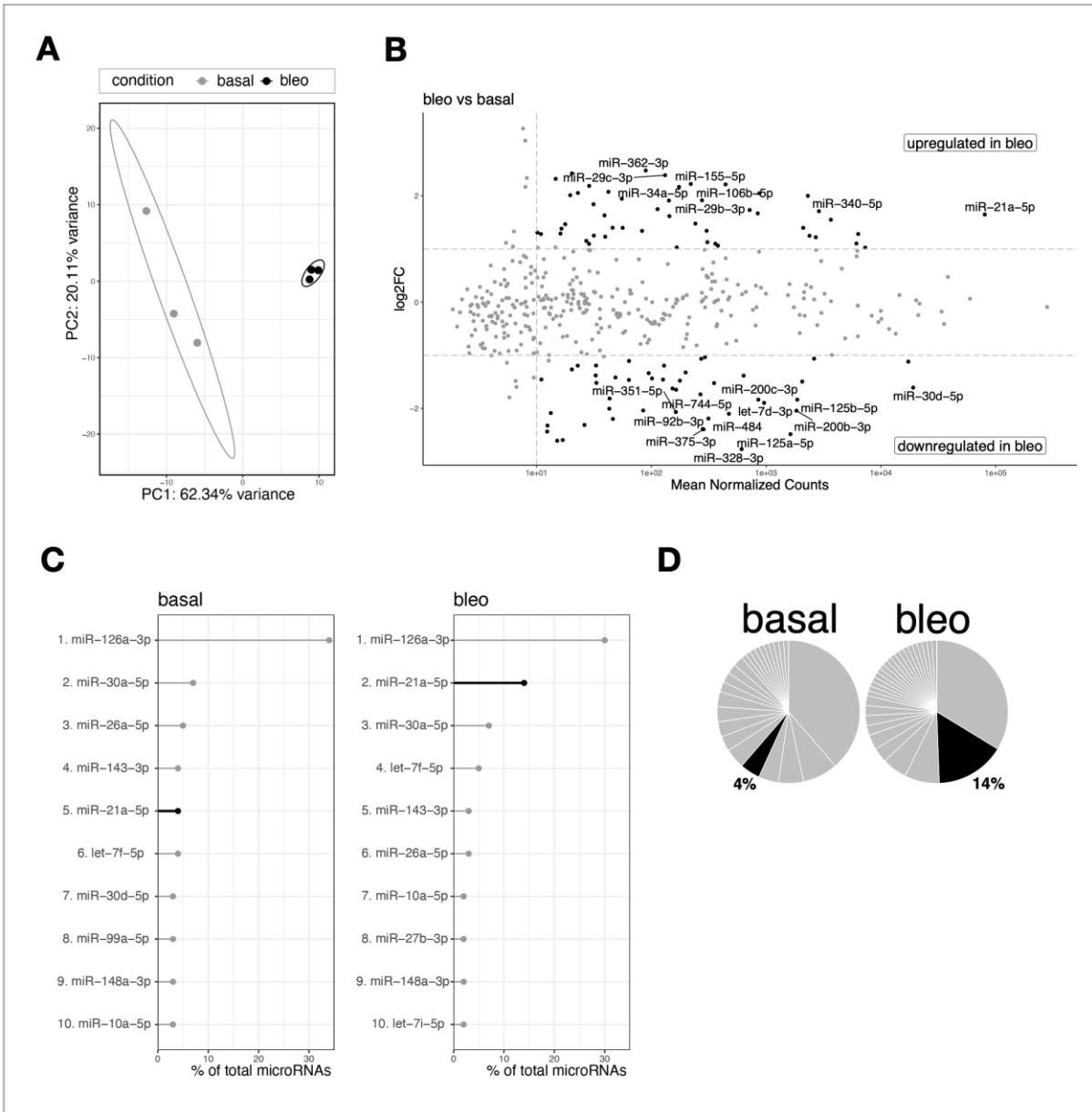


Figure 9 miRnome changes in bleomycin-induced lung fibrosis.

A. Principal component analysis of lungs in basal and lung fibrosis (bleo) conditions; n=3 for each condition. **B.** MA plot where significantly deregulated microRNAs in bleomycin-induced lung fibrosis are highlighted in black. **C.** Top 10 abundant microRNAs and their abundance with respect to total miR reads; miR-21a-5p is highlighted in black. **D.** Pie charts of miRs abundance; miR-21a-5p is highlighted in black and its percentage among all microRNAs is shown.

To gain a more in-depth understanding of how miRNAs are differentially regulated in the immune and non-immune cells, miRNA sequencing was performed on the CD45+ and CD45- cell fractions under bleomycin conditions (**Figure 10 A**). Out of more than 400

detected miRNAs, there were 100 miRs enriched in the CD45+ fraction and 113 miRs enriched in the CD45- fraction. In particular, miR-21a-5p was enriched in the CD45+ fraction (**Figure 10 B**).

Focusing specifically on the microRNAs that were deregulated in bleomycin compared to basal conditions, it was surprisingly found that all of them were enriched either on the CD45+ or the CD45- cell fractions in the bleomycin group (**Figure 10 C**). Among the upregulated miRs in bleomycin vs basal, miR-10b, miR-199b and miR-29c were enriched in the CD45- fraction, while miR-21a, miR-362 and miR-34a were enriched in the CD45+ fraction. Looking at the downregulated microRNAs in bleomycin, miR-205, miR-125b and miR-31 were de-enriched in the CD45+ fraction, while miR-342 was de-enriched in the CD45- fraction. In general terms, most upregulated microRNAs in bleomycin were enriched in the CD45+ fraction and most downregulated microRNAs were also de-enriched in the CD45+ fraction, suggesting an important role of microRNAs in gene expression regulation in immune cells.

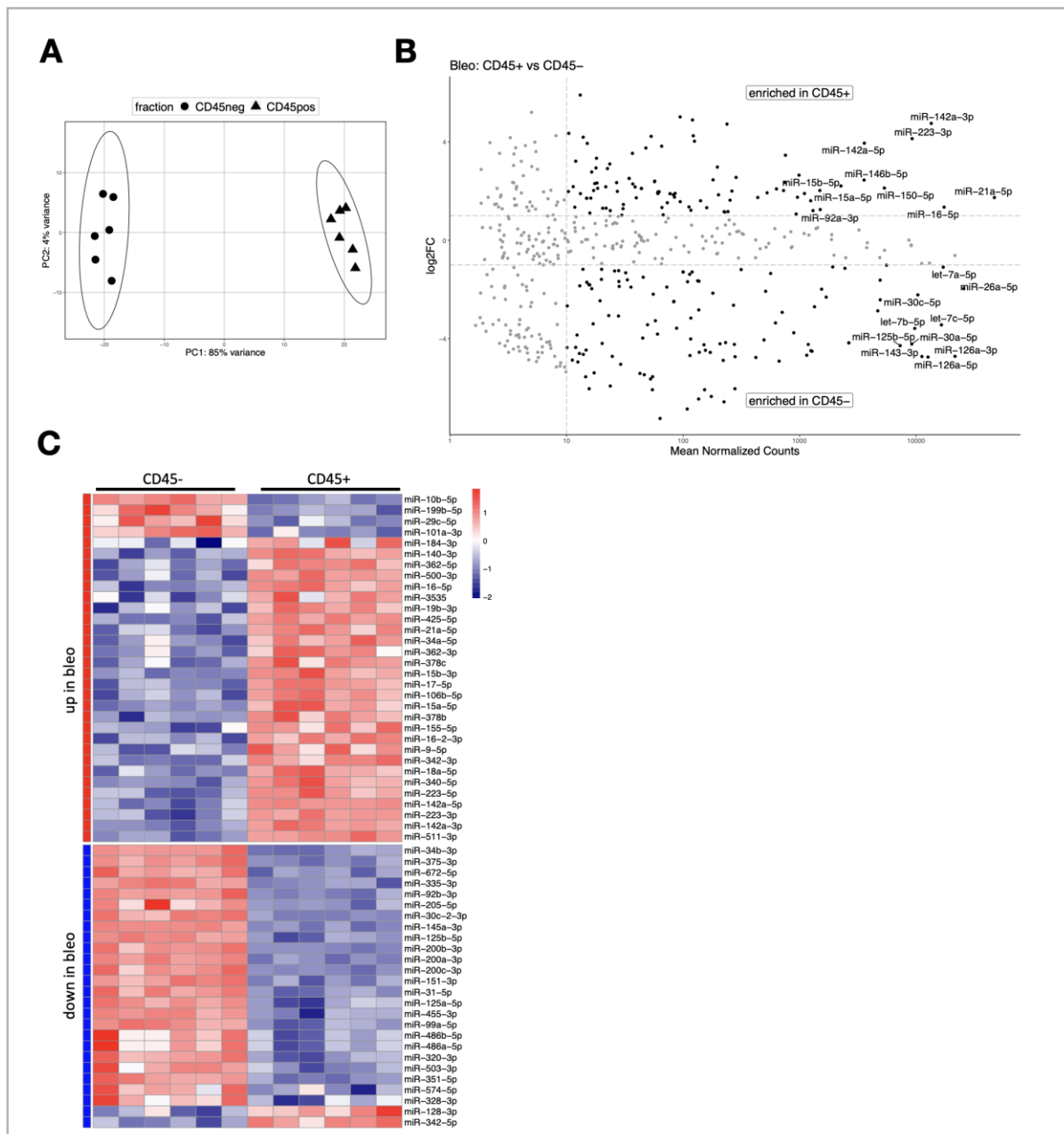


Figure 10 Enrichment of miRNAs in the CD45+ and CD45- fractions in the lungs of bleomycin-exposed mice.

A. Principal component analysis of CD45+ (CD45pos) and CD45- (CD45neg) cell fractions in bleomycin-induced lung fibrosis (bleo); n=6 for each cell fraction. **B.** MA plot showing the enriched microRNAs in CD45+ and CD45- fractions. **C.** Heatmap showing the enrichment in CD45+/- fractions of the deregulated miRs in bleomycin compared to basal conditions.

Since the highest upregulation of miR-21 was observed in the CD45+ fraction and infiltrating macrophages are known to have an important role in the development of lung fibrosis, the question was raised whether miR-21 targets repression in these cells could be detected. To

answer this question, a transcriptomic analysis was performed using a public RNA-Seq dataset (GSE94699, GSE94135) of SiglecF^{hi} and CD11b^{hi} macrophages under basal conditions and after bleomycin injury at the same timepoint of my miRnome analysis (**Figure 11 A**).

In a cumulative distribution of gene expression changes, a prominent leftwards shift of miR-21 predicted targets in CD11b^{hi} macrophages could be observed, while in SiglecF^{hi} macrophages, no shift was evident (**Figure 11 B**).

In order to study in which pathways the repressed miR-21 targets might be involved, gene ontology enrichment analysis was performed on the downregulated miR-21 targets in CD11b^{hi} macrophages and it could be seen that they are involved in important processes for lung fibrosis such as tissue remodeling, mesenchymal cell proliferation, lung epithelial cell differentiation and mononuclear cell differentiation (**Figure 11 C**).

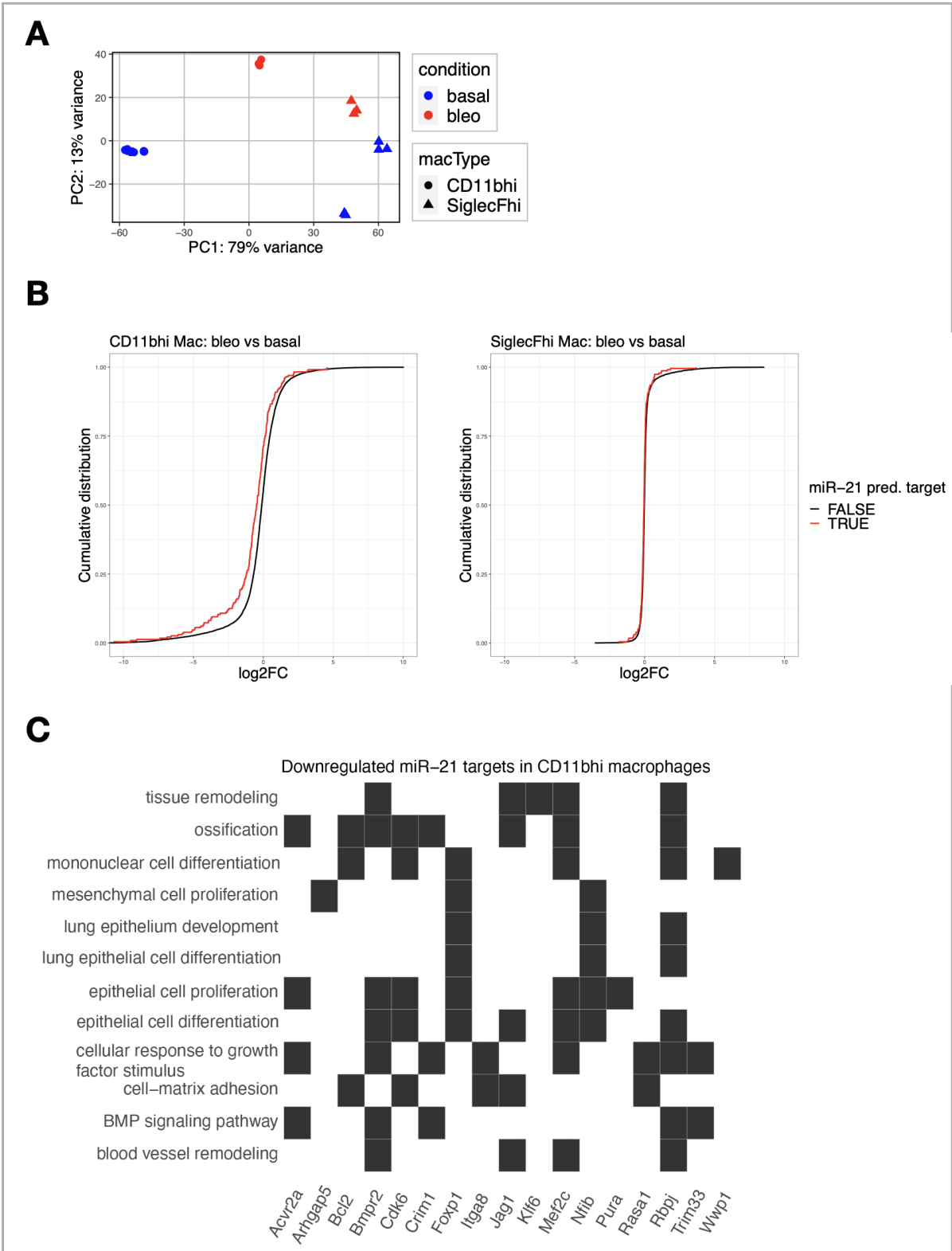


Figure 11 Analysis of the miR-21 targetome in murine macrophage subpopulations.

A. Principal component analysis of macrophage subpopulations (CD11bhi and SiglecFhi) under basal and bleomycin-induced lung fibrosis (bleo). **B.** Cumulative distribution in macrophage subpopulations; the black curve shows non-miR-21 predicted targets and the

red curve miR-21 predicted targets. **C.** Gene ontology analysis of miR-21 targets repressed in CD11b^{hi} SiglecF^{lo} macrophages. Mac: macrophages, pred.: predicted.

In summary, microRNAs changes that occur upon bleomycin injury of the lung were determined at the whole miRnome level and the dysregulated miRs were specifically associated with either the immune or non-immune cells. Interestingly, the majority of upregulated and downregulated miRNAs were enriched or de-enriched, respectively, in immune cells. The highest expressed upregulated miRNA miR-21, was enriched in the CD45⁺ cell fraction, its targetome was specifically repressed in the fibrosis-associated macrophage population CD11b^{hi} SiglecF^{lo} compared to CD11b^{lo} SiglecF^{hi} macrophages and the downregulation of these genes was associated to key processes in fibrotic remodeling. Taken together, these data suggest an important function of miR-21 in lung fibrosis, guided by macrophages.

Chapter 2: miRnome and miR-21 targetome in human IPF

Following the same idea as in the previous chapter of analyzing the overall miRnome changes in lung fibrosis, microRNA sequencing was performed on frozen lung tissue from human donors and IPF patients (**Figure 12 A and B**).

After filtering out miRs with low expression (mean expression ≤ 10), 31 differentially expressed microRNAs ($p\text{-adjusted} < 0.05$, $|\log_2\text{FoldChange}| \geq 1$) were found, of which 19 were upregulated and 12 downregulated (**Figure 12 C and D**).

Comparing the human miRnome to the deregulated miRNAs in murine bleomycin-induced pulmonary fibrosis, similarities and differences were observed. On the one hand, as in the mouse lung fibrosis model, miR-21-5p, miR-10b-5p and miR-199b-5p were upregulated, and miR-338-5p, miR-375-3p, miR-30d-5p and miR-200c-3p were downregulated. On the other hand, while miR-31-5p and miR-205-5p are upregulated in IPF, they are downregulated in mice; and while miR-223-3p and miR-30b-5p are downregulated in IPF, they are upregulated in mice.

In terms of abundance, as was seen for mouse lungs, out of more than 300 detected microRNAs, only a few (5-8) contribute to more than 50% of total microRNA reads (**Figure 12 E and F**). In detail, 7/10 of the top 10 abundant miRs in donor samples are also within the

top 10 in healthy mice, and 5/10 of the top 10 expressed miRs in IPF samples are also within the top 10 in mice with lung fibrosis.

In particular, miR-21-5p is significantly upregulated in IPF, its expression is doubled, and it is the upregulated miR with the highest abundance, as was also observed in bleomycin-induced fibrosis in mice. MiR-21-5p upregulation was further confirmed by RT-qPCR (**Figure 12 G**).

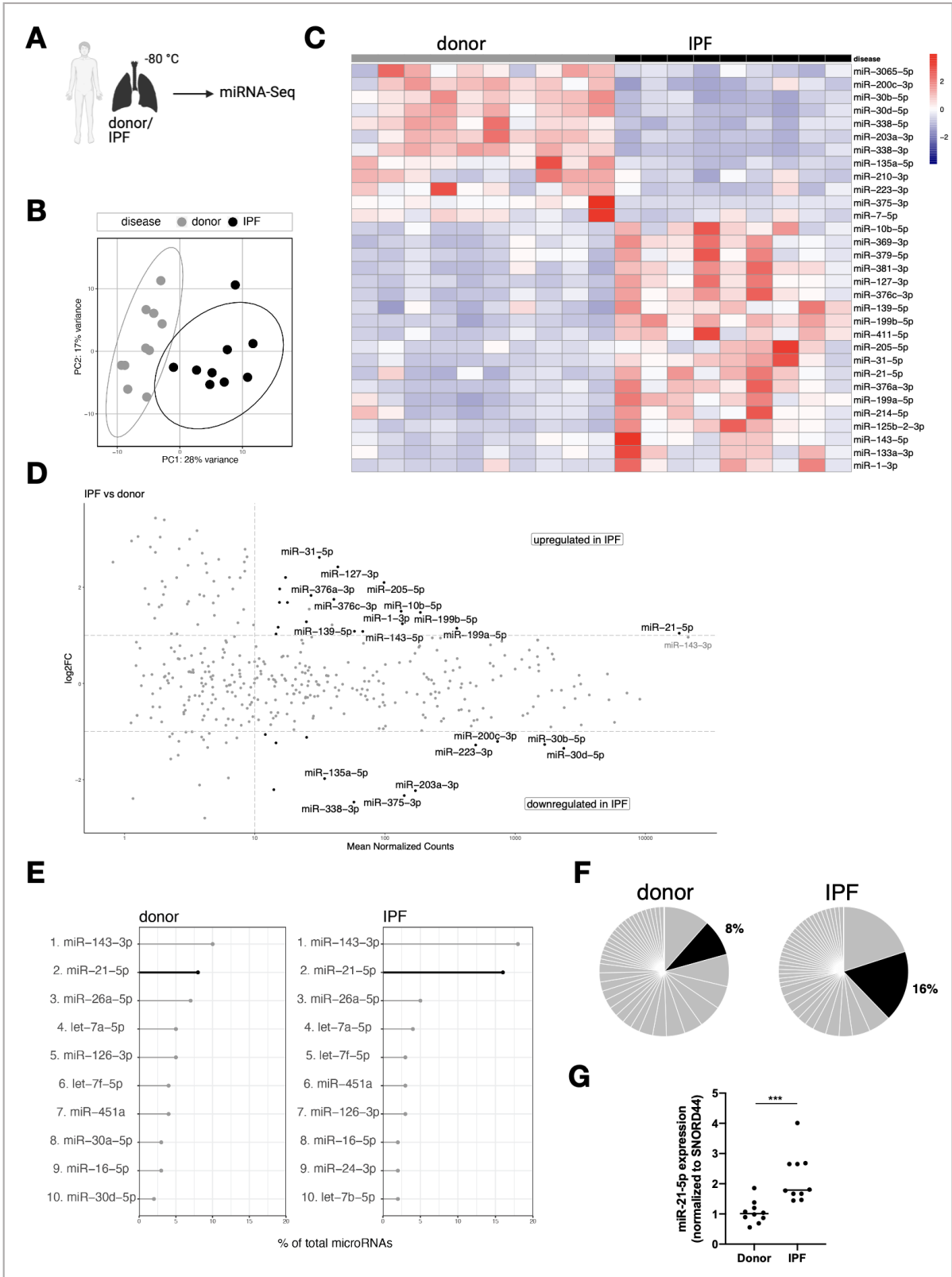


Figure 12 miRnome of human lungs from donors and patients with IPF.

A. Experiment outline: microRNA sequencing was performed on frozen lung tissue samples from IPF patients (n=9) and healthy donors (n=10). **B.** Principal Component Analysis showing the clustering of the samples according to the disease status. **C.** Heatmap of differentially

expressed miRs ($p\text{-adj}<0.05$, $|\log_2FC|\geq 1$). **D.** MA plot where significantly differentially expressed miRs are colored in black. **E.** Top10 abundant miRs in each condition and their percentages relative to all detected miRs; miR-21-5p is highlighted in black. **F.** Pie charts of miRs abundance in each condition; miR-21-5p is highlighted in black and its percentage is shown. **G.** RT-qPCR of miR-21-5p. Data are individual values and mean, and were analyzed by Student's unpaired t-test; *** $p<0.001$. IPF: idiopathic pulmonary fibrosis.

In order to study whether miR-21 upregulation was also evident at the level of its targetome, a public RNA-Seq dataset (GSE99621) of lung tissue from IPF patients and healthy donors ($n=8$) was analyzed. In this dataset, IPF samples were divided in normal-looking sections of the lung (IPFn, $n=10$) and scarred sections (IPFs, $n=8$). In a cumulative distribution plot of gene expression changes, the strongest miR-21 target deregulation was observed when comparing IPFs to healthy or IPFn, less prominent in IPF (IPFn and IPFs together) vs healthy and no repression in IPFn vs healthy, suggesting that the effects of miR-21 upregulation appear mainly at a later stage of the disease (**Figure 13 A**).

With the aim of identifying the relevant pathways related to miR-21 targets repression, gene ontology enrichment analysis was performed with the downregulated miR-21 predicted targets in each comparison. Significantly enriched terms ($p\text{-adjusted}<0.05$) were found when comparing IPFs vs healthy (**Figure 13 B**) and IPFs vs IPFn (**Figure 13 C**). In both analysis it was found that the repressed miR-21 predicted targets are involved in important processes for lung fibrosis such as regulation of fibroblast growth factor signaling pathway, mesenchymal cell differentiation and regulation of leukocyte mediated immunity.

Finally, to assess whether miR-21 target deregulation was also evident in BALF cells apart from lung tissue cells, a transcriptomic analysis was performed on the BALF from IPF patients ($n=16$) compared to healthy volunteers ($n=7$), using a public RNA-Seq dataset (GSE79544). In a cumulative distribution plot of gene expression changes (**Figure 13 D**), a leftward shift of miR-21 targets could be observed, but it was weaker than in the lung tissue and there were no significantly downregulated miR-21 targets. This finding suggests that miR-21 target deregulation is more prominent in the lung tissue cells than in the BALF cells.

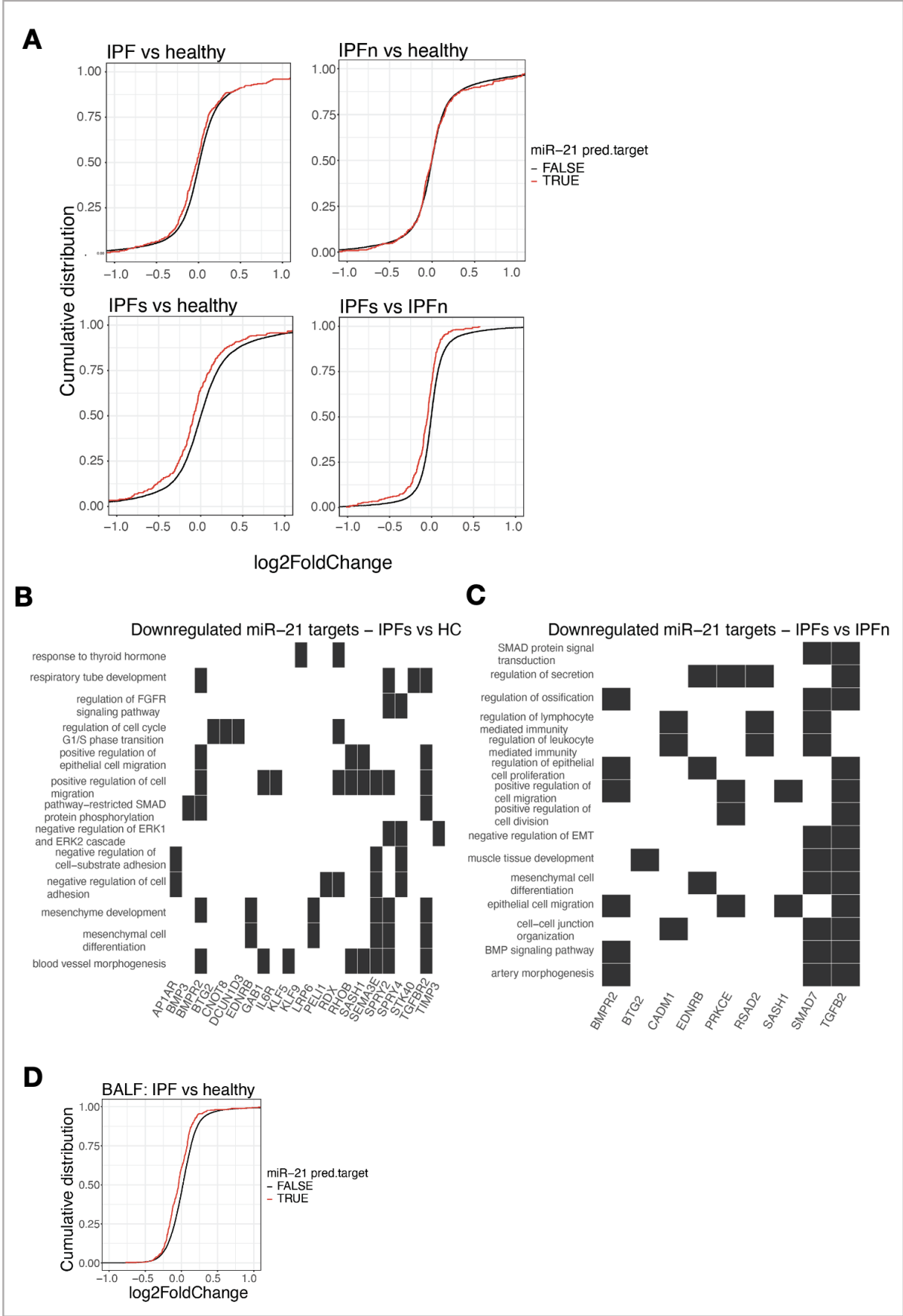


Figure 13 Analysis of the miR-21 targetome in lung tissue and BALF from IPF patients and healthy controls.

A. Cumulative distribution plots of gene expression changes comparing IPF, IPFn, IPFs and healthy lung tissue; miR-21 predicted targets are colored in red and non-miR-21 targets in black. **B.** Gene ontology enrichment analysis of downregulated miR-21 predicted targets in IPFs compared to healthy donors. **C.** Gene ontology enrichment analysis of downregulated miR-21 predicted targets in IPFs compared to IPFn. **D.** Cumulative distribution plot of gene expression changes in BALF from IPF compared to healthy volunteers; miR-21 predicted targets are colored in red and non-miR-21 predicted targets are colored in black. IPF: idiopathic pulmonary fibrosis; IPFn: normal-looking sections of IPF lungs; IPFs: scarred sections of IPF lungs, HC: healthy control, BALF: bronchoalveolar lavage fluid, pred.: predicted.

In summary, the dysregulation of miRNAs in IPF was identified at the whole miRnome level and compared to those occurring in the mouse model of bleomycin-induced lung fibrosis. As in mice, miR-21 was the upregulated miRNA with the highest expression. Furthermore, its targetome deregulation was stronger in scarred areas of the lung compared to normally-appearing or healthy areas or to the BALF and the associated pathways are key to the development of fibrosis, indicating that miR-21 has an important role in the progression of lung fibrosis.

Chapter 3: miRnome signature of mouse lung cells

With the aim of determining cell type-specific miRnome profiles, miRNA sequencing was performed on main murine lung cell types. Briefly, murine lungs were enzymatically digested, the resulting cell suspension was subjected to MACS separation based on CD45 expression and then each cell fraction (CD45+/-) was FACS-sorted according to standard surface markers expression. RNA was extracted from these sorted cells and the miRnomes were sequenced (**Figure 14 A**). For both CD45+ and CD45- cell fractions, live cells were gated based on their forward and side scatter, and doublets were excluded. Within CD45+ cells, macrophages were gated as F4/80+ CD24-, and further differentiated into alveolar macrophages (SiglecF^{hi} CD11b^{lo}) and interstitial macrophages (SiglecF^{lo} CD11b^{hi}); neutrophils were gated as Ly6G+ CD11b+, T cells being Ly6G- CD11b- CD3+ CD19- and B

cells Ly6G- CD11b- CD3- CD19+. Within CD45- cells, endothelial cells were gated as CD105+ EpCAM-, epithelial cells as CD105- EpCAM+, and fibroblasts CD105- EpCAM- CD140a+ (**Figure 14 B**).

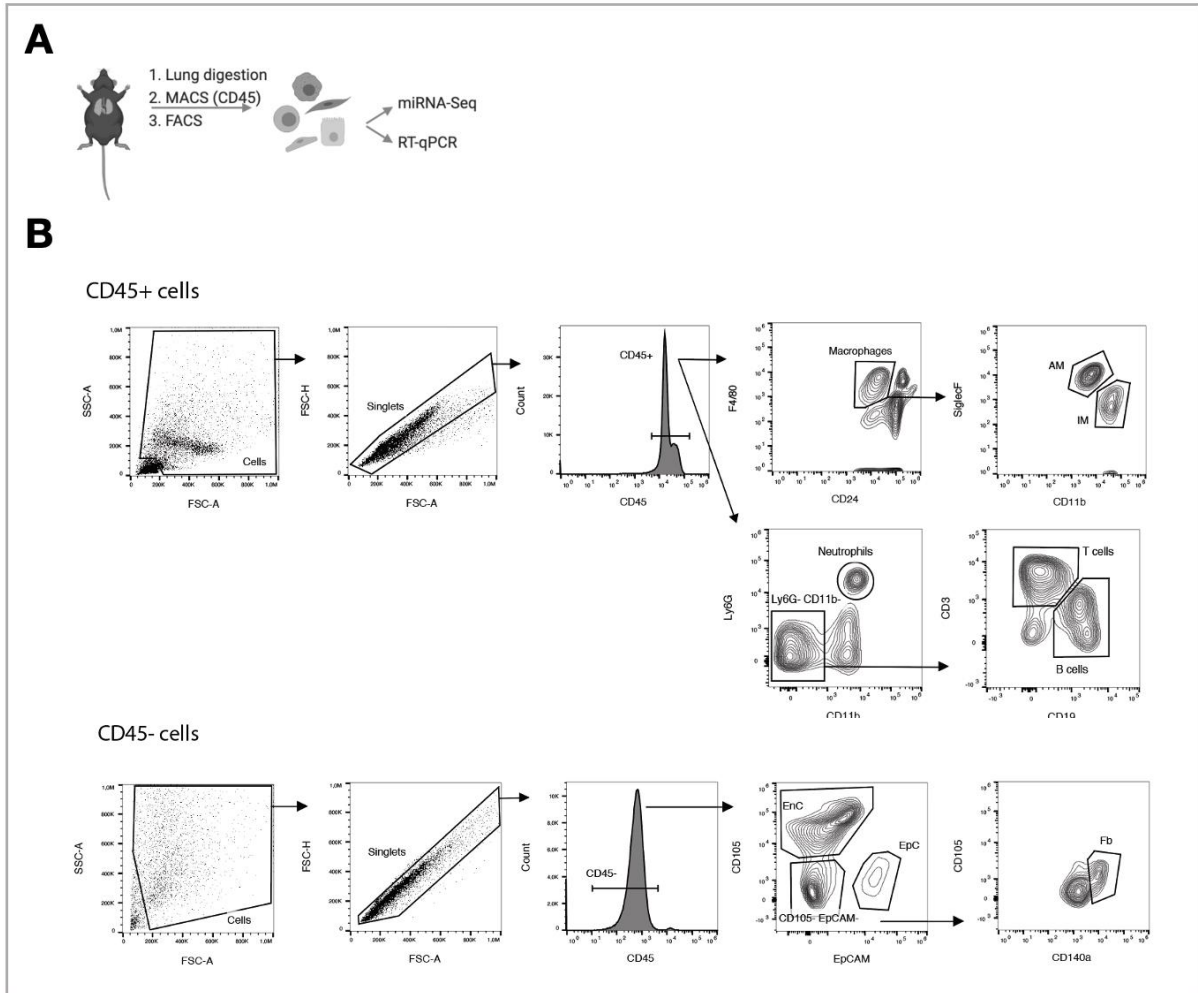


Figure 14 Sorting of mouse lung cells.

A. Experiment outline: cell suspensions from mouse lungs were obtained after enzymatic digestion, then separated by MACS according to their CD45 expression and further FACS-sorted to isolate the RNA from these main cell types, with which microRNA-Seq and RT-qPCR was performed. **B.** Flow cytometry gating strategies for the sorting of CD45+ and CD45- mouse lung cells according to classical markers. MACS: magnetic-activated-cell sorting, FACS: fluorescence-activated cell sorting, miRNA-Seq: microRNA sequencing, AM: alveolar macrophages, IM: interstitial macrophages, EnC: endothelial cells, EpC: epithelial cells, Fb: fibroblasts.

MicroRNA-Seq revealed that each cell type had a characteristic microRNA signature that enabled to distinguish them from one another (**Figure 15 A**). In this sense, marker miRs were classified as those miRs that were positively differentially expressed (mean expression ≥ 20 , $\log_2\text{FoldChange} \geq 1$, $\text{padj} < 0.05$) in one cell type compared to every other cell type (**Figure 15 B**). Among marker miRs there were miR-21a-5p, miR-146b-5p and miR-1298-5p for alveolar macrophages (AM), miR-146a-5p, miR-223-3p and miR-340-5p for interstitial macrophages (IM), miR-142a-5p, miR-150-5p, miR-92a-3p and miR-155-5p for T cells (Tc), miR-126a-3p, let-7b-5p and miR-30a-3p for endothelial cells (EnC), miR-148a-3p, miR-200b-3p and miR-200a-3p for epithelial cells (EpC) and miR-145a-5p, miR-222-3p and miR-100-5p for fibroblasts (Fb).

Examining the lung tissue cells in bulk, it was shown earlier that few miRNAs comprised the majority of miR reads (**Figure 9 D**). Likewise, only 3-7 microRNAs account for more than 50% of the total miR reads in individual pulmonary cell types (**Figure 15 C and D**).

A crosscheck was done to determine whether marker miRs from immune cells (AM, IM and T cells) and non-immune cells (EnC, EpC and Fb) were consistently enriched in the CD45 positive or negative fractions, respectively, in lungs exposed to bleomycin (**Figure 10**).

Indeed, among the microRNAs enriched in the CD45 positive cell fraction there were included miR markers for T cells (miR-142a-5p, and miR-150-5p), for interstitial macrophages (miR-223-3p) and for alveolar macrophages (miR-21a-5p and miR-146b-5p). Among the microRNAs enriched in the CD45 negative cell fraction of the bleomycin group, there were marker miRs for fibroblasts (miR-143-3p and miR-214-3p), for endothelial cells (miR-126a-5p, miR-126a-3p, miR-30a-5p and miR-30c-5p) and for epithelial cells (miR-200b-3p and miR-34c-5).

Moreover, miR-21a-5p, the highest expressed upregulated miR in bleomycin-induced pulmonary fibrosis (**Figure 9 B**), was mostly expressed in macrophages, especially in AM, where it represents the top1 abundant miR and it constitutes 22% of the total microRNAs. In IM it is also abundantly expressed, being the top 2 abundant miR and representing 11% of total microRNAs. This differential expression was further observed by RT-qPCR, being miR-21a-5p highest in AM compared to the total lung and compared to other lung cell types (**Figure 15 E**).

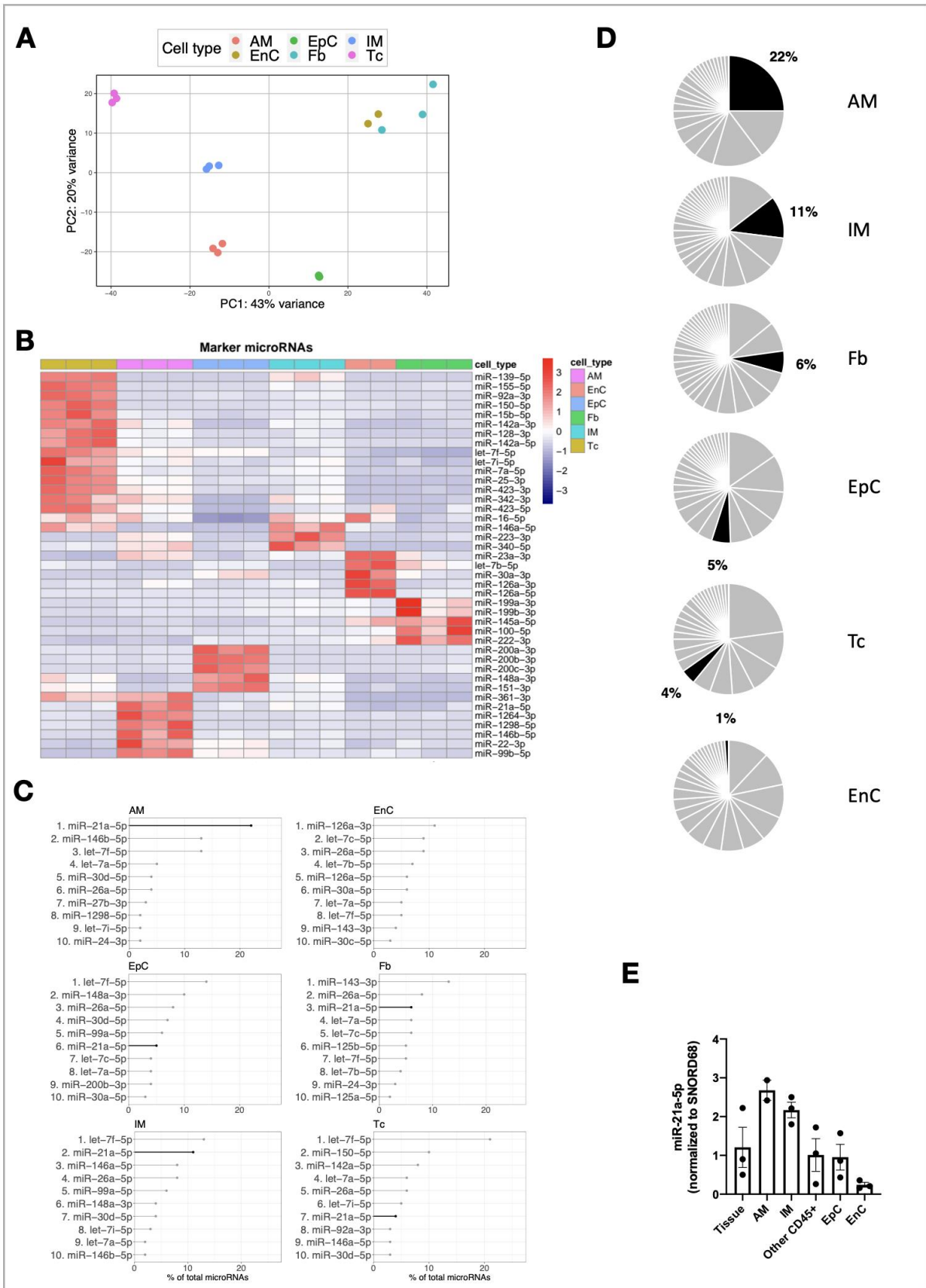


Figure 15 miRnome of sorted mouse lung cells at basal state.

A. Principal component analysis showing the clustering of lung cell types: AM (n=3), EnC (n=2), EpC (n=3), Fb (n=3), IM (n=3) and Tc (n=3). **B.** Heatmap of marker microRNAs in each

cell type. **C.** Top 10 expressed miRNAs percentage relative to all miRNAs in each cell type; miR-21 is highlighted in black. **D.** Pie charts showing the abundance of microRNAs in each cell type; miR-21 is highlighted in black. **E.** RT-qPCR of miR-21a-5p in lung cell types; data are individual values and mean \pm SEM. AM: alveolar macrophages, IM: interstitial macrophages, Fb: fibroblasts, EpC: epithelial cells, EnC: endothelial cells; Tc: T cells.

Taken together, microRNA sequencing of sorted lung cells revealed that different cell types possess a distinct miRnome signature and that few miRs account for the majority of total miRs expression. Furthermore, a set of marker miRNAs that clearly enables the identification of each cell type was delineated. In this detailed analysis it was found that miR-21 constitutes a marker miR for alveolar macrophages, where it is the miR with the highest expression levels and accounts for almost a quarter of total miR reads.

Chapter 4: miRnome signature of human lung cells

With the aim of determining cell type-specific miRnome profiles in human lungs, miRNA sequencing was performed on main lung cell types. For this, cells were isolated by enzymatic digestion from pathologically normal-looking sections of lungs from patients undergoing cancer lung resection or from the PCLS derived from those sections. Cell suspensions were then separated by MACS based on their CD45 expression and further FACS-sorted according to classical markers expression for each cell type. MicroRNA libraries were prepared from the isolated RNA or directly from the cell lysates (**Figure 16 A**).

For both CD45[±] cell fractions, live cells were gated based on their forward scatter, side scatter and the Zombie viability dye, and doublets were excluded. Within CD45 positive cells, macrophages (Mac) were gated as CD206⁺. Within CD45 negative cells, epithelial cells (EpC) were gated as EpCAM⁺ CD31⁻, endothelial cells (EnC) as EpCAM⁻ CD31⁺ and fibroblasts (Fb) as EpCAM⁻ CD31⁻ CD90⁺ (**Figure 16 B**).

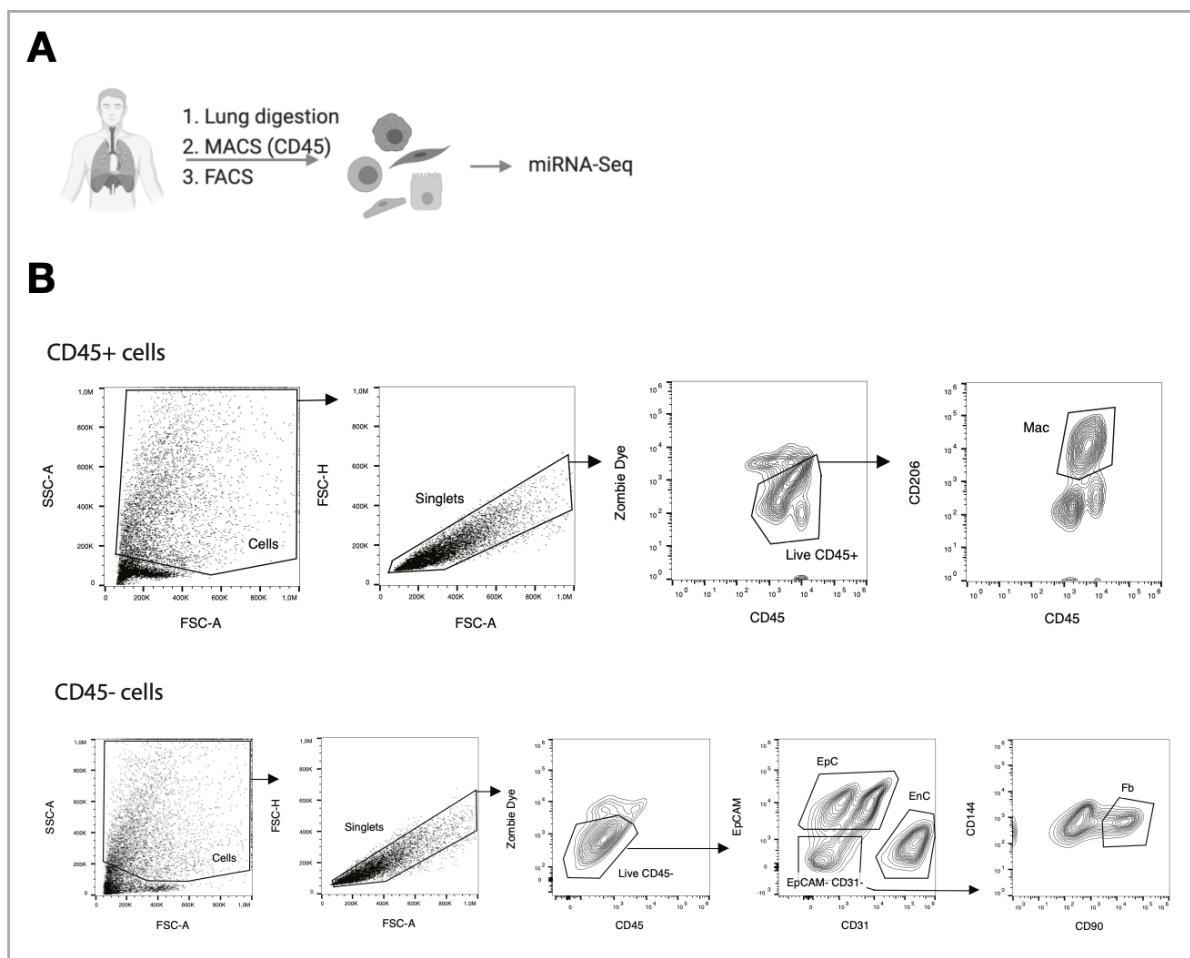


Figure 16 Sorting of human lung cells for microRNA sequencing.

A. Experiment outline: sections of human lungs were enzymatically digested and the cell suspension was then MACS-separated based on the CD45 expression and further sorting by FACS according to classical markers expression. MiRNA-Seq was performed on each cell type. **B.** Gating strategies used for FACS sorting. MACS(CD45): magnetic-activated cell sorting using CD45 microbeads, FACS: fluorescence-activated cell sorting, miRNA-Seq: microRNA sequencing, Mac: macrophages, Fb: fibroblasts, EpC: epithelial cells, EnC: endothelial cells.

MicroRNA sequencing showed a distinct miRnome signature for each cell type, with differentially expressed microRNAs ($p\text{-adjusted} < 0.05$, $|\log_2\text{FoldChange}| \geq 0.5$) compared to one or more other cell types (**Figure 17 A and B**). By taking the microRNAs that were differentially expressed in a cell type compared to every other cell type, the following positive ($\log_2\text{FoldChange} \geq 0.5$) marker miRs were found: miR-126-3p for endothelial cells, miR-1-3p, miR-10a-5p and miR-27b-3p for fibroblasts, and miR-155-5p, miR-197-3p and miR-142-5p for macrophages.

Comparing the cell type-specific miRnome profiles from mouse and human lungs, macrophages from these species shared the marker miR-223-3p and endothelial cells shared the marker miR-126.

Some of the microRNAs that were classified as marker miRs for mouse lung cells were not in human, but were differentially expressed compared to some of the other cell types. For instance, miR-21 is a marker miR for mouse macrophages, and in human macrophages it is differentially expressed compared to endothelial and epithelial cells, though not compared to fibroblasts. MiR-151, a marker for mouse epithelial cells, is differentially expressed in human epithelial cells compared to fibroblasts and macrophages, though not compared to endothelial cells. Lastly, miR-145, a marker miR for mouse lung fibroblasts, is significantly higher in human fibroblasts compared to macrophages and endothelial cells, but not in comparison to epithelial cells.

In terms of abundance of microRNAs in each cell type, as was the case in mice, only 3-7 individual microRNAs accounted for more than 50% of all microRNA reads (**Figure 16 C and D**).

To further assess the similarities in the miRnome profiles across species, the top 10 abundant microRNAs of the respective cell type in human and mouse were compared with each other. In macrophages, 5 microRNAs were shared in both species (miR-21-5p, let-7a-5p, let-7a-5p, miR-146b-5p and miR-26a-5p); in endothelial cells, also 5 were shared (let-7b-5p, miR-143-3p, let-7a-5p, let-7f-5p and miR-26a-5p); epithelial cells had 4 common microRNAs between mouse and human (let-7a-5p, let-7f-5p, miR-21-5p and miR-26a-5p) and fibroblasts had 7 microRNAs in common (miR-143-3p, let-7a-5p, miR-26a-5p, let-7b-5p, let-7f-5p, miR-125b-5p, miR-24-3p).

In particular, miR-21-5p, the upregulated miRNA in IPF with the highest expression (**Figure 12 D**) was primarily expressed in macrophages and this was the most abundant miR therein as was the case for mice (**Figure 15 D**), though, in contrast, it was not classified as marker miR because it was not differentially expressed compared to fibroblasts ($\log_2\text{FoldChange}=0.4$, $p\text{-adjusted}=0.48$).

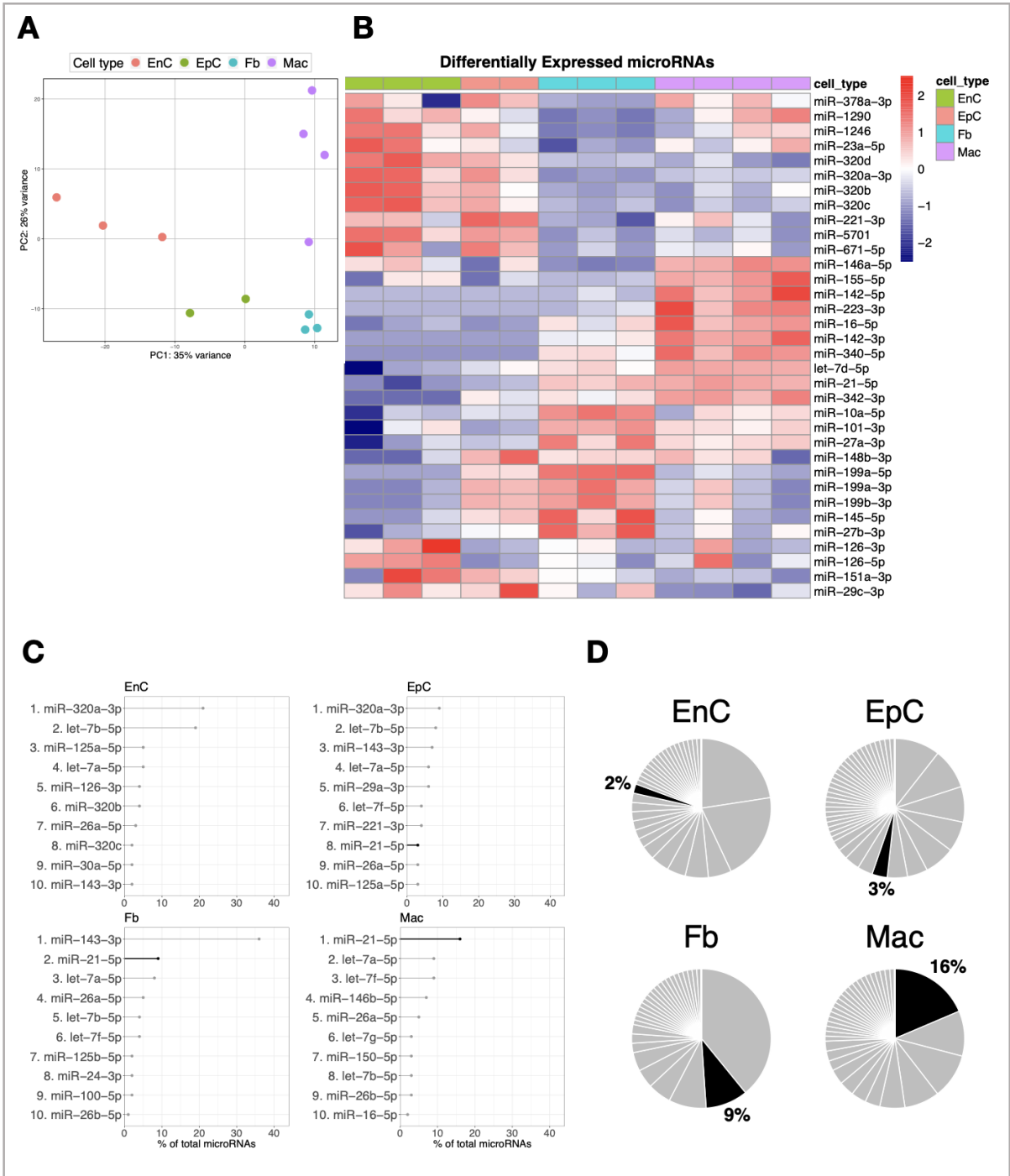


Figure 17 miRnome of human sorted lung cells.

A. Principal component analysis showing the clustering of samples according to the cell type, i.e., EnC (n=3), EpC (n=2), Fb (n=3) and Mac (n=4). **B.** Heatmap showing differentially expressed (p -adjusted<0.05, $|\log_2\text{FoldChange}| \geq 0.5$) microRNAs between one cell type and one or more other cell types. **C.** Representation of the top 10 abundant microRNAs in each cell type and their percentages relative to all detected microRNAs; miR-21-5p is highlighted in black. **D.** Pie charts depicting miRs abundance; miR-21-5p is highlighted in black and its

percentage is shown. Mac: macrophages, Fb: fibroblasts, EpC: epithelial cells, EnC: endothelial cells.

All in all, this experiment revealed that human lung cell types have a characteristic miRnome profile similar to that of their murine counterparts, though the differences were less pronounced. As in mice, miR-21 was mainly and highly expressed in macrophages, but it was not classified as a marker miR for this cell type.

Chapter 5: Characterization of human blood monocyte-derived macrophages

In order to assess whether *in vitro* differentiated human macrophages also highly express miR-21 like mouse and human lung macrophages and whether there are differences between macrophage subtypes, human blood monocyte-derived macrophages (Mo-Mac) were characterized in terms of miR-21 expression and similarity to lung macrophages.

To obtain the Mo-Mac, peripheral blood mononuclear cells (PBMCs) were isolated by Ficoll-gradient centrifugation from fresh blood and monocytes were purified with magnetic separation using a human monocyte isolation kit. Monocytes were differentiated to macrophages by culturing them in the presence of GM-CSF or M-CSF (GM-Mac and M-Mac, respectively). At day 6, the differentiation was completed (**Figure 18 A**). The successful purification of monocytes from PBMCs is depicted in **Figure 18 B**.

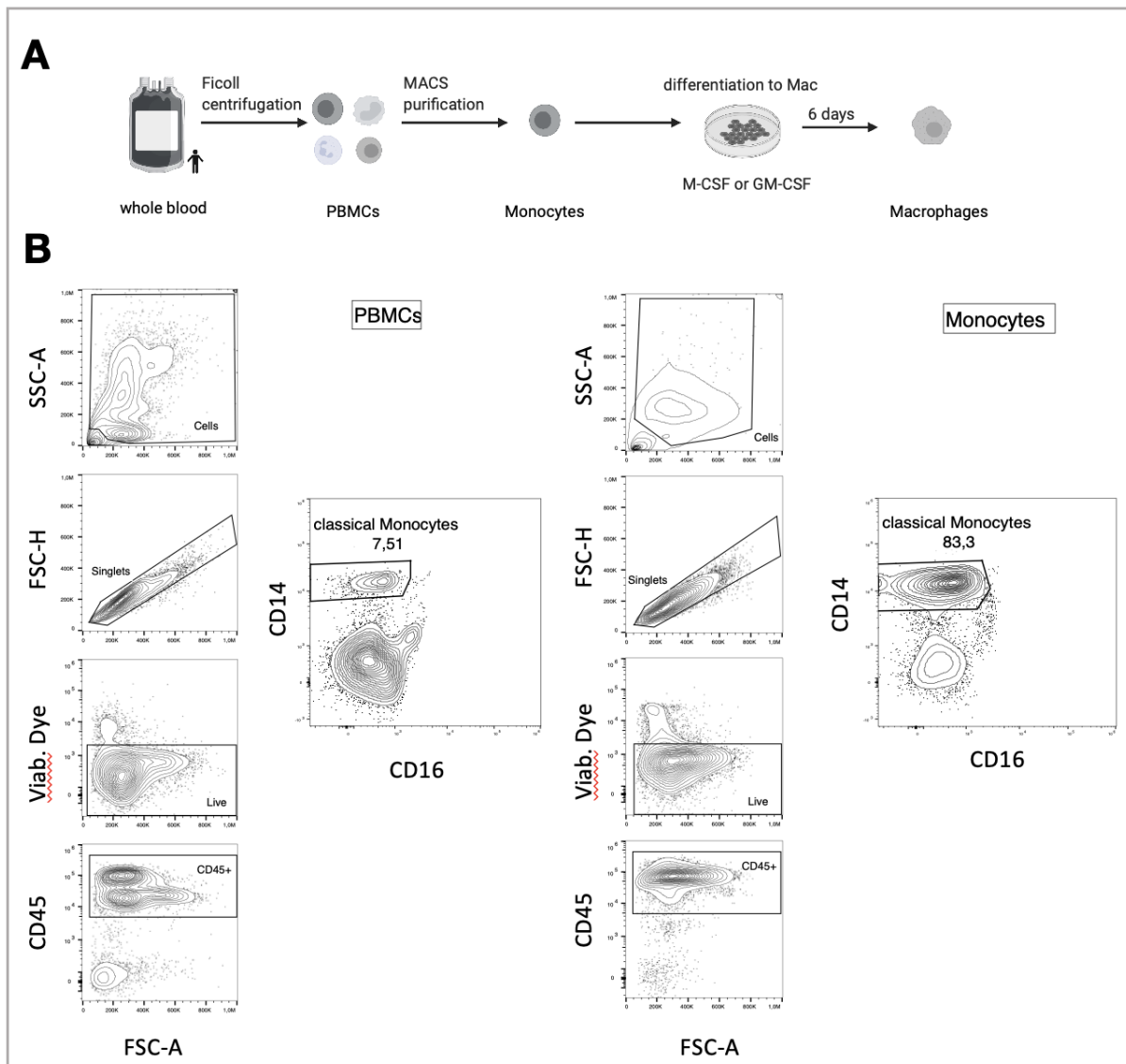


Figure 18 Differentiation of human blood monocytes to macrophages.

A. Workflow for the procurement of blood monocyte-derived macrophages: PBMCs were purified from fresh human blood, then subjected to MACS using a monocyte isolation kit to enrich the monocytes, which were subsequently cultured in the presence of M-CSF or GM-CSF for 6 days to promote the differentiation to macrophages. **B.** Flow cytometry analysis of the isolated PBMCs and monocytes to confirm the enrichment of monocytes after MACS separation. PBMCs: peripheral blood mononuclear cells, MACS: magnetic-activated cell sorting, PBMCs: peripheral blood mononuclear cells, Mac: macrophages.

First, an optimization of the differentiation and culture of the macrophages was performed to retain high viability and surface proteins expression given that it is known that, on the one hand, detachment of cultured cells with trypsinization or scraping can alter the expression of

surface proteins and induce apoptosis [80]–[82], but on the other hand, macrophages are very adherent cells and difficult to detach. Therefore, two different kinds of cell culture plates were tested, namely, Corning Ultra-Low Attachment plates, which have a hydrophilic surface that minimizes adherence and spreading, and Nunc UpCell plates, which have a hydrophobic surface at cell culture temperature (37 °C) but become hydrophilic at RT, facilitating detachment of cells.

To test the performance of these plates, monocytes were differentiated in the presence of GM-CSF and medium was changed on day 2, day 4 or not changed at all. After 6 days, cells morphology was observed under the microscope (**Figure 19 A**) and then cells were harvested by treatment with Accutase and gentle flushing. The number of recovered cells and viability was quantified using an automated cell counter (**Figure 19 B**).

By visual inspection under the microscope, cells had a classic macrophage morphology under all conditions tested. However, when analyzing the number of recovered cells and viability, a 2-way ANOVA test revealed that, overall, more cells ($5.84E4 \pm 2E4$, $p=0.013$) and with higher viability ($24.8\% \pm 8.4\%$, $p=0.012$) were recovered when cultured in Nunc UpCell plates than in Corning Ultra-Low Attachment plates, while the change of medium had no significant effect.

The surface expression of CD68, a pan macrophage marker, and CD206, a lung macrophage marker, as well as viability, was assessed by flow cytometry in GM- and M-Mac cultured in Corning Ultra-Low Attachment and Nunc UpCell plates (**Figure 19 C and D**). The viability was high (>80%) in both plates, either assessed by Trypan Blue staining in an automated cell counter or with a viability dye (Zombie violet) by flow cytometry. However, differentiation was stronger in the Nunc UpCell plates, in terms of CD68 and CD206 expression.

Taken together the higher viability, higher number of recovered cells and better differentiation of macrophages in Nunc UpCell plates compared to Corning Ultra-Low Attachment, these plates were chosen to culture macrophages in the following experiments.

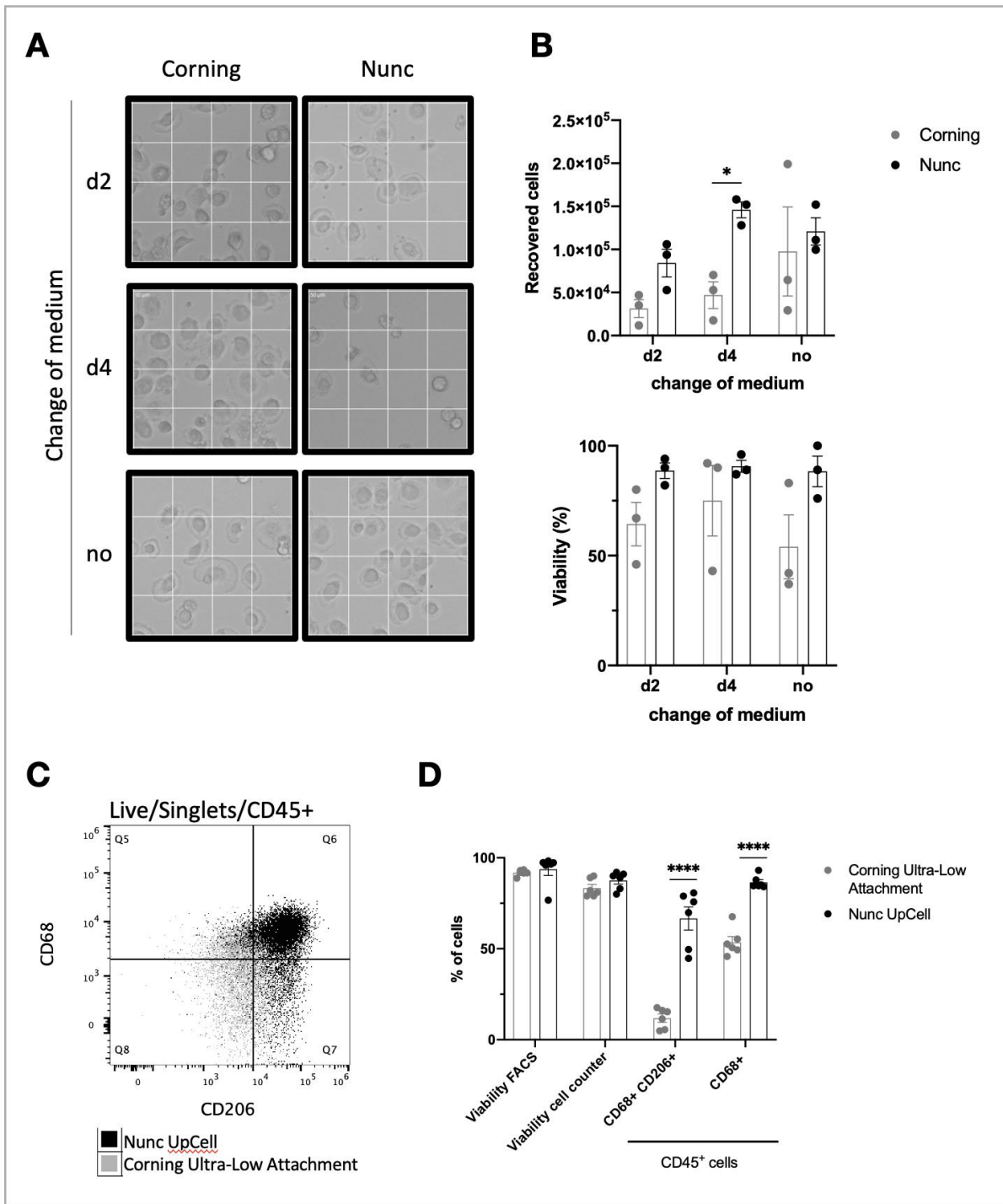


Figure 19 Influence of cell culture surface in macrophage differentiation.

A. Morphology of G-Mac when cultured in Corning Ultra-Low Attachment plates (Corning) or Nunc UpCell plates (Nunc), with change of medium on day 2 (d2), day 4 (d4) or no change of medium (no). **B.** Quantification of recovered cells and viability using an automated cell counter; n=3 for each condition. **C.** Representative flow cytometry dot plot of CD68 and CD206 expression in differentiated macrophages in the two cell culture plates. **D.** Quantification of viability and macrophage surface markers expression of G-Mac when

cultured in Corning or Nunc plates (n=6 for each) by automatic cell counting and flow cytometry. Data are individual values and mean \pm SEM and were analyzed with 2-way ANOVA, *p<0.05, ****p<0.0001.

Once the culture conditions were optimized, it was next assessed whether M- or GM-Mac could be associated with an AM- or IM-like phenotype. Therefore, differences between M- and GM-Mac were assessed in terms of morphology, surface markers expression and miR-21 levels.

By microscopy it was observed that monocytes differentiated from small round cells to have a distinct macrophage morphology. GM-Mac had a “fried-egg” morphology, while M-Mac were heterogenous, some adopted a rounder morphology as GM-Mac, while others adopted a spindle-like morphology (**Figure 20 A**).

In order to determine whether blood monocyte-derived macrophages expressed high levels of miR-21 as was previously observed in primary lung macrophages (**Figure 15**), microRNA sequencing was performed on macrophages derived from monocytes from one donor, using two replicates per growth factor. MiR-21-5p was indeed highly expressed, representing 38% and 29% of total microRNA reads in GM- and M-Mac, respectively, and constituting the most abundant microRNA in both macrophage subtypes (**Figure 20 B**). However, miR-21 was not differentially expressed between both macrophage types, which was also corroborated by RT-qPCR (**Figure 20 C**).

In terms of surface markers expression, CD68, CD206, CD14 and CD169 levels were analyzed in macrophages derived from 3 different donors. As quantified by flow cytometry, >88% of cells were macrophages (CD45+ CD68+). It is known that human alveolar macrophages express higher levels of CD206 and CD169, and lower levels of CD14 compared to interstitial macrophages [83], [84]. However, between GM- and M-Mac there was no significant difference in surface expression of CD68, CD206 or CD169, though M-Mac had a slightly higher surface expression of CD14 (**Figure 20 D and E**).

Taken together, both M- and GM-Mac share similarities and differences with human lung alveolar and interstitial macrophages.

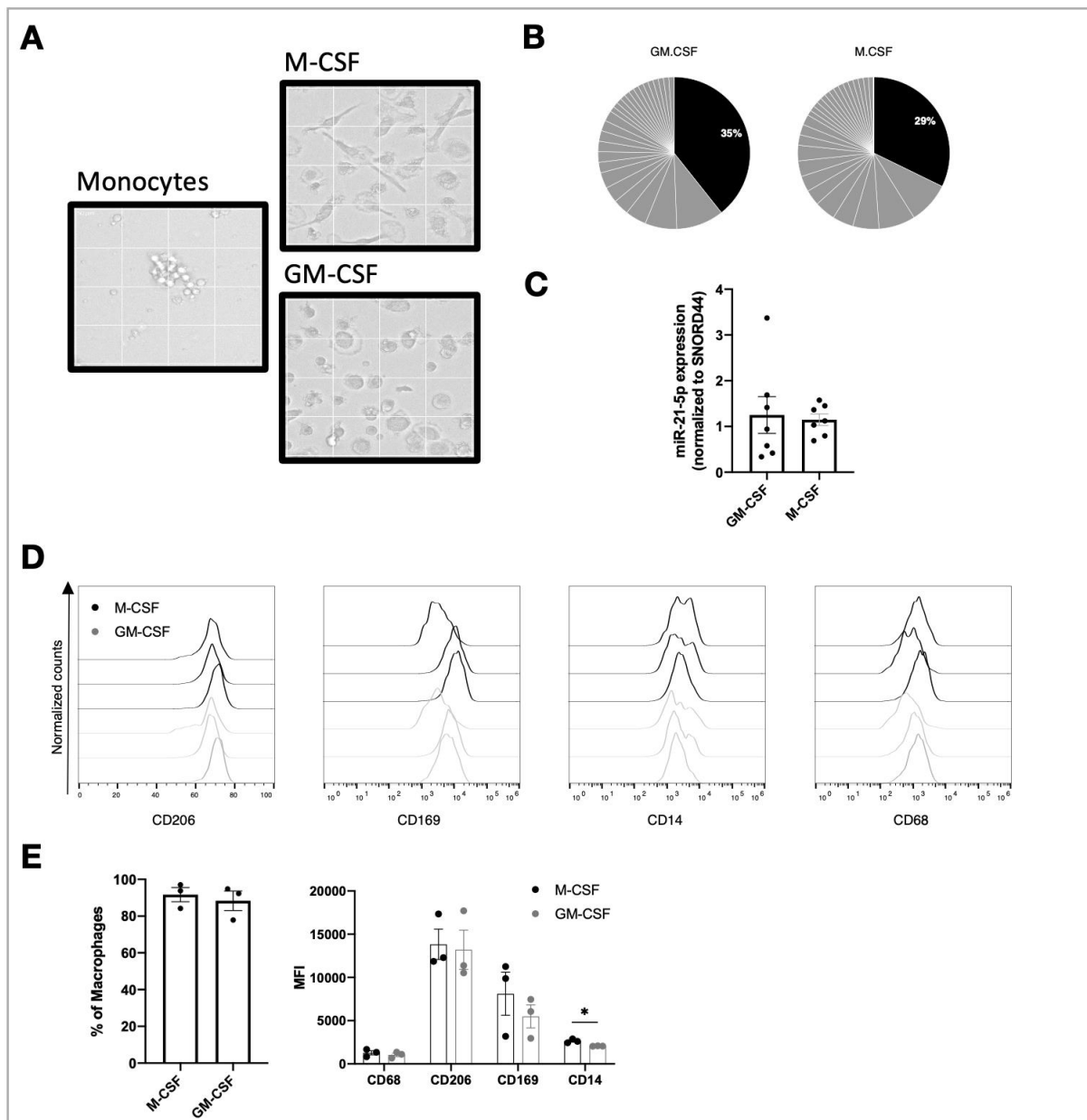


Figure 20 Characterization of GM- and M-Mac.

A. Morphology of monocytes and macrophages differentiated with M-CSF or GM-CSF as assessed by light microscopy. **B.** Pie charts of microRNAs abundance in G-Mac and M-Mac (n=2 for each); miR-21-5p is highlighted in black and its percentage among all microRNAs is shown. **C.** MiR-21 expression quantified by RT-qPCR in G-Mac and M-Mac (n=7 for each). **D.** Histograms of surface markers expression in G-Mac and M-Mac studied with flow cytometry (n=3 for each). **E.** Flow cytometry quantification of percentage of macrophages, and intensity of surface markers expression as assessed by median fluorescence intensity (MFI)

in G-Mac and M-Mac (n=3 for each). Data are individual values and mean \pm SEM and were analyzed with Student's unpaired t-tests; *p< 0.05.

Finally, to study the effects of a profibrotic environment on macrophage miR-21 levels, human blood monocyte-derived macrophages were treated with the pro-fibrotic cytokine TGF- β . Given the evidence of previous studies where it has been shown that TGF- β induces miR-21 expression in cultured lung epithelial cells [46] and lung fibroblasts [45], [48], it could be hypothesized that TGF- β also promotes an increase in miR-21 levels in macrophages, which could be reversed by antimiR-21 treatment. To test this hypothesis, monocytes from one donor were differentiated with GM- or M-CSF into macrophages; on day 6, macrophages were treated with increasing concentrations of TGF- β (0, 5, 25 and 50 ng/mL) for 48 h and, on day 8, they were transfected with antimiR-21 or antimiR-scr (**Figure 21 A**).

Nevertheless, under these conditions, miR-21 was not upregulated under any of the TGF- β concentrations tested in GM- nor in M-Mac (**Figure 21 B**).

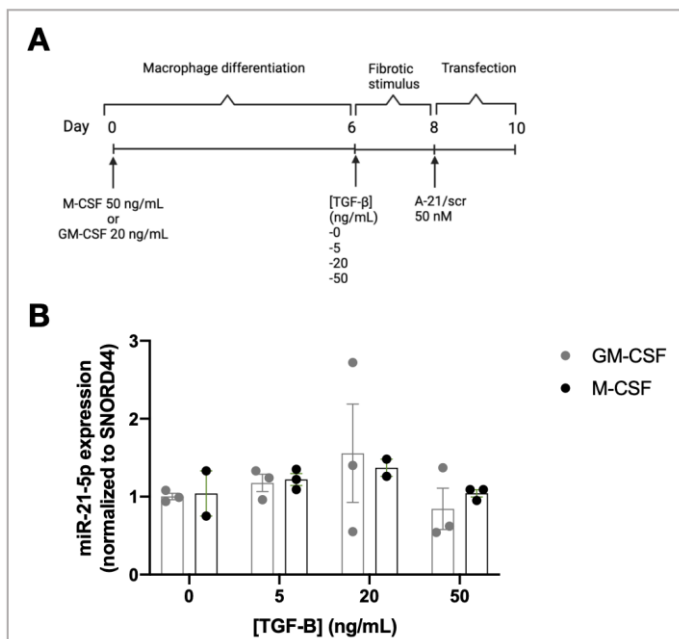


Figure 21 miR-21 levels in GM- and M-Mac upon TGF- β treatment.

A. Experiment outline: macrophages were differentiated in the presence of M-CSF or GM-CSF for 6 days, then treated for two days with increasing concentrations of TGF- β and on day 8, they were transfected with antimiR-21 (A-21) or scrambled control (scr). **B.** miR-21

levels in the anti-miR-scr group quantified by RT-qPCR. Data are individual values and mean \pm SEM and were statistically analyzed with 2-way ANOVA.

Summing up, in this chapter the culture of human blood monocyte-derived macrophages was optimized in terms of viability and macrophage markers expression by testing the performance of two cell culture plates with different physical properties, highlighting the importance of choosing an appropriate surface for the culture of adherent cells. In addition, comparisons between macrophages differentiated in the presence of M-CSF or GM-CSF revealed that they differed in morphology and CD14 expression, but not in CD68, CD169 nor CD206 expression. Furthermore, miRNA analysis showed that miR-21 was the most expressed miRNA as was the case for human and murine macrophages, but its expression levels did not change upon TGF- β treatment.

Chapter 6: Transcriptome analysis of a human *ex vivo* model of lung fibrosis using PCLS and anti-miR-21 treatment

With the aim of assessing the therapeutic efficacy of miR-21 inhibition in dampening fibrosis in a relevant human model of lung fibrosis, the *ex vivo* fibrosis model in human precision-cut lung slices (PCLS) introduced by *Alsafadi et al* [85] was used, where the disease onset is driven by a cocktail of profibrotic cytokines and growth factors (TGF- β , TNF- α , PDGF-AB and LPA). Briefly, PCLS derived from tumor-free sections of lungs from two patients were treated with fibrosis (FC) or control cocktail (CC) on days 0 and 2, medium was changed on day 4, and on day 5, PCLS were treated with 30 pmol anti-miR-21 or anti-miR-scr. Transcriptomic analysis was performed two days later (**Figure 22 A and B**).

To analyze at the whole transcriptomic level the similarity of this model to human lung fibrosis, differential expression analysis was carried out after filtering out genes with low expression (mean expression ≥ 20). This analysis showed 225 differentially expressed genes (p -adjusted < 0.05 and $|\log_2\text{FoldChange}| \geq 0.5$) between FC and CC-treated PCLS, of which 204 were upregulated and 21 downregulated (**Figure 22 C**). Included in these gene expression changes was the upregulation of classical IPF markers such as CCL11, MMP10 and S100A8.

In addition, gene ontology analysis performed using two databases, namely GO and MSigDB, identified relevant terms like “extracellular matrix organization”, “inflammatory

response” and “epithelial mesenchymal transition”, all processes involved in the development of lung fibrosis (**Figure 22 D**). Furthermore, gene set enrichment analysis using the Reactome database also showed activated inflammatory pathways, like “Interleukin-1 signaling” and “Toll-like Receptor Cascades” (**Figure 22 E**).

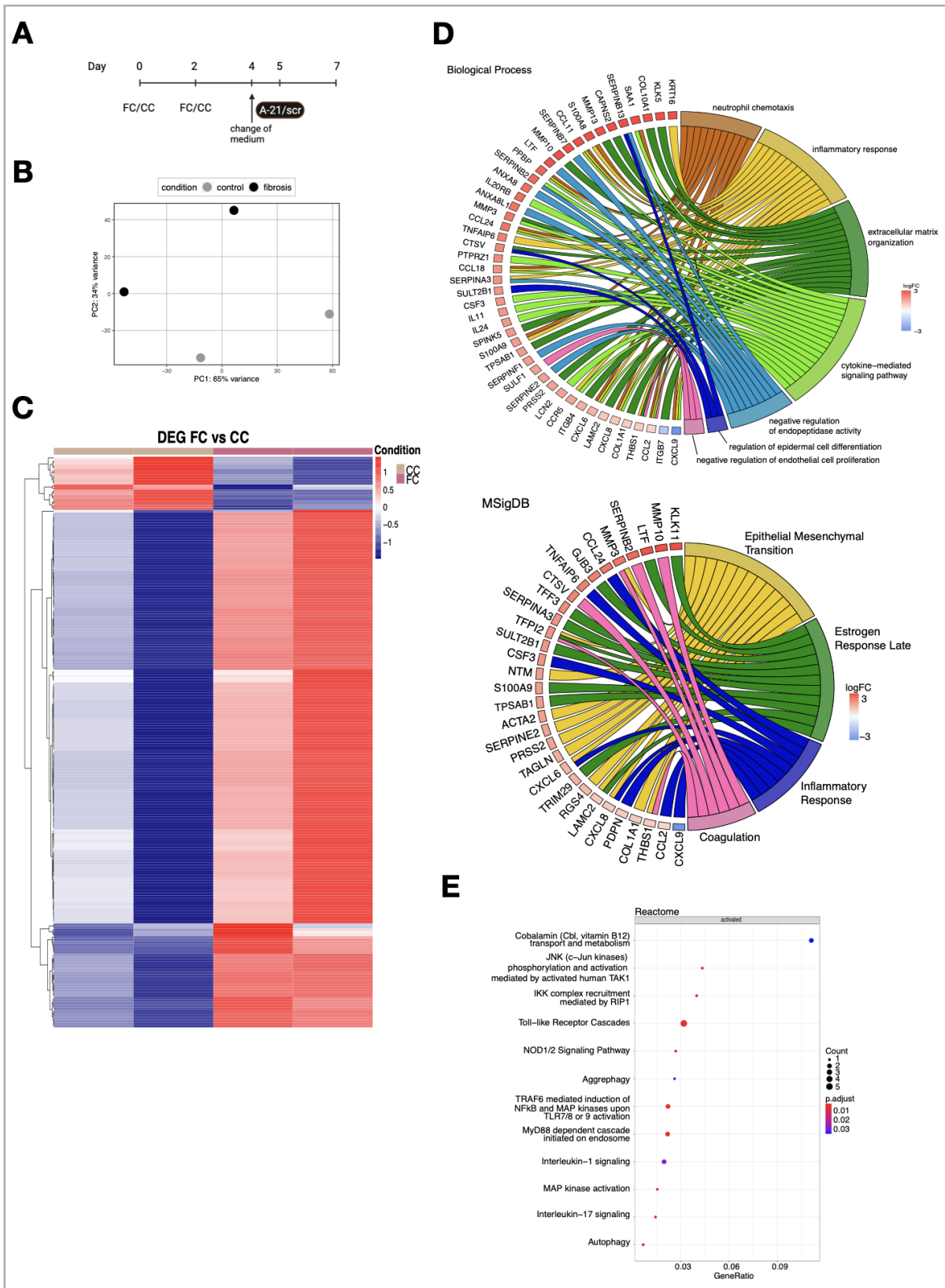


Figure 22 Transcriptomic analysis of a human *ex vivo* fibrosis model using PCLS.

A. Experiment outline: PCLS were treated with CC or FC on days 0 and 2, medium was changed on day 4 and PCLS were transfected with antimiR-21/-scr on day 5; two days later

RNA sequencing analysis was performed; n=2 for each condition. **B.** Principal component analysis of FC- and CC-treated PCLS. **C.** Heatmap clustering of differentially expressed genes ($p\text{-adjusted} < 0.05$ and $|\log_2\text{FoldChange}| \geq 0.5$) between FC- and CC-treated PCLS. **D.** Gene ontology overrepresentation analysis with the Biological Process and MSigDB databases, showing which genes contribute to each GO term and their $\log_2\text{FoldChanges}$. **E.** Gene set enrichment analysis using the Reactome database. A-21: antimiR-21, scr: antimiR-scr, FC: fibrosis cocktail, CC: control cocktail, DEG: differentially expressed genes.

In order to assess the similarities of this model to IPF, the differentially expressed genes in FC- vs CC-treated PCLS were compared to the differentially expressed genes from a public RNA-Seq dataset (GSE99621) of IPF (n=18) and healthy (n=8) donors. There were 46 genes upregulated both in the *ex vivo* model and in IPF patients and 1 gene was downregulated in both datasets (**Figure 23 A**). From the genes that were differentially expressed in both datasets, most of the genes that are upregulated in IPF patients were also upregulated in FC-PCLS, including commonly fibrosis-associated genes such as ACTA2, COL1A1, COL10A1, CCL11 and TAGLN (**Figure 23 B**).

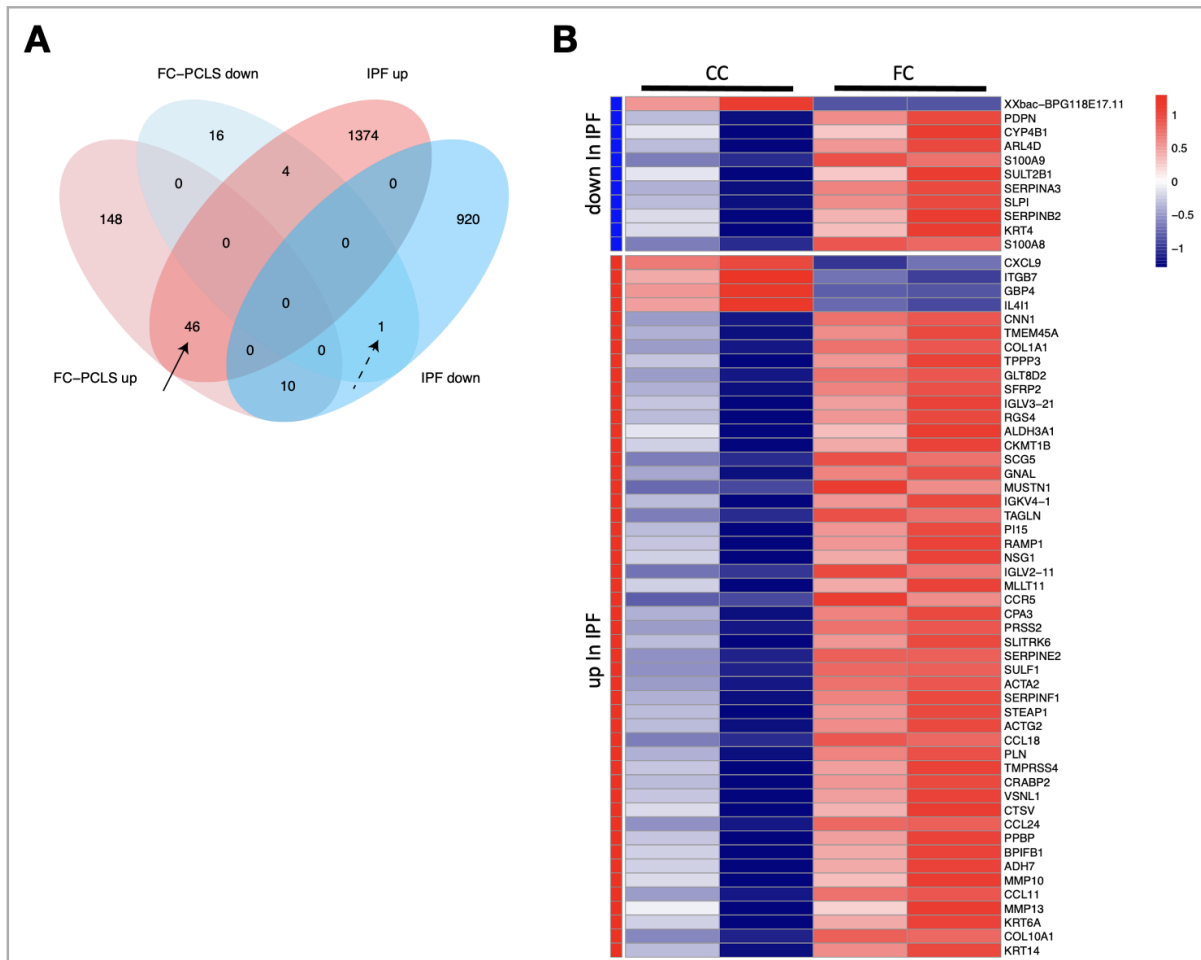


Figure 23 Comparison of human *ex vivo* PCLS fibrosis model to IPF.

A. Venn diagram showing intersections of up- and downregulated genes in FC-PCLS and IPF; the uniform line arrow indicates the commonly upregulated genes and the dashed arrow points to the commonly downregulated genes. **B.** Heatmap of differentially expressed genes in FC-PCLS and IPF. FC-PCLS: precision-cut lung slices treated with fibrosis cocktail, IPF: idiopathic pulmonary fibrosis, CC: control cocktail, FC: fibrosis cocktail, down: downregulated, up: upregulated.

After having found relevant transcriptomic similarities between the PCLS fibrosis model and IPF, the effects of miR-21 inhibition in the FC-treated PCLS (FC-PCLS) were analyzed to assess whether it would have anti-fibrotic properties as in animal models and cultured cells [45], [46], [48].

The treatment with anti-miR-21 produced an overall trend of miR-21 target de-repression (**Figure 24 A**). Even though it was a modest shift, it led to significant changes at the whole transcriptome level; the fibrosis-related genes that were upregulated in FC-PCLS, such as

MMP3, MMP13, MMP10, CCL11 and CCL20, were downregulated after miR-21 inhibition (**Figure 24 B**).

Moreover, gene set enrichment analysis showed that inhibition of miR-21 reduced inflammatory signaling pathways (NF-kappaB, IL-1 family), keratinization, leukocyte migration, phagocytosis, apoptosis, and proliferation; processes that are activated in FC-PCLS (**Figure 24 C**).

Despite the significant anti-fibrotic effects observed at the transcriptome level after anti-miR-21 treatment of FC-PCLS, there were no significantly (p -adjusted <0.05) de-repressed miR-21 targets. A possible explanation could be that 48 h after transfection might be too early to observe significant increases in particular genes, but the combined effect is sufficient to alter signaling pathways. In this sense, miR-21 targets with $\log_2\text{FoldChanges}>0.3$ were further analyzed by gene ontology enrichment to identify the involved pathways (**Figure 24 D**). The most prominent pathways were BMP, TGF- β and activin signaling pathways, with some genes being activators or downstream targets (BMP3, TGFBR2 and MSX1) and others negative regulators (CRIM1, LEMD3, SKI and SMAD7).

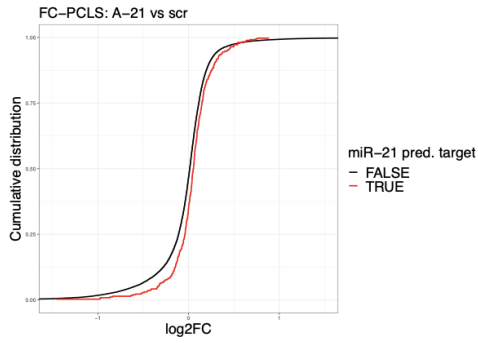
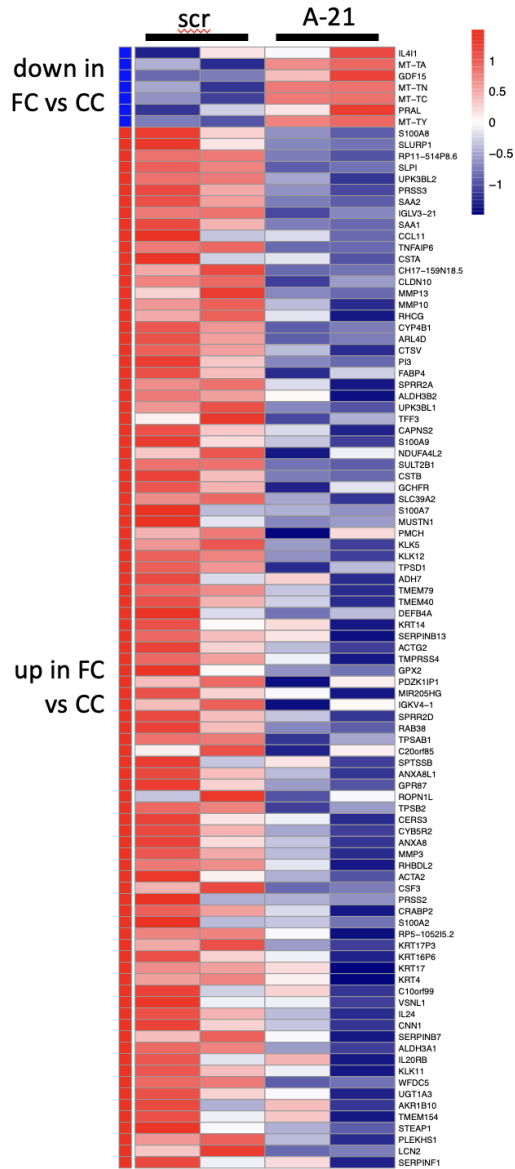
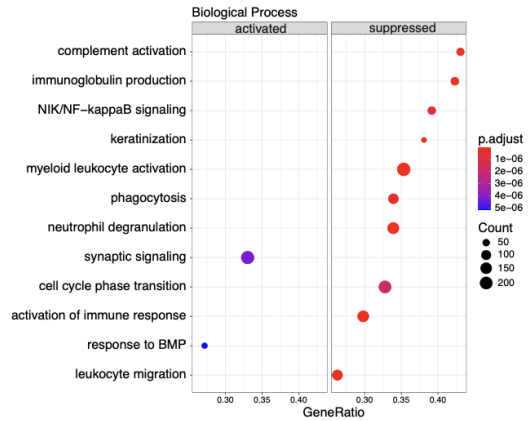
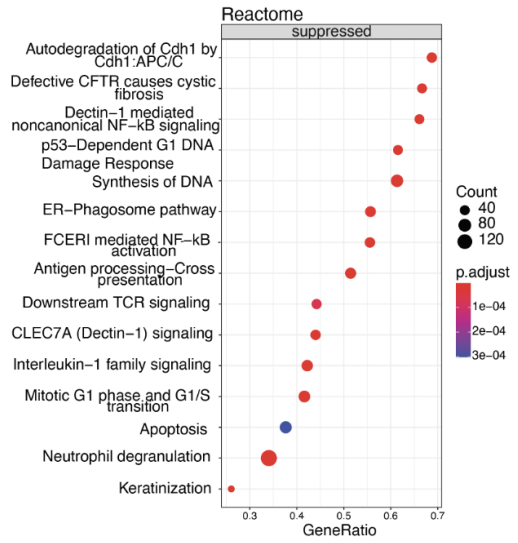
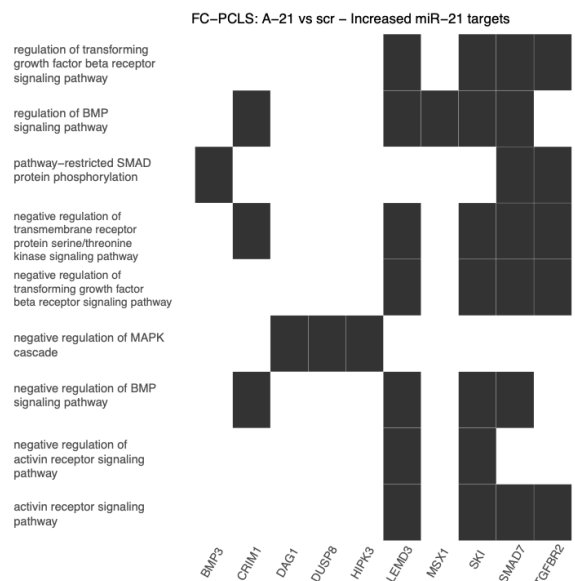
A**B****C****D**

Figure 24 MiR-21 inhibition reduces the fibrotic phenotype of FC-PCLS.

A. Heatmap of differentially expressed genes between FC-PCLS treated with antimiR-21 (A-21) or antimiR-scr (scr), compared to deregulated genes in FC-PCLS versus CC-PCLS. **B.** Gene set enrichment analysis of the differentially expressed genes between FC-PCLS treated with antimiR-21 (A-21) or antimiR-scr (scr), using the Reactome and Biological Process databases. **C.** Cumulative distribution plot of gene expression changes; the black curve shows non-miR-21 predicted targets and the red curve miR-21 predicted targets. **D.** Gene ontology analysis of the de-repressed miR-21 targets showing which genes are related to each pathway. PCLS: precision-cut lung slices, FC-PCLS: PCLS treated with fibrosis cocktail, CC-PCLS: PCLS treated with control cocktail, down: downregulated, up: upregulated; pred.: predicted.

To further delineate the relevance of the gene expression changes upon miR-21 inhibition, a comparison was done with the same public IPF RNA-Seq dataset as before. When FC-PCLS were treated with antimiR-21, 64 of the genes that are upregulated in IPF, became downregulated, including classic fibrosis markers such as ACTA2, CCL11, CCL19, MMP13 and MMP10. Likewise, 19 genes, mainly mitochondrial genes, that are downregulated in IPF, are upregulated in the antimiR-21-treated FC-PCLS (**Figure 25 A and B**).

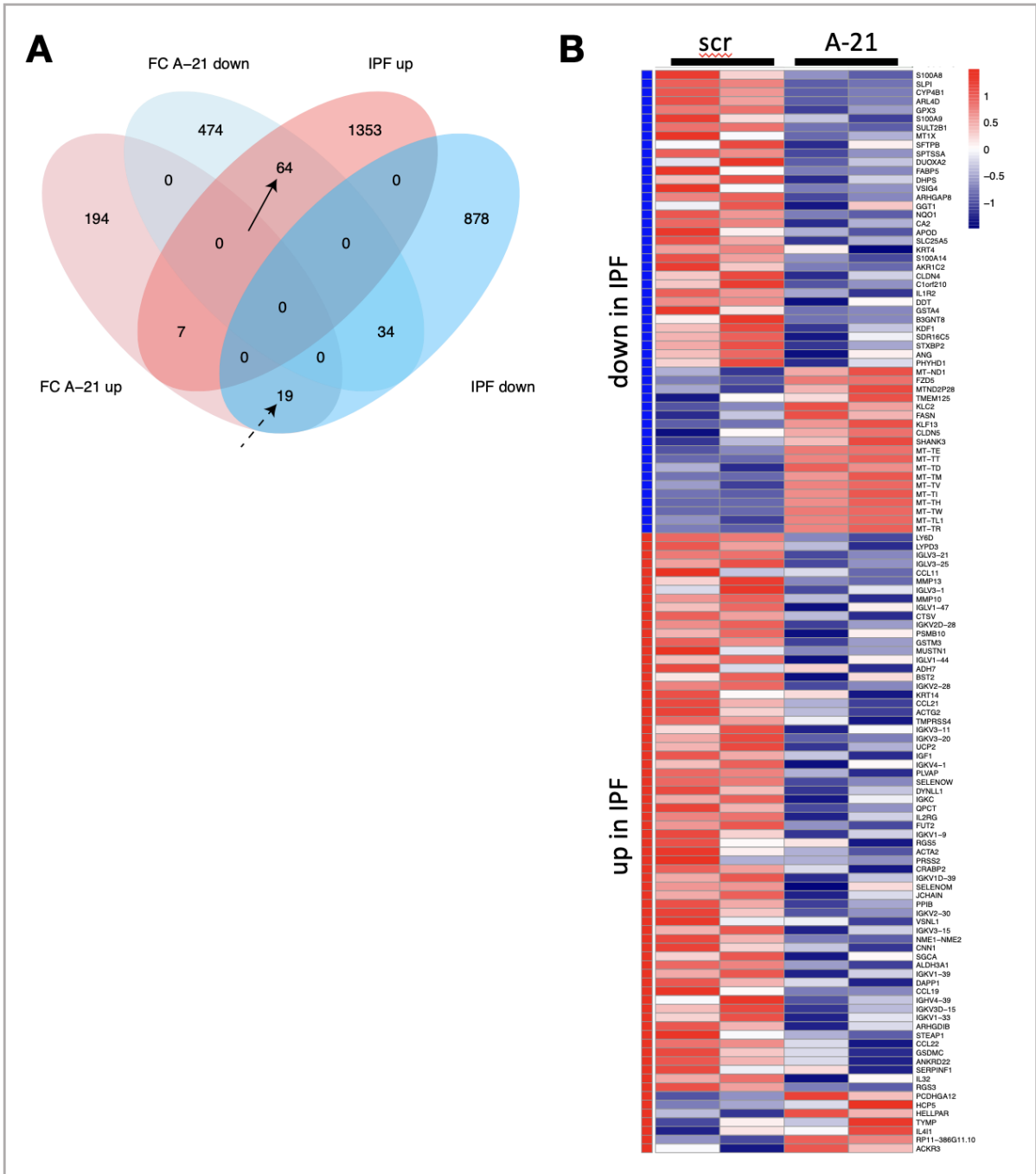


Figure 25 Comparison of transcriptome changes between IPF and FC-PCLS treated with A-21.

A. Venn diagram showing intersections of up- and downregulated genes in FC-PCLS treated with anti-miR-21 (A-21) or scrambled control (scr) and IPF; the uniform line arrow indicates the genes that are upregulated in IPF but downregulated in A-21-treated FC-PCLS and the dashed arrow points to genes that are downregulated in IPF but upregulated in A-21-treated FC-PCLS. **B.** Heatmap of differentially expressed genes between FC-PCLS treated with A-21 or scr, compared to deregulated genes in IPF lungs versus healthy donors. FC-PCLS: PCLS

treated with fibrosis cocktail, FC A-21: FC-PCLS treated with antimiR-21, down:
downregulated, up: upregulated, IPF: idiopathic pulmonary fibrosis.

Taken together, the transcriptomic data on the *ex vivo* human fibrosis model in PCLS revealed similarities with IPF and relevant fibrosis-associated pathways were connected. What is more, antimiR-21 transfection of PCLS treated with the fibrosis cocktail reduced the expression of fibrosis-related genes and led to the suppression of pathways activated in fibrosis cocktail-treated PCLS.

DISCUSSION

Chapter 1: miRnome and miR-21 targetome in bleomycin-induced pulmonary fibrosis

While other groups have previously studied microRNA deregulation in mouse models of pulmonary fibrosis in a high throughput manner with the use of microRNA arrays [86], [87], this methodology requires previous knowledge about the sequences, and a pre-selected pool of microRNAs is studied. In contrast, sequencing methods do not need this a priori information because the alignment of the sequenced nucleic acids to the genome represents a downstream step. This provides the additional advantage that when advancements in genome annotation are introduced, such as the annotation of new miRNAs and annotations for new species, among others, the (mi)RNA-Seq raw data does not become outdated; instead, it can be reanalyzed with this new information. With these advantages in mind, in this study, microRNA sequencing was performed on mouse lung cells after bleomycin-induced pulmonary fibrosis to study the changes of microRNAs expression at the whole miRnome level.

On the one hand, previously reported upregulated and downregulated microRNAs in mouse models of lung fibrosis were confirmed, such as the upregulation of miR-21a and miR-34a [65] and the downregulation of miR-125a [88] and miR-484 [89]. On the other hand, formerly unreported upregulated microRNAs in bleomycin-induced pulmonary fibrosis were also found, e.g. miR-340 and miR-16 and miR-10b, which was found to be associated with EMT in breast cancer [90].

In addition, the differential enrichment of these microRNAs in immune and non-immune cells was analyzed under bleomycin conditions, providing guidance for future studies on which cell types these microRNAs are more likely to exert their effects. For instance, miR-34a was found to be upregulated in bleomycin and enriched in immune cells, though this microRNA has been mainly studied in epithelial cells [91], [92]. Also, it was found that miR-142 is upregulated in bleomycin and enriched in the CD45+ fraction, consistent with Su *et al* 2015 [93] findings that miR-142 inhibition in profibrotic macrophages inhibits macrophage-induced fibrogenesis in co-cultured fibroblasts but not in fibroblasts cultured alone.

In particular, one of the crucial findings was that microRNA-21 represented the upregulated miR with the highest expression, which suggests that it is a key microRNA in lung fibrosis,

since it is known that a microRNA needs to have a strong expression for effective repression of its target genes [94]. Furthermore, Liu *et al* 2010 [65] showed that inhibition of miR-21 reduced the progression of bleomycin-induced lung fibrosis.

With the aim to identify the cell type in which this microRNA may be exerting its pathologic effects, the identification of its targetome in lung fibrosis was carried out. Taken together the facts that miR-21 was found to be enriched in the CD45+ fraction of fibrotic lungs, that macrophage numbers increase upon bleomycin injury [95], [96] and that infiltrating monocyte-derived macrophages as opposed to resident alveolar macrophages drive lung fibrosis [25], [97], miR-21 targets repression was assessed in CD11b^{hi} and SiglecF^{hi} lung macrophages and it was found that strong target repression occurs in CD11b^{hi} macrophages, but not in SiglecF^{hi} macrophages, suggesting that the role of miR-21 might be associated with these profibrotic macrophages.

By gene ontology analysis of the significantly downregulated miR-21 targets in CD11b^{hi} macrophages, relevant pathways in the development of lung fibrosis were identified, such as tissue remodeling, mononuclear cell differentiation, mesenchymal cell proliferation and lung epithelial cell differentiation. For example, Bmpr2 (Macrophage bone morphogenic protein receptor 2), a target related to several of the fibrotic pathways, was shown by Chen *et al* 2016 [98] to be reduced in IPF and bleomycin-induced pulmonary fibrosis; furthermore, it was expressed in macrophages of healthy subjects and mice, but depleted in IPF patients and bleomycin-exposed mice. Another example is Cdk6 (cyclin-dependent kinase 6); Birnhuber *et al* 2020 [99] recently showed that inhibition of this kinase in bleomycin-induced lung fibrosis augmented the recruitment of inflammatory cells, including macrophages.

In summary, microRNA sequencing was applied for the first time in murine lung cells after bleomycin-induced lung fibrosis, confirming previously reported deregulated miRs and identifying new ones. Additionally, their relative enrichment in immune and non-immune lung cells was quantified. Furthermore, the putative role of miR-21, the upregulated miR with the highest expression and enriched in immune cells, was delineated in macrophages by studying its targetome in these cells.

Chapter 2: miRnome and miR-21 targetome in human IPF

In order to study the changes of microRNAs expression at the whole miRnome level in human idiopathic pulmonary fibrosis, microRNA sequencing was performed on lung samples

from healthy subjects and IPF patients. With this analysis, previously reported deregulated microRNAs were confirmed, such as the upregulation of miR-21 [65] and miR-199b [40] and the downregulation of miR-30d and miR-338 [40]. Newly identified upregulated microRNAs in IPF were also found, namely, miR-205, miR-379, miR-125b (which is upregulated in cystic fibrosis [100]) and downregulated miRs, namely, miR-1260b, miR-1260, miR-582-3p, miR-3065, miR-519a-3p and miR-135a.

Comparing the human and mouse miRnome datasets, correlations between both were identified. For example, in both species miR-21-5p, miR-10b-5p and miR-199b-5p were upregulated, and miR-338-5p, miR-375-3p, miR-30d-5p and miR-200c-3p were downregulated. However, there were also differences; while miR-31-5p and miR-205-5p are upregulated in IPF, they are downregulated bleomycin-induced lung fibrosis in mice. In fact, Qian *et al* 2021 [101] showed that, not only is miR-205 downregulated in silica-induced pulmonary fibrosis in mice, but treatment with miR-205 mimics could reduce collagen levels. Similarly, while miR-223-3p and miR-30b-5p are downregulated in IPF, they are upregulated in the mouse model. This highlights the importance of taking into account possible species differences and the degree to which an animal model recapitulates the human disease when proposing novel treatments.

Further comparing both miRnome datasets, a good correlation between microRNAs abundance in mouse and human lungs was observed: 7/10 of the top 10 abundant miRs in human donor lungs are also within the top 10 in healthy mouse lungs, and 5/10 of the top 10 abundant miRs in IPF samples are also within the top 10 in mice with lung fibrosis.

Like in bleomycin-induced lung fibrosis in mice, miR-21 appeared as the highest expressed upregulated microRNA in IPF. With the aim of gaining understanding of the role of this miR in IPF, the deregulation of its targets was studied in the lung transcriptomes of IPF patients and healthy donors. The strongest miR-21 target deregulation was observed when comparing scarred IPF tissue to healthy lungs or normal-looking sections of IPF lungs, a weaker repression of miR-21 targets when comparing all IPF samples (scarred and non-scarred) to healthy samples, and no repression when comparing non-fibrotic sections of IPF lungs to healthy controls, suggesting that the effects of miR-21 upregulation are observed mainly at a later stage of the disease.

To identify the pathways associated to miR-21 deregulation, gene ontology analysis was performed on the downregulated miR-21 targets and it was found that the repressed miR-21

targets are involved in important processes for lung fibrosis such as regulation of the fibroblast growth factor signaling pathway, mesenchymal cell differentiation and regulation of leukocyte-mediated immunity.

In more detail, among the downregulated miR-21 targets there was BMP2, as was also seen in the mouse model of bleomycin-induced pulmonary fibrosis. In addition, SEMA3E (Semaphorin 3E) was also a downregulated miR-21 target, which was classified by Wang *et al* 2017 [102] as part of the core set of genes (containing only 11 genes) that allowed to distinguish IPF from healthy controls, and was also found by Schiller *et al* 2015 [103] to be downregulated at the protein level in the BALF of mice exposed to bleomycin. Another downregulated miR-21 target related to several of the GO enriched terms was SPRY2 (Sprouty RTK Signaling Antagonist 2), which is consistent with Zhao *et al* 2014 [74] findings that miR-21 regulates EMT in hepatic stellate cells by directly targeting SPRY2.

Finally, it was assessed whether miR-21 target deregulation was also evident in the BALF cells of IPF patients. However, miR-21 target repression was weaker in comparison to the lung tissue, suggesting that, in IPF, miR-21 may exert its profibrotic role primarily in lung cells compared to BALF cells.

Summing up, microRNA sequencing of IPF lung tissue confirmed previously reported deregulated miRNAs and identified new ones. The observed changes in miRs expression and the overall miRs abundance were compared to those in mouse lungs, and correlations and differences between both were delineated. One of the important similarities between human IPF and the animal model of lung fibrosis was the fact that, among the upregulated microRNAs, miR-21 is the one with the highest expression. The targetome of miR-21 was studied in lung tissue and BALF cells, and it was found that the strongest repression is observed in scarred areas of lung tissue. This target repression was further contextualized in relevant fibrosis-associated pathways.

Chapter 3: miRnome signature of mouse lung cells

To further delineate the cell type-specific expression of microRNAs in the lung, microRNA sequencing was performed on sorted mouse lung cells, namely alveolar macrophages, interstitial macrophages, T cells, endothelial cells, epithelial cells and fibroblasts. It was observed that each cell type had a characteristic microRNA signature that enabled to distinguish them from one another. Furthermore, marker microRNAs for each cell type were

identified, i.e., microRNAs that were differentially expressed compared to every other cell type.

This study showed that, in the lung, miR-21 is a marker miR of alveolar macrophages and that miR-21 is also the strongest expressed miR in this cell type, and the second most expressed miR in interstitial macrophages. This was consistent with the findings of *Ramanujam et al 2021* [104] that miR-21 was primarily expressed in mouse cardiac macrophages compared to other cardiac cells, and further increased in these cells upon cardiac fibrosis. Furthermore, *Vegh et al 2013* [105] also showed by microRNA sequencing that miR-21 was the highest expressed microRNA in bovine alveolar macrophages. At a functional level, several studies have shown that miR-21 regulates macrophage polarization [104], [106]–[110].

T cell marker and most abundant miR let-7f was shown to regulate the polarization of T cells to memory Th17 cells by repressing IL-23R [111] and *Wu et al 2007* [112] similarly showed that let-7f levels are lower in memory T cells compared to naïve cells.

Consistent with the miRnome results showing that miR-126a is a marker miR of lung endothelial cells and the most expressed miR in these cells, *Harris et al 2007* [113] showed by microRNA array that it is the highest expressed miR in the human endothelial cell line HUVEC, that it directly binds to VCAM-1 and therefore its overexpression reduces leukocyte adherence to endothelial cells.

Zhang et al 2015 [114] showed that miR-148a, which was classified in this study as a marker miR for lung epithelial cells and the second most expressed in this cell type, induces the expression of epithelial cell markers like E-cadherin, while reducing that of mesenchymal markers like N-cadherin in hepatoma cells.

MiR-145a, which was classified as a marker miR of lung fibroblasts, was shown by *Yang et al 2013* [115] to promote the differentiation of mouse and human lung fibroblasts to myofibroblasts by enhancing α -SMA expression, contractility and the formation of focal and fibrillar adhesions.

Overall, it was found that the defined marker miRs are important regulators of the functions of the corresponding cell types under homeostatic and disease conditions.

Chapter 4: miRnome signature of human lung cells

In order to analyze the cell type-specific expression of microRNAs in the human lung, microRNA sequencing was performed on sorted cells, namely macrophages, endothelial cells, epithelial cells and fibroblasts. As was the case with mouse lung cells, a characteristic microRNA profile was observed in each cell type with differentially expressed microRNAs compared to one or more other cell types and a set of marker miRs were defined, i.e., microRNAs that were differentially expressed in a cell type compared to every other cell type, for macrophages, endothelial cells and fibroblasts.

Comparing to the miRnomes of mouse lung cells, murine and human macrophages shared the marker miRNA miR-223-3p, and endothelial cells from both species shared the marker miRNA miR-126. Partial similarities were also observed, i.e., some of the microRNAs that were classified as marker miRs for mouse lung cells were not for human, but were differentially expressed compared to some of the other cell types. For instance, miR-21 is a marker miR for mouse macrophages, and in human macrophages it is differentially expressed compared to endothelial and epithelial cells, though not compared to fibroblasts. MiR-151, a marker for mouse epithelial cells, is differentially expressed in epithelial cells compared to fibroblasts and macrophages in human lungs, though not compared to endothelial cells. Lastly, miR-145, a marker miR for mouse lung fibroblasts, is differentially expressed in fibroblasts compared to macrophages and endothelial cells in human lungs, but not compared to epithelial cells.

As in the mouse lung, the microRNAs that were classified as marker for each cell type regulate important physiological functions within them. Among the newly identified marker miRs in fibroblasts there is miR-27b, which was shown by *Zeng et al 2017* [116] to be decreased in fibroblasts from bleomycin-exposed mouse lungs and TGF- β -activated human lung fibroblasts; furthermore, overexpressing miR-27b in activated human lung fibroblasts decreased collagens and α -SMA expression at the RNA and protein level, as well as the contractile activity by directly binding to SMAD2 and TGFBR1. As an additional example, deletion or inhibition of miR-155, which was classified in the present study as a marker miR in human lung macrophages, was shown by *Wang et al 2016* [117] to reduce inflammatory genes in alveolar macrophages from LPS-exposed rodents and LPS-treated bone marrow-derived macrophages by derepressing SOCS-1, a negative inflammation regulator.

In terms of abundance of microRNAs in each cell type, as was the case in mice, only 3-7 microRNAs accounted for more than 50% of all the microRNA reads. Furthermore, there was a good correlation among the 10 most abundant microRNAs in mouse and human lung cells. In macrophages and endothelial cells, 5 of the top 10 abundant miRs in the corresponding cell type were shared in mouse and human; in epithelial cells 4, and in fibroblasts 7.

In summary, microRNA sequencing of sorted human lung cells enabled the definition of cell type-specific miRnome signatures, which shared similarities and differences with their murine counterparts. Furthermore, these signature miRs were associated to key functions of these microRNAs in their corresponding cell types in health and disease.

Even though lung tissue sections from tumor-free areas of lungs from cancer patients without metastasis were used, the possibility that cancer had an effect on the transcriptome of cells away from the tumor cannot be ruled out.

Chapter 5: Characterization of human blood monocyte-derived macrophages

For the study of tissue-resident macrophage development and physiology *in vitro*, several models are traditionally used, including human blood monocyte-derived macrophages, THP-1-derived macrophages and iPSC-derived macrophages.

In the *in vitro* culture of highly adherent cells like macrophages, a common issue is the difficulty of detaching the cells from the culture plate. However, harsh methods like long trypsinization or cell scraping, which provide efficient recovery, negatively impact the viability and surface protein expression of cells and can also alter cells phenotype [80], [81], [118]–[120]. In recent years, cell culture plates with novel surface chemistry have been developed that reduce overall adherence, or when temperature is lowered, the so called thermo-responsive surfaces. *Malheiro et al 2017* [121] showed that detaching THP-1-derived macrophages by cooling from a commercial plate coated with a thermo-responsive polymer yielded higher viability than after detaching them with EDTA + scraping, independent from macrophage polarization. Therefore, with the aim of optimizing the differentiation and culture of primary monocyte-derived macrophages used in this study to retain high viability and surface proteins expression, two different commercially available cell culture plates were tested, namely, Corning Ultra-Low Attachment plates, which have a hydrophilic surface that

minimizes adherence and spreading, and Nunc UpCell plates, which have a hydrophobic surface at cell culture temperature (37 °C) but become hydrophilic at RT, facilitating detachment of cells.

In terms of morphology, macrophage differentiation was successful in both plates. However, more cells, with higher viability and higher surface expression of the macrophage markers CD68 and CD206 were obtained after detaching them from Nunc UpCell plates in comparison to Corning plates. Nevertheless, incubation at low temperature for 20 min was not sufficient to effectively recover most macrophages, so a mild enzymatic treatment with Accutase was included to aid in the detachment. *Chen et al 2015* [118] reported that Accutase-driven detachment of monocyte-derived macrophages yielded a higher cell viability than scraping, and a higher surface protein expression than trypsinization. Indeed, in the present study it was observed that the viability of cells was high after detachment (>80%) and the flow cytometry signals from surface markers were bright and clearly shifted with respect to unstained cells.

Once the culture of the monocyte-derived macrophages was optimized, it was assessed whether there were differences between macrophages differentiated in the presence of GM-CSF or M-CSF that could be associated to either an AM- or IM-like phenotype. For this, differences between M- and GM-Mac were assessed in terms of morphology, surface markers expression and miR-21 expression.

Monocytes differentiated from small round cells to have a distinct macrophage morphology. GM-Mac had a “fried-egg” morphology, more similar to the morphology of isolated primary alveolar macrophages, while M-Mac were more heterogeneous, some adopted a rounder shape as GM-Mac, whereas others adopted a spindle-like morphology. These differences in morphology were also observed by *Brocheriou et al 2011* [122].

In order to study whether blood monocyte-derived macrophages highly expressed miR-21 as lung macrophages, microRNA sequencing was performed on Mo-Mac and it was found that miR-21 was indeed highly expressed, constituting the most abundant microRNA in both macrophage subtypes. However, miR-21-5p was not differentially expressed between the two macrophage types, which was also corroborated by RT-qPCR.

In terms of surface markers expression, CD68, CD206, CD14 and CD169 were analyzed by flow cytometry. CD68 is a pan-monocyte/macrophage marker [123], [124]; CD206, though commonly used as a marker of M2 macrophage polarization in other tissues [93], [125],

[126], it is highly expressed in lung macrophages under homeostatic conditions, especially in alveolar macrophages compared to interstitial macrophages [83], [84], [124]; CD14 is a pan-monocyte marker, which is also expressed in most macrophages, with alveolar macrophages having a marked lower expression compared to interstitial macrophages [83], [124], and CD169 is commonly used as marker for alveolar macrophages [83], [84], [127]. As quantified by flow cytometry, >88% of cells were macrophages (SSC^{hi} CD45⁺ CD68⁺). There was no significant difference in surface expression of CD68, CD206 or CD169 between GM- and M-Mac, but M-Mac had a slightly higher surface expression of CD14. Discordant results have been reported in the literature regarding these markers expression in GM- and M-Mac; *Brocheriou et al 2011* [122] observed higher expression levels of CD206 at the RNA level in GM-Mac compared to M-Mac and no differences for CD68 or CD14, while *Lescoat et al 2018* [128] did not find differences in CD206 levels by flow cytometry and *Lukic et al 2017* [129] observed higher CD14 surface protein expression in M-Mac compared to GM-Mac. These disagreements in results are likely due to differences in growth factors concentrations used and time of differentiation.

Taking together morphology, surface markers expression and miR-21 levels, both M- and GM-Mac share similarities and differences with human lung alveolar and interstitial macrophages.

Finally, it was assessed how M- and GM-Mac responded to TGF- β , a profibrotic cytokine known to be upregulated in IPF [52], in terms of miR-21 expression. *Yamada et al 2013* [46] found that miR-21 is upregulated in epithelial cells from mice with bleomycin-induced pulmonary fibrosis, in IPF patients and upon TGF- β -induced EMT in cultured mouse epithelial cells; furthermore, they found that *in vitro* inhibition of miR-21 reversed TGF- β -induced EMT. MiR-21 was also found upregulated in fibroblasts from IPF lungs [130], in mice with bleomycin-induced pulmonary fibrosis [46] and in TGF- β -stimulated human fibroblasts cell lines [48], [65]; furthermore, both *Liu et al 2010* and *Yao et al 2011* observed that TGF- β -induced fibroblast activation was enhanced or reversed upon treatment with miR-21 mimics or anti-miR-21, respectively. Nonetheless, under the experimental conditions used in this study, there was no upregulation of miR-21 levels upon TGF- β treatment at any of the concentrations tested in GM- nor in M-Mac. It is of importance then, to employ a more complex milieu that better represents the cytokines environment in IPF.

Shortly, in this chapter the relevance of surface properties of cell culture plates in the culture and differentiation of human blood monocyte-derived macrophages was highlighted, and the

similarities and differences between Mo-Mac differentiated in the presence of GM-CSF or M-CSF were characterized in terms of morphology, surface markers expression and endogenous miR-21 levels.

Chapter 6: Transcriptome analysis of a human *ex vivo* model of lung fibrosis using PCLS and antimiR-21 treatment

MiR-21 inhibition or knock-out has proven successful in dampening fibrosis *in vivo* in several tissues and species [65], [104], [131] as well as in *in vitro* human and non-human models [48], [65]. However, the majority of studies in human cells have focused on a single cell type, mostly cell lines, or at most in co-culture with a few other cell types [132], [133], which fails to recapitulate the morphology and cells heterogeneity and cross-talk in native lungs. In the last decades, more advanced models have been developed, such as organoids [134], [135], organ-on-a-chip [136], [137] and PCLS [138], [139]. From these, PCLS naturally resemble the most native lungs, as they are *ex vivo* sections from real lungs, and have proved useful in the study of cytotoxicity [140], bronchoconstriction [138] and, especially interestingly for us, lung fibrosis. Recently, *Alsafadi et al 2017* [85] presented an *ex vivo* model of lung fibrosis using PCLS and *Lehmann et al 2018* used it to study the effects of Nintedanib (an approved drug against IPF) treatment.

The characterization of this human lung fibrosis model was made with a few fibrosis marker genes and proteins. In this study, the aims were to analyze at the whole transcriptome level by RNA-Seq the similarities to IPF and to test whether inhibition of antimiR-21 has a therapeutic effect.

Differential expression analysis between FC- and CC-PCLS showed the upregulation of classically elevated genes and proteins in IPF such as COL10A1 [141], CCL18 [142], [143], MMP10 [144] and MMP3 [145]. The upregulation of genes reported in the original study was also observed, namely, ACTA2 and COL1A1. Even though there was no upregulation of SERPINE1, MMP7 nor WNT5A as in the publication, there was upregulations of genes of the same families, such as SERPINE2, MMP10 and WNT5B. In terms of associated signaling pathways, gene ontology and gene set enrichment analysis performed using multiple databases, all identified relevant processes like “extracellular matrix organization”, “MAP kinase activation” and “epithelial mesenchymal transition”, which are hallmarks in lung fibrosis [27], [146], [147].

Furthermore, when comparing the transcriptome of FC-PCLS to a public RNA-Seq dataset of IPF and healthy donors [143], similarities were observed between the fibrosis PCLS model and IPF: 46 genes were upregulated both in the *ex vivo* fibrosis model and in IPF patients, including ACTA2, COL1A1, COL10A1, CCL11 and TAGLN; and 1 gene was downregulated in both datasets. There were fewer genes that displayed an opposite regulation, e.g., CXCL9 and ITGB7 are upregulated in IPF, but downregulated in FC-treated PCLS, while SERPINB2 and S100A8 are downregulated in the IPF dataset but upregulated in FC-PCLS. Other studies have shown opposing results in terms of SERPINB2 and S100A8 regulation; *Sivakumar et al 2019* [148] reported that SERPINB2 expression was upregulated in transplant-stage IPF patients; similarly, *Kotani et al 1995* [149] observed increased protein levels of SERPINB2 (also known as PAI-2) in the BALF of IPF patients. S100A8 protein levels were shown to be increased in the serum of IPF patients with acute exacerbation [150], while *Sivakumar et al 2019* [148] observed downregulation of its gene expression in lungs from IPF patients.

Taken together, at the whole transcriptome level remarkable similarities between the *ex vivo* fibrosis model and IPF were shown and further evidence was provided towards the suitability of this model to study the pathological features of lung fibrosis. As an *ex vivo* model, a clear drawback is the lack of input of circulating blood cells, such as monocytes, which have been shown to be key players in *in vivo* models of lung fibrosis [25], [97].

In a therapeutic approach against lung fibrosis, it was studied whether miR-21 inhibition in the FC-treated PCLS would have an anti-fibrotic effect. Indeed, the fibrosis-related genes that were upregulated in FC-PCLS, such as MMP3, MMP13, MMP10, CCL11 and CCL20, were downregulated after miR-21 inhibition. From an overall pathway perspective, gene set enrichment analysis showed that inhibition of miR-21 reduced inflammatory signaling pathways (NF- κ B, IL-1 family), keratinization, leukocyte migration, phagocytosis, apoptosis, and proliferation; processes that are activated in FC-PCLS. In order to further study the relevance of the transcriptomic changes after miR-21 inhibition in FC-PCLS in relation to IPF, the gene expression was compared to that of a public IPF RNA-Seq dataset [143]. When FC-PCLS were treated with anti-miR-21, 64 of the genes that are upregulated in IPF, became downregulated, including ACTA2, CCL11, CCL19, MMP13 and MMP10. Likewise, 19 genes that are downregulated in IPF, were upregulated in the anti-miR-21-treated FC-PCLS, mostly mitochondrial genes.

Even though anti-miR-21 treatment at the utilized concentration had mild effects on miR-21 targetome regulation, the slight de-repression of miR-21 targets were indicative of negative regulation of TGF- β , activin and MAPK signaling pathways, which are activated in IPF [52], [147], [151]–[153], though there was also indication of negative regulation of the BMP signaling pathway, which is also inhibited in lung fibrosis [154], [155]. Stronger miR-21 targetome de-repression might be observed at a longer timepoint after transfection and/or with higher anti-miR-21 concentrations, which would be interesting to study in the future to gain a clearer vision of the mechanisms of action.

Collectively, these results show that miR-21 inhibition dampens fibrosis-associated gene expression in a human *ex vivo* model of lung fibrosis. Further studies are required to assess if these observed changes are also reflected at the protein and functional level, and to investigate the molecular mechanisms that drive them. Additionally, experiments involving a larger number of biological samples should be conducted to ensure that the effects are independent of patient-to-patient variability. What is more, a step further would be to investigate whether PCLS derived from IPF lungs are also able to respond to the treatment.

CONCLUSION AND FUTURE PERSPECTIVES

In the present study, microRNA sequencing was performed for the first time in the lungs from IPF patients and bleomycin-induced lung fibrosis in mice, which allowed to assess at the whole miRnome level the expression changes of these small non-coding RNAs during disease, confirming previous findings and identifying newly dysregulated microRNAs.

A crucial finding was that miR-21 was the highest expressed upregulated microRNA. In mice, its increase was correlated with miR-21 gene targets repression in a population of CD11b^{hi} SiglecF^{lo} but not CD11b^{lo} SiglecF^{hi} macrophages, consistent with previous studies categorizing the first as important drivers of fibrosis [25], [97], as well as the fact that miR-21 was found to be enriched in the immune cell fraction compared to non-immune cells. In humans, the increase in miR-21 levels was correlated with miR-21 target repression in scarred lung tissue from IPF patients. In contrast, such a correlation was not observed with non-scarred IPF lung tissue sections, nor was it observed with BALF cells. Furthermore, putative fibrosis-associated pathways were identified, where the deregulated gene targets might be involved.

In addition, the miRnome signatures and miRNAs relative abundances in several cell types from healthy mouse and human lungs, as well as in human blood monocyte-derived macrophages were characterized. In particular, miR-21 was mainly and highly expressed in macrophages compared to T cells, endothelial cells, epithelial cells and fibroblasts. These data should provide a solid starting point to the investigation of microRNAs cell type-specific functions.

A limitation of this work is that, even though main cell types in the lung were characterized, information is lacking on other cell types, e.g., B cells and mast cells, though these are encountered in lower proportions than other immune cells like macrophages [124]. Moreover, the analysis of microRNA expression changes in disease within defined cell populations will be important, as this was so far studied in bulk.

Given the prospective therapeutic effects of miR-21 inhibition in *in vivo* and *in vitro* models of fibrotic diseases observed in several species [48], [65], I sought to determine whether miR-21 inhibition had a therapeutic potential in a human *ex vivo* model of lung fibrosis using PCLS. It was first corroborated at the whole transcriptome level that this is a suitable model

for IPF and it was further observed that the fibrosis-associated phenotype was reduced upon miR-21 inhibition.

Even though this is a promising finding and provides additional evidence of the suitability of antimiR-21 as an anti-fibrotic and anti-inflammatory drug, it is yet to be determined whether the observed transcriptomic changes translate to the protein and functional level. In addition, testing this treatment in IPF-derived PCLS is crucial to assess whether it could provide a therapeutic effect in already established disease.

In summary, this study suggests an important pathological role of miR-21 in lung fibrosis and the potential of using miR-21 inhibitors as an anti-fibrotic and anti-inflammatory therapeutic strategy against pulmonary disease.

REFERENCES

- [1] F. J. Martinez *et al.*, "Idiopathic pulmonary fibrosis," *Nat. Rev. Dis. Prim.*, vol. 3, pp. 1–20, 2017, doi: 10.1038/nrdp.2017.74.
- [2] J. Hutchinson, A. Fogarty, R. Hubbard, and T. McKeever, "Global incidence and mortality of idiopathic pulmonary fibrosis: A systematic review," *Eur. Respir. J.*, vol. 46, no. 3, pp. 795–806, 2015, doi: 10.1183/09031936.00185114.
- [3] B. Kaul, V. Cottin, H. R. Collard, and C. Valenzuela, "Variability in Global Prevalence of Interstitial Lung Disease," *Front. Med.*, vol. 8, no. November, pp. 1–10, 2021, doi: 10.3389/fmed.2021.751181.
- [4] B. Ley and H. Collard, "Epidemiology of idiopathic pulmonary fibrosis," *Clin. Epidemiol.*, p. 483, Nov. 2013, doi: 10.2147/CLEP.S54815.
- [5] O. Kalchiem-Dekel, J. R. Galvin, A. P. Burke, S. P. Atamas, and N. W. Todd, "Interstitial lung disease and pulmonary fibrosis: A practical approach for general medicine physicians with focus on the medical history," *J. Clin. Med.*, vol. 7, no. 12, 2018, doi: 10.3390/jcm7120476.
- [6] ATS; ERS, "American Thoracic Society Idiopathic Pulmonary Fibrosis : Diagnosis and Treatment," *Am. J. Respir. Crit. Care Med.*, vol. 161, pp. 646–664, 2000, doi: 10.1164/ajrccm.161.2.ats3-00.
- [7] W. A. Wuyts, A. Cavazza, G. Rossi, F. Bonella, N. Sverzellati, and P. Spagnolo, "Differential diagnosis of usual interstitial pneumonia: When is it truly idiopathic?," *Eur. Respir. Rev.*, vol. 23, no. 133, pp. 308–319, 2014, doi: 10.1183/09059180.00004914.
- [8] M. L. Smith, "The histologic diagnosis of usual interstitial pneumonia of idiopathic pulmonary fibrosis. Where we are and where we need to go," *Mod. Pathol.*, vol. 35, no. June 2021, pp. 8–14, 2022, doi: 10.1038/s41379-021-00889-5.
- [9] B. Ley, H. R. Collard, and T. E. King, "Clinical course and prediction of survival in idiopathic pulmonary fibrosis," *Am. J. Respir. Crit. Care Med.*, vol. 183, no. 4, pp. 431–440, 2011, doi: 10.1164/rccm.201006-0894CI.
- [10] J. Kaunisto *et al.*, "Demographics and survival of patients with idiopathic pulmonary fibrosis in the FinnishIPF registry," *ERJ Open Res.*, vol. 5, no. 3, 2019, doi: 10.1183/23120541.00170-2018.
- [11] T. A. Wynn, "Integrating mechanisms of pulmonary fibrosis," *J. Exp. Med.*, vol. 208, no. 7, pp. 1339–1350, 2011, doi: 10.1084/jem.20110551.
- [12] J. Tashiro *et al.*, "Exploring animal models that resemble idiopathic pulmonary fibrosis," *Front. Med.*, vol. 4, no. JUL, pp. 1–11, 2017, doi: 10.3389/fmed.2017.00118.
- [13] R. Peng *et al.*, "Bleomycin Induces Molecular Changes Directly Relevant to Idiopathic Pulmonary Fibrosis: A Model for 'Active' Disease," *PLoS One*, vol. 8, no. 4, 2013, doi: 10.1371/journal.pone.0059348.
- [14] G. Izbicki, M. J. Segel, T. G. Christensen, M. W. Conner, and R. Breuer, "Time course of bleomycin-induced lung fibrosis," *Int. J. Exp. Pathol.*, vol. 83, no. 3, pp. 111–119, 2002, doi: 10.1046/j.1365-2613.2002.00220.x.
- [15] P. W. Noble, "Epithelial fibroblast triggering and interactions in pulmonary fibrosis," *Eur. Respir. Rev.*, vol. 17, no. 109, pp. 123–129, 2008, doi: 10.1183/09059180.00010904.
- [16] M. Selman and A. Pardo, "The leading role of epithelial cells in the pathogenesis of

- idiopathic pulmonary fibrosis," *Cell. Signal.*, vol. 66, p. 109482, 2020, doi: 10.1016/j.cellsig.2019.109482.
- [17] F. Chua and G. Laurent, "Encyclopedia of Respiratory Medicine," in *Encyclopedia of Respiratory Medicine*, 1st ed., G. J. Laurent and S. Shapiro, Eds. Academic Press, 2006, pp. 213–219.
- [18] R. T. Kendall and C. A. Feghali-Bostwick, "Fibroblasts in fibrosis: Novel roles and mediators," *Front. Pharmacol.*, vol. 5 MAY, no. May, pp. 1–13, 2014, doi: 10.3389/fphar.2014.00123.
- [19] J. West and A. Luks, *West's Respiratory physiology*, 10th ed. Wolters Kluwer Health, 2016.
- [20] C. K. Probst, S. B. Montesi, B. D. Medoff, B. S. Shea, and R. S. Knipe, "Vascular permeability in the fibrotic lung," *Eur. Respir. J.*, vol. 56, no. 1, 2020, doi: 10.1183/13993003.00100-2019.
- [21] J. Schyns, F. Bureau, and T. Marichal, "Lung interstitial macrophages: Past, present, and future," *J. Immunol. Res.*, vol. 2018, 2018, doi: 10.1155/2018/5160794.
- [22] T. Ogawa, S. Shichino, S. Ueha, and K. Matsushima, "Macrophages in lung fibrosis," *Int. Immunol.*, vol. 33, no. 12, pp. 665–671, 2021, doi: 10.1093/intimm/dxab040.
- [23] A. V. Misharin *et al.*, "Monocyte-derived alveolar macrophages drive lung fibrosis and persist in the lung over the life span," *J. Exp. Med.*, vol. 214, no. 8, pp. 2387–2404, 2017, doi: 10.1084/jem.20162152.
- [24] B. B. Moore *et al.*, "Protection from Pulmonary Fibrosis in the Absence of CCR2 Signaling," *J. Immunol.*, vol. 167, no. 8, pp. 4368–4377, 2001, doi: 10.4049/jimmunol.167.8.4368.
- [25] J. J. Osterholzer *et al.*, "Implicating Exudate Macrophages and Ly-6C high Monocytes in CCR2-Dependent Lung Fibrosis following Gene-Targeted Alveolar Injury," *J. Immunol.*, vol. 190, no. 7, pp. 3447–3457, 2013, doi: 10.4049/jimmunol.1200604.
- [26] M. A. Gibbons *et al.*, "Ly6Chi monocytes direct alternatively activated profibrotic macrophage regulation of lung fibrosis," *Am. J. Respir. Crit. Care Med.*, vol. 184, no. 5, pp. 569–581, 2011, doi: 10.1164/rccm.201010-1719OC.
- [27] S. Kolahian, I. E. Fernandez, O. Eickelberg, and D. Hartl, "Immune mechanisms in pulmonary fibrosis," *Am. J. Respir. Cell Mol. Biol.*, vol. 55, no. 3, pp. 309–322, 2016, doi: 10.1165/rcmb.2016-0121TR.
- [28] L. Barron and T. A. Wynn, "Fibrosis is regulated by Th2 and Th17 responses and by dynamic interactions between fibroblasts and macrophages," *Am. J. Physiol. - Gastrointest. Liver Physiol.*, vol. 300, no. 5, pp. 723–729, 2011, doi: 10.1152/ajpgi.00414.2010.
- [29] M. E. Snyder and D. L. Farber, "Human lung tissue resident memory T cells in health and disease," *Curr. Opin. Immunol.*, vol. 59, pp. 101–108, 2019, doi: 10.1016/j.coi.2019.05.011.
- [30] G. Cruse and P. Bradding, "Mast cells in airway diseases and interstitial lung disease," *Eur. J. Pharmacol.*, vol. 778, pp. 125–138, May 2016, doi: 10.1016/j.ejphar.2015.04.046.
- [31] J. M. Felton, C. D. Lucas, A. G. Rossi, and I. Dransfield, "Eosinophils in the Lung - Modulating Apoptosis and Efferocytosis in Airway Inflammation," *Front. Immunol.*, vol. 5, no. 302, Jul. 2014, doi: 10.3389/fimmu.2014.00302.
- [32] P. C. Cook and A. S. MacDonald, "Dendritic cells in lung immunopathology," *Semin. Immunopathol.*, vol. 38, no. 4, pp. 449–460, Jul. 2016, doi: 10.1007/s00281-016-0571-

- 3.
- [33] F. Polverino, L. J. M. Seys, K. R. Bracke, and C. A. Owen, "B cells in chronic obstructive pulmonary disease: moving to center stage," *Am. J. Physiol. Cell. Mol. Physiol.*, vol. 311, no. 4, pp. L687–L695, Oct. 2016, doi: 10.1152/ajplung.00304.2016.
- [34] M. Menon, T. Hussell, and H. Ali Shuwa, "Regulatory B cells in respiratory health and diseases," *Immunol. Rev.*, vol. 299, no. 1, pp. 61–73, Jan. 2021, doi: 10.1111/imr.12941.
- [35] S. W. Eichhorn *et al.*, "MRNA Destabilization Is the dominant effect of mammalian microRNAs by the time substantial repression ensues," *Mol. Cell*, vol. 56, no. 1, pp. 104–115, 2014, doi: 10.1016/j.molcel.2014.08.028.
- [36] D. P. Bartel, R. Lee, and R. Feinbaum, "MicroRNAs : Genomics , Biogenesis , Mechanism , and Function Genomics : The miRNA Genes," vol. 116, pp. 281–297, 2004, doi: 10.1016/j.cell.2004.12.035.
- [37] I. G. Gomez, N. Nakagawa, and J. S. Duffield, "MicroRNAs as novel therapeutic targets to treat kidney injury and fibrosis," *Am. J. Physiol. - Ren. Physiol.*, vol. 310, no. 10, pp. F931–F944, 2016, doi: 10.1152/ajprenal.00523.2015.
- [38] E. Rooij and S. Kauppinen, " Development of micro RNA therapeutics is coming of age ," *EMBO Mol. Med.*, vol. 6, no. 7, pp. 851–864, 2014, doi: 10.15252/emmm.201100899.
- [39] J. Hanna, G. S. Hossain, and J. Kocerha, "The potential for microRNA therapeutics and clinical research," *Front. Genet.*, vol. 10, no. MAY, 2019, doi: 10.3389/fgene.2019.00478.
- [40] K. V. Pandit *et al.*, "Inhibition and role of let-7d in idiopathic pulmonary fibrosis," *Am. J. Respir. Crit. Care Med.*, vol. 182, no. 2, pp. 220–229, 2010, doi: 10.1164/rccm.200911-1698OC.
- [41] D. Lacedonia *et al.*, "Downregulation of exosomal let-7d and miR-16 in idiopathic pulmonary fibrosis," *BMC Pulm. Med.*, vol. 21, no. 1, p. 188, Dec. 2021, doi: 10.1186/s12890-021-01550-2.
- [42] X. Yu *et al.*, "miR-let-7d attenuates EMT by targeting HMGA2 in silica-induced pulmonary fibrosis," *RSC Adv.*, vol. 9, no. 34, pp. 19355–19364, 2019, doi: 10.1039/C9RA01031A.
- [43] C. Mao *et al.*, "MiRNA-30a inhibits AECs-II apoptosis by blocking mitochondrial fission dependent on Drp-1," *J. Cell. Mol. Med.*, vol. 18, no. 12, pp. 2404–2416, Dec. 2014, doi: 10.1111/jcmm.12420.
- [44] S. Zhang *et al.*, "miR-30a as Potential Therapeutics by Targeting TET1 through Regulation of Drp-1 Promoter Hydroxymethylation in Idiopathic Pulmonary Fibrosis," *Int. J. Mol. Sci.*, vol. 18, no. 3, p. 633, Mar. 2017, doi: 10.3390/ijms18030633.
- [45] G. Liu *et al.*, "miR-21 mediates fibrogenic activation of pulmonary fibroblasts and lung fibrosis," *J. Exp. Med.*, vol. 207, no. 8, pp. 1589–1597, 2010, doi: 10.1084/jem.20100035.
- [46] M. Yamada *et al.*, "The increase of microRNA-21 during lung fibrosis and its contribution to epithelial-mesenchymal transition in pulmonary epithelial cells," *Respiratory Research*, vol. 14, no. 1. 2013, doi: 10.1186/1465-9921-14-95.
- [47] H. Dirol *et al.*, "Alterations in plasma miR-21, miR-590, miR-192 and miR-215 in idiopathic pulmonary fibrosis and their clinical importance," *Mol. Biol. Rep.*, Jan. 2022, doi: 10.1007/s11033-021-07045-x.
- [48] Q. Yao, S. Cao, C. Li, A. Mengesha, B. Kong, and M. Wei, "Micro-RNA-21 regulates

- TGF- β -induced myofibroblast differentiation by targeting PDCD4 in tumor-stroma interaction," *Int. J. Cancer*, vol. 128, no. 8, pp. 1783–1792, 2011, doi: 10.1002/ijc.25506.
- [49] J. Milosevic *et al.*, "Profibrotic Role of miR-154 in Pulmonary Fibrosis," *Am. J. Respir. Cell Mol. Biol.*, vol. 47, no. 6, pp. 879–887, Dec. 2012, doi: 10.1165/rcmb.2011-0377OC.
- [50] S. Rajasekaran, P. Rajaguru, and P. S. Sudhakar Gandhi, "MicroRNAs as potential targets for progressive pulmonary fibrosis," *Front. Pharmacol.*, vol. 6, no. NOV, pp. 1–15, 2015, doi: 10.3389/fphar.2015.00254.
- [51] K. V. Pandit, J. Milosevic, and N. Kaminski, "MicroRNAs in idiopathic pulmonary fibrosis," *Transl. Res.*, vol. 157, no. 4, pp. 191–199, 2011, doi: 10.1016/j.trsl.2011.01.012.
- [52] I. E. Fernandez and O. Eickelberg, "New cellular and molecular mechanisms of lung injury and fibrosis in idiopathic pulmonary fibrosis," *Lancet*, vol. 380, no. 9842, pp. 680–688, 2012, doi: 10.1016/S0140-6736(12)61144-1.
- [53] X. Liu, H. Liu, X. Jia, R. He, X. Zhang, and W. Zhang, "Changing Expression Profiles of Messenger RNA, MicroRNA, Long Non-coding RNA, and Circular RNA Reveal the Key Regulators and Interaction Networks of Competing Endogenous RNA in Pulmonary Fibrosis," *Front. Genet.*, vol. 11, Sep. 2020, doi: 10.3389/fgene.2020.558095.
- [54] D. Bautista-Sánchez *et al.*, "The Promising Role of miR-21 as a Cancer Biomarker and Its Importance in RNA-Based Therapeutics," *Mol. Ther. - Nucleic Acids*, vol. 20, pp. 409–420, Jun. 2020, doi: 10.1016/j.omtn.2020.03.003.
- [55] M. V. Iorio *et al.*, "MicroRNA Signatures in Human Ovarian Cancer," *Cancer Res.*, vol. 67, no. 18, pp. 8699–8707, Sep. 2007, doi: 10.1158/0008-5472.CAN-07-1936.
- [56] I. Akagi *et al.*, "Combination of Protein Coding and Noncoding Gene Expression as a Robust Prognostic Classifier in Stage I Lung Adenocarcinoma," *Cancer Res.*, vol. 73, no. 13, pp. 3821–3832, Jul. 2013, doi: 10.1158/0008-5472.CAN-13-0031.
- [57] K. Danielsson, Y. B. Wahlin, X. Gu, L. Boldrup, and K. Nylander, "Altered expression of miR-21, miR-125b, and miR-203 indicates a role for these microRNAs in oral lichen planus," *J. Oral Pathol. Med.*, vol. 41, no. 1, pp. 90–95, Jan. 2012, doi: 10.1111/j.1600-0714.2011.01084.x.
- [58] C. B. Lajer *et al.*, "Different miRNA signatures of oral and pharyngeal squamous cell carcinomas: a prospective translational study," *Br. J. Cancer*, vol. 104, no. 5, pp. 830–840, Mar. 2011, doi: 10.1038/bjc.2011.29.
- [59] R. Kumarswamy, I. Volkmann, and T. Thum, "Regulation and function of miRNA-21 in health and disease," *RNA Biol.*, vol. 8, no. 5, pp. 706–713, 2011, doi: 10.4161/rna.8.5.16154.
- [60] S. Surina, R. A. Fontanella, L. Scisciola, R. Marfella, G. Paolisso, and M. Barbieri, "miR-21 in Human Cardiomyopathies," *Front. Cardiovasc. Med.*, vol. 8, Oct. 2021, doi: 10.3389/fcvm.2021.767064.
- [61] T. Zhang, Z. Yang, P. Kusumanchi, S. Han, and S. Liangpunsakul, "Critical Role of microRNA-21 in the Pathogenesis of Liver Diseases," *Front. Med.*, vol. 7, Jan. 2020, doi: 10.3389/fmed.2020.00007.
- [62] E. Raitoharju *et al.*, "miR-21, miR-210, miR-34a, and miR-146a/b are up-regulated in human atherosclerotic plaques in the Tampere Vascular Study," *Atherosclerosis*, vol. 219, no. 1, pp. 211–217, Nov. 2011, doi: 10.1016/j.atherosclerosis.2011.07.020.
- [63] Y. Zhang, J. Jia, S. Yang, X. Liu, S. Ye, and H. Tian, "MicroRNA-21 controls the

- development of osteoarthritis by targeting GDF-5 in chondrocytes," *Exp. Mol. Med.*, vol. 46, no. 2, pp. e79–e79, Feb. 2014, doi: 10.1038/emm.2013.152.
- [64] "clinicaltrials.gov." <https://clinicaltrials.gov/> (accessed Feb. 04, 2022).
- [65] G. Liu *et al.*, "miR-21 mediates fibrogenic activation of pulmonary fibroblasts and lung fibrosis," *J. Exp. Med.*, vol. 207, no. 8, pp. 1589–1597, 2010, doi: 10.1084/jem.20100035.
- [66] J. Wang *et al.*, "Resveratrol inhibits pulmonary fibrosis by regulating miR-21 through MAPK/AP-1 pathways," *Biomed. Pharmacother.*, vol. 105, no. May, pp. 37–44, 2018, doi: 10.1016/j.biopha.2018.05.104.
- [67] Y. Hiyoshi *et al.*, "MicroRNA-21 regulates the proliferation and invasion in esophageal squamous cell carcinoma," *Clin. Cancer Res.*, vol. 15, no. 6, pp. 1915–1922, 2009, doi: 10.1158/1078-0432.CCR-08-2545.
- [68] I. A. Asangani *et al.*, "MicroRNA-21 (miR-21) post-transcriptionally downregulates tumor suppressor Pcd4 and stimulates invasion, intravasation and metastasis in colorectal cancer," *Oncogene*, vol. 27, no. 15, pp. 2128–2136, Apr. 2008, doi: 10.1038/sj.onc.1210856.
- [69] A. Das, K. Ganesh, S. Khanna, C. K. Sen, and S. Roy, "Engulfment of Apoptotic Cells by Macrophages: A Role of MicroRNA-21 in the Resolution of Wound Inflammation," *J. Immunol.*, vol. 192, no. 3, pp. 1120–1129, 2014, doi: 10.4049/jimmunol.1300613.
- [70] F. Meng *et al.*, "Involvement of Human Micro-RNA in Growth and Response to Chemotherapy in Human Cholangiocarcinoma Cell Lines," *Gastroenterology*, vol. 130, no. 7, pp. 2113–2129, Jun. 2006, doi: 10.1053/j.gastro.2006.02.057.
- [71] S. Roy *et al.*, "MicroRNA expression in response to murine myocardial infarction: MiR-21 regulates fibroblast metalloprotease-2 via phosphatase and tensin homologue," *Cardiovasc. Res.*, vol. 82, no. 1, pp. 21–29, 2009, doi: 10.1093/cvr/cvp015.
- [72] F. Meng, R. Henson, H. Wehbe-Janek, K. Ghoshal, S. T. Jacob, and T. Patel, "MicroRNA-21 Regulates Expression of the PTEN Tumor Suppressor Gene in Human Hepatocellular Cancer," *Gastroenterology*, vol. 133, no. 2, pp. 647–658, 2007, doi: 10.1053/j.gastro.2007.05.022.
- [73] T. Thum *et al.*, "MicroRNA-21 contributes to myocardial disease by stimulating MAP kinase signalling in fibroblasts," *Nature*, vol. 456, no. 7224, pp. 980–984, 2008, doi: 10.1038/nature07511.
- [74] J. Zhao *et al.*, "MiR-21 simultaneously regulates ERK1 signaling in HSC activation and hepatocyte EMT in hepatic fibrosis," *PLoS One*, vol. 9, no. 10, pp. 1–10, 2014, doi: 10.1371/journal.pone.0108005.
- [75] Y. Zhang *et al.*, "Co-treatment with miR-21-5p inhibitor and Aurora kinase inhibitor reversine suppresses breast cancer progression by targeting sprouty RTK signaling antagonist 2," *Bioengineered*, vol. 13, no. 1, pp. 455–468, 2022, doi: 10.1080/21655979.2021.2009410.
- [76] W. Qin, B. Zhao, Y. Shi, C. Yao, L. Jin, and Y. Jin, "BMPRII is a direct target of miR-21," *Acta Biochim. Biophys. Sin. (Shanghai)*, vol. 41, no. 7, pp. 618–623, Jul. 2009, doi: 10.1093/abbs/gmp049.
- [77] S. Yang *et al.*, "MiR-21 regulates chronic hypoxia-induced pulmonary vascular remodeling," *Am. J. Physiol. - Lung Cell. Mol. Physiol.*, vol. 302, no. 6, pp. 521–529, 2012, doi: 10.1152/ajplung.00316.2011.
- [78] J. Zhou, Q. Xu, Q. Zhang, Z. Wang, and S. Guan, "A novel molecular mechanism of microRNA-21 inducing pulmonary fibrosis and human pulmonary fibroblast

- extracellular matrix through transforming growth factor β 1-mediated SMADs activation," *J. Cell. Biochem.*, no. May, pp. 1–10, 2018, doi: 10.1002/jcb.27185.
- [79] A. Loboda, M. Sobczak, A. Jozkowicz, and J. Dulak, "TGF- β 1/Smads and miR-21 in Renal Fibrosis and Inflammation," *Mediators Inflamm.*, vol. 2016, pp. 1–12, 2016, doi: 10.1155/2016/8319283.
- [80] H.-L. Huang *et al.*, "Trypsin-induced proteome alteration during cell subculture in mammalian cells," *J. Biomed. Sci.*, vol. 17, no. 1, p. 36, Dec. 2010, doi: 10.1186/1423-0127-17-36.
- [81] K. Tsuji *et al.*, "Effects of Different Cell-Detaching Methods on the Viability and Cell Surface Antigen Expression of Synovial Mesenchymal Stem Cells," *Cell Transplant.*, vol. 26, no. 6, pp. 1089–1102, Jun. 2017, doi: 10.3727/096368917X694831.
- [82] A. Nowak-Terpiłowska, P. Śledziński, and J. Zeyland, "Impact of cell harvesting methods on detection of cell surface proteins and apoptotic markers," *Brazilian J. Med. Biol. Res.*, vol. 54, no. 2, 2021, doi: 10.1590/1414-431x202010197.
- [83] Y. R. A. Yu *et al.*, "Flow cytometric analysis of myeloid cells in human blood, bronchoalveolar lavage, and lung tissues," *Am. J. Respir. Cell Mol. Biol.*, vol. 54, no. 1, pp. 13–24, 2016, doi: 10.1165/rcmb.2015-0146OC.
- [84] A. Bharat *et al.*, "Flow Cytometry Reveals Similarities Between Lung Macrophages in Humans and Mice," *Am. J. Respir. Cell Mol. Biol.*, vol. 54, no. 1, pp. 147–149, Jan. 2016, doi: 10.1165/rcmb.2015-0147LE.
- [85] H. N. Alsafadi *et al.*, "An ex vivo model to induce early fibrosis-like changes in human precision-cut lung slices," *Am. J. Physiol. - Lung Cell. Mol. Physiol.*, vol. 312, no. 6, pp. L896–L902, 2017, doi: 10.1152/ajplung.00084.2017.
- [86] T. Xie, J. Liang, R. Guo, N. Liu, P. W. Noble, and D. Jiang, "Comprehensive microRNA analysis in bleomycin-induced pulmonary fibrosis identifies multiple sites of molecular regulation," *Physiological Genomics*, vol. 43, no. 9. pp. 479–487, 2011, doi: 10.1152/physiolgenomics.00222.2010.
- [87] L. Honeyman, M. Bazett, T. G. Tomko, and C. K. Haston, "MicroRNA profiling implicates the insulin-like growth factor pathway in bleomycin-induced pulmonary fibrosis in mice," *Fibrogenes. Tissue Repair*, vol. 6, no. 1, pp. 1–10, 2013, doi: 10.1186/1755-1536-6-16.
- [88] Q. Xu *et al.*, "Aberrant expression of miR-125a-3p promotes fibroblast activation via Fyn/STAT3 pathway during silica-induced pulmonary fibrosis," *Toxicology*, vol. 414, pp. 57–67, Feb. 2019, doi: 10.1016/j.tox.2019.01.007.
- [89] T. Konaka, M. Kawami, A. Yamamoto, R. Yumoto, and M. Takano, "miR-484: A Possible Indicator of Drug-Induced Pulmonary Fibrosis," *J. Pharm. Pharm. Sci.*, vol. 23, pp. 486–495, Nov. 2020, doi: 10.18433/jpps31448.
- [90] X. Han *et al.*, "Critical role of miR-10b in transforming growth factor- β 1-induced epithelial–mesenchymal transition in breast cancer," *Cancer Gene Ther.*, vol. 21, no. 2, pp. 60–67, Feb. 2014, doi: 10.1038/cgt.2013.82.
- [91] H. Cui *et al.*, "miR-34a promotes fibrosis in aged lungs by inducing alveolarepithelial dysfunctions," *Am. J. Physiol. Cell. Mol. Physiol.*, vol. 312, no. 3, pp. L415–L424, Mar. 2017, doi: 10.1152/ajplung.00335.2016.
- [92] S. K. Shetty *et al.*, "p53 and miR-34a Feedback Promotes Lung Epithelial Injury and Pulmonary Fibrosis," *Am. J. Pathol.*, vol. 187, no. 5, pp. 1016–1034, May 2017, doi: 10.1016/j.ajpath.2016.12.020.
- [93] S. Su *et al.*, "miR-142-5p and miR-130a-3p are regulated by IL-4 and IL-13 and control

- profibrogenic macrophage program," *Nat. Commun.*, vol. 6, pp. 1–19, 2015, doi: 10.1038/ncomms9523.
- [94] A. D. Bosson, J. R. Zamudio, and P. A. Sharp, "Endogenous miRNA and Target Concentrations Determine Susceptibility to Potential ceRNA Competition," *Mol. Cell*, vol. 56, no. 3, pp. 347–359, Nov. 2014, doi: 10.1016/j.molcel.2014.09.018.
- [95] X. Lin, M. Barravecchia, R. Matthew Kottmann, P. Sime, and D. A. Dean, "Caveolin-1 gene therapy inhibits inflammasome activation to protect from bleomycin-induced pulmonary fibrosis," *Sci. Rep.*, vol. 9, no. 1, p. 19643, Dec. 2019, doi: 10.1038/s41598-019-55819-y.
- [96] M.-H. Liu, A.-H. Lin, H.-K. Ko, D.-W. Perng, T.-S. Lee, and Y. R. Kou, "Prevention of Bleomycin-Induced Pulmonary Inflammation and Fibrosis in Mice by Paeonol," *Front. Physiol.*, vol. 8, Mar. 2017, doi: 10.3389/fphys.2017.00193.
- [97] A. L. McCubbrey *et al.*, "Deletion of c-FLIP from CD11bhi macrophages prevents development of bleomycin-induced lung fibrosis," *American Journal of Respiratory Cell and Molecular Biology*, vol. 58, no. 1, pp. 66–78, 2018, doi: 10.1165/rcmb.2017-0154OC.
- [98] N.-Y. Chen *et al.*, "Macrophage bone morphogenic protein receptor 2 depletion in idiopathic pulmonary fibrosis and Group III pulmonary hypertension," *Am. J. Physiol. Cell. Mol. Physiol.*, vol. 311, no. 2, pp. L238–L254, Aug. 2016, doi: 10.1152/ajplung.00142.2016.
- [99] A. Birnhuber *et al.*, "CDK4/6 inhibition enhances pulmonary inflammatory infiltration in bleomycin-induced lung fibrosis," *Respir. Res.*, vol. 21, no. 1, p. 167, Dec. 2020, doi: 10.1186/s12931-020-01433-w.
- [100] M. Pelullo *et al.*, "miR-125b/NRF2/HO-1 axis is involved in protection against oxidative stress of cystic fibrosis: A pilot study," *Exp. Ther. Med.*, vol. 21, no. 6, p. 585, Apr. 2021, doi: 10.3892/etm.2021.10017.
- [101] Q. Qian *et al.*, "MicroRNA-205-5p targets E2F1 to promote autophagy and inhibit pulmonary fibrosis in silicosis through impairing SKP2-mediated Beclin1 ubiquitination," *J. Cell. Mol. Med.*, vol. 25, no. 19, pp. 9214–9227, Oct. 2021, doi: 10.1111/jcmm.16825.
- [102] Y. Wang, J. Yella, J. Chen, F. X. McCormack, S. K. Madala, and A. G. Jegga, "Unsupervised gene expression analyses identify IPF-severity correlated signatures, associated genes and biomarkers," *BMC Pulm. Med.*, vol. 17, no. 1, pp. 1–10, 2017, doi: 10.1186/s12890-017-0472-9.
- [103] H. B. Schiller *et al.*, "Time- and compartment-resolved proteome profiling of the extracellular niche in lung injury and repair," *Mol. Syst. Biol.*, vol. 11, no. 7, pp. 819–819, 2015, doi: 10.15252/msb.20156123.
- [104] D. Ramanujam *et al.*, "MicroRNA-21-Dependent Macrophage-to-Fibroblast Signaling Determines the Cardiac Response to Pressure Overload," *Circulation*, vol. 143, no. 15, pp. 1513–1525, Apr. 2021, doi: 10.1161/CIRCULATIONAHA.120.050682.
- [105] P. Vegh *et al.*, "Profiling microRNA expression in bovine alveolar macrophages using RNA-seq," *Vet. Immunol. Immunopathol.*, vol. 155, no. 4, pp. 238–244, Oct. 2013, doi: 10.1016/j.vetimm.2013.08.004.
- [106] J. Xi *et al.*, "miR-21 depletion in macrophages promotes tumoricidal polarization and enhances PD-1 immunotherapy," *Oncogene*, vol. 37, no. 23, pp. 3151–3165, Jun. 2018, doi: 10.1038/s41388-018-0178-3.
- [107] W. Zhu, J. Xu, M. Zhang, T. Zhu, Y. Zhang, and K. Sun, "MicroRNA-21 inhibits

- lipopolysaccharide-induced acute lung injury by targeting nuclear factor- κ B,” *Exp. Ther. Med.*, pp. 4616–4622, Sep. 2018, doi: 10.3892/etm.2018.6789.
- [108] M. Sahraei *et al.*, “Suppressing miR-21 activity in tumor-associated macrophages promotes an antitumor immune response,” *J. Clin. Invest.*, vol. 129, no. 12, pp. 5518–5536, Nov. 2019, doi: 10.1172/JCI127125.
- [109] R. E. Barnett *et al.*, “Anti-inflammatory effects of miR-21 in the macrophage response to peritonitis,” *J. Leukoc. Biol.*, vol. 99, no. 2, pp. 361–371, Feb. 2016, doi: 10.1189/jlb.4A1014-489R.
- [110] Z. Wang *et al.*, “MicroRNA 21 Is a Homeostatic Regulator of Macrophage Polarization and Prevents Prostaglandin E2-Mediated M2 Generation,” *PLoS One*, vol. 10, no. 2, p. e0115855, Feb. 2015, doi: 10.1371/journal.pone.0115855.
- [111] Z. Li, F. Wu, S. R. Brant, and J. H. Kwon, “IL-23 Receptor Regulation by Let-7f in Human CD4 + Memory T Cells,” *J. Immunol.*, vol. 186, no. 11, pp. 6182–6190, Jun. 2011, doi: 10.4049/jimmunol.1000917.
- [112] H. Wu *et al.*, “miRNA Profiling of Naïve, Effector and Memory CD8 T Cells,” *PLoS One*, vol. 2, no. 10, p. e1020, Oct. 2007, doi: 10.1371/journal.pone.0001020.
- [113] T. A. Harris, M. Yamakuchi, M. Ferlito, J. T. Mendell, and C. J. Lowenstein, “MicroRNA-126 regulates endothelial expression of vascular cell adhesion molecule 1,” *Proc. Natl. Acad. Sci.*, vol. 105, no. 5, pp. 1516–1521, Feb. 2008, doi: 10.1073/pnas.0707493105.
- [114] J. Zhang *et al.*, “MiR-148b suppresses cell proliferation and invasion in hepatocellular carcinoma by targeting WNT1/ β -catenin pathway,” *Sci. Rep.*, vol. 5, no. 1, p. 8087, Jul. 2015, doi: 10.1038/srep08087.
- [115] S. Yang *et al.*, “miR-145 regulates myofibroblast differentiation and lung fibrosis,” *FASEB J.*, vol. 27, no. 6, pp. 2382–2391, Jun. 2013, doi: 10.1096/fj.12-219493.
- [116] X. Zeng, C. Huang, L. Senavirathna, P. Wang, and L. Liu, “miR-27b inhibits fibroblast activation via targeting TGF β signaling pathway,” *BMC Cell Biol.*, vol. 18, no. 1, p. 9, Dec. 2017, doi: 10.1186/s12860-016-0123-7.
- [117] W. Wang *et al.*, “Macrophage micro-RNA-155 promotes lipopolysaccharide-induced acute lung injury in mice and rats,” *Am. J. Physiol. Cell. Mol. Physiol.*, vol. 311, no. 2, pp. L494–L506, Aug. 2016, doi: 10.1152/ajplung.00001.2016.
- [118] S. Chen, E. C. So, S. E. Strome, and X. Zhang, “Impact of Detachment Methods on M2 Macrophage Phenotype and Function,” *J. Immunol. Methods*, vol. 426, pp. 56–61, 2015, doi: 10.1016/j.jim.2015.08.001.
- [119] H. Komatsu *et al.*, “Trypsin inhibits lipopolysaccharide signaling in macrophages via toll-like receptor 4 accessory molecules,” *Life Sci.*, vol. 91, no. 3–4, pp. 143–150, Aug. 2012, doi: 10.1016/j.lfs.2012.06.030.
- [120] M. J. V. White and R. H. Gomer, “Trypsin, Trypsinase, and Thrombin Polarize Macrophages towards a Pro-Fibrotic M2a Phenotype,” *PLoS One*, vol. 10, no. 9, p. e0138748, Sep. 2015, doi: 10.1371/journal.pone.0138748.
- [121] V. Malheiro, Y. Elbs-Glatz, M. Obarzanek-Fojt, K. Maniura-Weber, and A. Bruinink, “Harvesting pre-polarized macrophages using thermo-responsive substrates,” *Sci. Rep.*, vol. 7, no. 1, p. 42495, Mar. 2017, doi: 10.1038/srep42495.
- [122] I. Brochériou *et al.*, “Antagonistic regulation of macrophage phenotype by M-CSF and GM-CSF: Implication in atherosclerosis,” *Atherosclerosis*, vol. 214, no. 2, pp. 316–324, 2011, doi: 10.1016/j.atherosclerosis.2010.11.023.
- [123] A. Frafjord *et al.*, “Antibody combinations for optimized staining of macrophages in human lung tumours,” *Scand. J. Immunol.*, vol. 92, no. 1, Jul. 2020, doi:

- 10.1111/sji.12889.
- [124] P. A. Reyfman *et al.*, "Single-Cell Transcriptomic Analysis of Human Lung Provides Insights into the Pathobiology of Pulmonary Fibrosis," *Am J Respir Crit Care Med*, vol. 199, no. 12, pp. 1517–1536, 2019.
- [125] Z.-J. Xu *et al.*, "The M2 macrophage marker CD206 : a novel prognostic indicator for acute myeloid leukemia," *Oncoimmunology*, vol. 9, no. 1, Jan. 2020, doi: 10.1080/2162402X.2019.1683347.
- [126] M. Orecchioni, Y. Ghosheh, A. B. Pramod, and K. Ley, "Macrophage Polarization: Different Gene Signatures in M1(LPS+) vs. Classically and M2(LPS-) vs. Alternatively Activated Macrophages," *Front. Immunol.*, vol. 10, May 2019, doi: 10.3389/fimmu.2019.01084.
- [127] M. Liao *et al.*, "Single-cell landscape of bronchoalveolar immune cells in patients with COVID-19," *Nat. Med.*, vol. 26, no. 6, pp. 842–844, 2020, doi: 10.1038/s41591-020-0901-9.
- [128] A. Lescoat *et al.*, "Distinct properties of human M-CSF and GM-CSF monocyte-derived macrophages to simulate pathological lung conditions in vitro: Application to systemic and inflammatory disorders with pulmonary involvement," *Int. J. Mol. Sci.*, vol. 19, no. 3, 2018, doi: 10.3390/ijms19030894.
- [129] A. Lukic *et al.*, "GM-CSF- and M-CSF-primed macrophages present similar resolving but distinct inflammatory lipid mediator signatures," *FASEB J.*, vol. 31, no. 10, pp. 4370–4381, 2017, doi: 10.1096/fj.201700319R.
- [130] S. Mullenbrock *et al.*, "Systems Analysis of Transcriptomic and Proteomic Profiles Identifies Novel Regulation of Fibrotic Programs by miRNAs in Pulmonary Fibrosis Fibroblasts," *Genes (Basel)*, vol. 9, no. 12, p. 588, Nov. 2018, doi: 10.3390/genes9120588.
- [131] R. Hinkel *et al.*, "AntimiR-21 Prevents Myocardial Dysfunction in a Pig Model of Ischemia/Reperfusion Injury," *J. Am. Coll. Cardiol.*, vol. 75, no. 15, pp. 1788–1800, Apr. 2020, doi: 10.1016/j.jacc.2020.02.041.
- [132] S. Prasad, C. M. Hogaboam, and G. Jarai, "Deficient repair response of IPF fibroblasts in a co-culture model of epithelial injury and repair," *Fibrogenesis Tissue Repair*, vol. 7, no. 1, p. 7, Dec. 2014, doi: 10.1186/1755-1536-7-7.
- [133] J. He *et al.*, "Modeling alveolar injury using microfluidic co-cultures for monitoring bleomycin-induced epithelial/fibroblastic cross-talk disorder," *RSC Adv.*, vol. 7, no. 68, pp. 42738–42749, 2017, doi: 10.1039/C7RA06752F.
- [134] A. J. Miller *et al.*, "Generation of lung organoids from human pluripotent stem cells in vitro," *Nat. Protoc.*, vol. 14, no. 2, pp. 518–540, Feb. 2019, doi: 10.1038/s41596-018-0104-8.
- [135] H. Hirai *et al.*, "The sodium/glucose cotransporters as potential therapeutic targets for CF lung diseases revealed by human lung organoid swelling assay," *Mol. Ther. - Methods Clin. Dev.*, vol. 24, pp. 11–19, Mar. 2022, doi: 10.1016/j.omtm.2021.11.008.
- [136] P. Zamprogno *et al.*, "Second-generation lung-on-a-chip with an array of stretchable alveoli made with a biological membrane," *Commun. Biol.*, vol. 4, no. 1, p. 168, Dec. 2021, doi: 10.1038/s42003-021-01695-0.
- [137] D. Huh, B. D. Matthews, A. Mammoto, M. Montoya-Zavala, H. Y. Hsin, and D. E. Ingber, "Reconstituting Organ-Level Lung Functions on a Chip," *Science (80-.)*, vol. 328, no. 5986, pp. 1662–1668, Jun. 2010, doi: 10.1126/science.1188302.
- [138] M. Schlepütz *et al.*, "Neurally Mediated Airway Constriction in Human and Other

- Species: A Comparative Study Using Precision-Cut Lung Slices (PCLS)," *PLoS One*, vol. 7, no. 10, p. e47344, Oct. 2012, doi: 10.1371/journal.pone.0047344.
- [139] A. Wohlsen *et al.*, "The early allergic response in small airways of human precision-cut lung slices," *Eur. Respir. J.*, vol. 21, no. 6, pp. 1024–1032, Jun. 2003, doi: 10.1183/09031936.03.00027502.
- [140] J. Tigges, F. Eggerbauer, F. Worek, H. Thiermann, U. Rauen, and T. Wille, "Optimization of long-term cold storage of rat precision-cut lung slices with a tissue preservation solution," *Am. J. Physiol. Cell. Mol. Physiol.*, vol. 321, no. 6, pp. L1023–L1035, Dec. 2021, doi: 10.1152/ajplung.00076.2021.
- [141] J. E. McDonough *et al.*, "Transcriptional regulatory model of fibrosis progression in the human lung," *JCI Insight*, vol. 4, no. 22, 2019, doi: 10.1172/jci.insight.131597.
- [142] J. Lee *et al.*, "Bronchoalveolar lavage (BAL) cells in idiopathic pulmonary fibrosis express a complex pro-inflammatory, pro-repair, angiogenic activation pattern, likely associated with macrophage iron accumulation," *PLoS One*, vol. 13, no. 4, p. e0194803, Apr. 2018, doi: 10.1371/journal.pone.0194803.
- [143] I. G. Luzina *et al.*, "Transcriptomic evidence of immune activation in macroscopically normal-appearing and scarred lung tissues in idiopathic pulmonary fibrosis," *Cell. Immunol.*, vol. 325, no. December 2017, pp. 1–13, 2018, doi: 10.1016/j.cellimm.2018.01.002.
- [144] A. Sokai *et al.*, "Matrix metalloproteinase-10: a novel biomarker for idiopathic pulmonary fibrosis," *Respir. Res.*, vol. 16, no. 1, p. 120, Dec. 2015, doi: 10.1186/s12931-015-0280-9.
- [145] C. M. Yamashita *et al.*, "Matrix Metalloproteinase 3 Is a Mediator of Pulmonary Fibrosis," *Am. J. Pathol.*, vol. 179, no. 4, pp. 1733–1745, Oct. 2011, doi: 10.1016/j.ajpath.2011.06.041.
- [146] S. Barratt, A. Creamer, C. Hayton, and N. Chaudhuri, "Idiopathic Pulmonary Fibrosis (IPF): An Overview," *J. Clin. Med.*, vol. 7, no. 8, p. 201, Aug. 2018, doi: 10.3390/jcm7080201.
- [147] K. Yoshida *et al.*, "MAP kinase activation and apoptosis in lung tissues from patients with idiopathic pulmonary fibrosis," *J. Pathol.*, vol. 198, no. 3, pp. 388–396, Nov. 2002, doi: 10.1002/path.1208.
- [148] P. Sivakumar *et al.*, "RNA sequencing of transplant-stage idiopathic pulmonary fibrosis lung reveals unique pathway regulation," *ERJ Open Res.*, vol. 5, no. 3, 2019, doi: 10.1183/23120541.00117-2019.
- [149] I. Kotani, A. Sato, H. Hayakawa, T. Urano, Y. Takada, and A. Takada, "Increased procoagulant and antifibrinolytic activities in the lungs with idiopathic pulmonary fibrosis," *Thromb. Res.*, vol. 77, no. 6, pp. 493–504, Mar. 1995, doi: 10.1016/0049-3848(95)00025-9.
- [150] K. Tanaka *et al.*, "Serum S100A8 and S100A9 as prognostic biomarkers in acute exacerbation of idiopathic pulmonary fibrosis," *Respir. Investig.*, vol. 59, no. 6, pp. 827–836, Nov. 2021, doi: 10.1016/j.resinv.2021.05.008.
- [151] T. Xie, L. Han, Y. Chen, and H. Wu, "Progranulin and Activin A Concentrations are Elevated in Serum from Patients with Acute Exacerbations of Idiopathic Pulmonary Fibrosis," *Lung*, vol. 199, no. 5, pp. 467–473, Oct. 2021, doi: 10.1007/s00408-021-00470-6.
- [152] F. Aoki, M. Kurabayashi, Y. Hasegawa, and I. Kojima, "Attenuation of Bleomycin-induced Pulmonary Fibrosis by Follistatin," *Am. J. Respir. Crit. Care Med.*, vol. 172, no.

- 6, pp. 713–720, Sep. 2005, doi: 10.1164/rccm.200412-1620OC.
- [153] Y. Kasuya, J.-D. Kim, M. Hatano, K. Tatsumi, and S. Matsuda, “Pathophysiological Roles of Stress-Activated Protein Kinases in Pulmonary Fibrosis,” *Int. J. Mol. Sci.*, vol. 22, no. 11, p. 6041, Jun. 2021, doi: 10.3390/ijms22116041.
- [154] M. Myllärniemi *et al.*, “Gremlin-mediated Decrease in Bone Morphogenetic Protein Signaling Promotes Pulmonary Fibrosis,” *Am. J. Respir. Crit. Care Med.*, vol. 177, no. 3, pp. 321–329, Feb. 2008, doi: 10.1164/rccm.200706-945OC.
- [155] N. Murphy *et al.*, “Altered Expression of Bone Morphogenetic Protein Accessory Proteins in Murine and Human Pulmonary Fibrosis,” *Am. J. Pathol.*, vol. 186, no. 3, pp. 600–615, Mar. 2016, doi: 10.1016/j.ajpath.2015.10.032.

ACKNOWLEDGMENTS

First of all, I would like to thank my supervisor Prof. Dr. Dr. Stefan Engelhardt for giving me the opportunity to conduct my PhD in his lab, for his valuable input throughout these years and for his trust in giving me the freedom to shape my project. I thank as well my mentor Dr. Deepak Ramanujam for his continuous guidance and always being there for questions, discussions and brainstorming.

I would also like to thank my other supervisors and mentors, Prof. Dr. med. Christian Schulz, Prof. Dr. med. Jürgen Behr and Dr. Herbert Schiller for their helpful contributions and giving a fresh perspective. I want to thank as well our collaborators Dr. Claudia Staab-Weijnitz who provided the lung tissues from IPF patients and donors, and Prof. Dr. Hans Hoffmann and Dr. med. Seyer Safi for providing the lung sections for the PCLS experiments.

This PhD was also possible thanks to Prof. Dr. med. Thomas Gudermann, who founded the research training program “Targets in Toxicology” I am part of, and Dr. Julia Brandt and Stefanie Rosenberger who made a great work in coordination.

I would also like to express my gratitude to all my colleagues in the institute for the friendly and helpful environment they create, with a special mention to Sabine, Jessi, Toni and Julia for their great help with experiments.

Ile, Chris, Regi, you are not just good scientists but wonderful people; thank you for the chats, laughs, coffee breaks and daily support. You are the best I take from my time here.

Finally, I would like to give the greatest thanks to my family. You provided me with the biggest motivation, encouragement and hope, even from an ocean apart.